



**ON-LINE QUALITY MONITORING AND LIFETIME  
PREDICTION OF THICK AL WIRE BONDS USING  
SIGNALS OBTAINED FROM ULTRASONIC  
GENERATOR**

**Elaheh Arjmand**

Thesis submitted to the University of Nottingham

For the degree of Doctor of Philosophy

Department of Electrical and Electronic Engineering

The University of Nottingham

August 2016

## **Abstract**

The reliable performance of power electronic modules has been a concern for many years due to their increased use in applications which demand high availability and longer lifetimes. Thick Al wire bonding is a key technique for providing interconnections in power electronic modules. Today, wire bond lift-off and heel cracking are often considered the most lifetime limiting factors of power electronic modules as a result of cyclic thermomechanical stresses. Therefore, it is important for power electronic packaging manufacturers to address this issue at the design stage and on the manufacturing line. Techniques for the non-destructive, real-time evaluation and control of wire bond quality have been proposed to detect defects in manufacture and predict reliability prior to in-service exposure. This approach has the potential to improve the accuracy of lifetime prediction for the manufactured product.

In this thesis, a non-destructive technique for detecting bond quality by the application of a semi-supervised classification algorithm to process signals obtained from an ultrasonic generator is presented. Experimental tests verified that the classification method is capable of accurately predicting bond quality, indicated by bonded area as measured by X-ray tomography. Samples classified during bonding were subjected to both passive and active cycling and the distribution of bond life amongst the different classes analysed. It is demonstrated that the as-bonded quality classification is closely correlated with cycling life and can therefore be used as a non-destructive tool for monitoring bond quality and predicting useful service life.

*To Saeed, Viyana, my father and  
in loving memory of my mother "Mah-Parvin"*



## Acknowledgments

After four and half years, finally, the journey of my Ph.D comes to an end and I would like to take this opportunity to express my deepest gratitude to many people who enriched my experiences at University of Nottingham.

Firstly, I would like to express my most sincere gratitude and appreciation to my supervisors, Prof. C. Mark Johnson and Dr. Pearl Agyakwa, who have helped me during this research and have been supporting me throughout my study. I have learned so much from you, both professionally and personally.

I am also grateful to Prof. Chris Bailey (University of Greenwich) and Dr. Alberto Castellazi for examining this work and for your comments and suggestions.

Especially, I would like to acknowledge members of power electronics integration, packaging and thermal management team, including, Dr. Jianfeng Li, Dr. Martin Corfield, Dr. Li Yang, Dr. Paul Evans, Dr. Imran Yaqub, Dr. Bassem Mouawad, Dr. Amir Eleffendi, Dr. Yun Wang and Miss Dai Jingru for their kind guidance, help and support throughout my study.

I would also like to acknowledge the EPSRC funding through the HubNet Project under Grant EP/I013636/1 for providing financial support through this study. I am also grateful to Dynex Semiconductor Ltd. for providing Silicon dies and substrate tiles.

I would like to thank my friends: Salma, Fathemeh, Shiva, Farkhondeh, Parisa, Zahra, Sara, Yasaman, Atefeh and Mina, for their love and support.

I would like to thank my father and sisters for their constant encouragement and endless support throughout my life.

I would like to extend my sincerest thanks and appreciation to my beloved husband Saeed for his love, patience and support throughout the years. Finally, I deeply appreciate my lovely daughter, Viyana for her sincere love, sweet spirit and understanding of my time. Without her cheerful presence, it would have been impossible to finish this thesis.

## Table of Contents

<b>ABSTRACT.....</b>	<b>i</b>
<b>List of Figures.....</b>	<b>viii</b>
<b>List of Tables.....</b>	<b>xii</b>
<b>Abbreviations.....</b>	<b>xiii</b>
<b>Nomenclature.....</b>	<b>xiv</b>
<b>CHAPTER 1 INTRODUCTION.....</b>	<b>1</b>
1.1. OVERVIEW AND MOTIVATION.....	1
1.2. CONTRIBUTIONS.....	8
1.3. THESIS STRUCTURE.....	10
1.4. LIST OF PUBLICATIONS .....	11
<b>CHAPTER 2 BACKGROUND AND LITERATURE REVIEW.....</b>	<b>12</b>
2.1. WIRE BONDING TECHNOLOGY .....	12
2.2. ULTRASONIC WEDGE BONDING .....	13
2.2.1. Ultrasonic Wedge Wire Bonder.....	13
2.2.2. Ultrasonic Wedge Wire Bonding Process .....	14
2.3. WIRE BONDING PROCESS VARIATION AND PROCESS PARAMETERS OPTIMIZATION .....	16
2.4. WIRE BONDING FAILURE MECHANISMS .....	16
2.5. WIRE BOND RELIABILITY ASSESSMENT AND LIFETIME PREDICTION ..	21
2.6. WIRE BONDING CHARACTERIZATION/EVALUATION .....	23
2.6.1. Wire Bond Pull Test .....	23
2.6.2. Wire Bond Shear Test.....	24
2.6.3. 3D X-Ray Tomography .....	25
2.6.4. On-Line Wire Bonding Process Monitoring.....	28
2.7. SUMMARY.....	34
<b>CHAPTER 3 EXPERIMENTAL METHOD FOR ON-LINE QUALITY ASSESSMENT OF WIRE BONDING PROCESS.....</b>	<b>36</b>

3.1.	NON-DESTRUCTIVE WIRE BOND LIFETIME PREDICTION TECHNIQUE	36
3.1.1.	Signal Detection Principle and Set-up	37
3.1.2.	Signal Pre-processing	39
3.2.	TECHNIQUE OF NON-DESTRUCTIVE ANALYSIS AND VISUAL OBSERVATION OF DEGRADATION	41
3.2.1.	Process Parameters Optimization	41
3.2.2.	Passive Thermal Cycling	41
3.2.3.	Active Power Cycling Test	43
3.2.4.	3D X-ray Tomography	46
3.2.5.	Tweezer Test	49
3.3.	TECHNIQUE FOR DATA ANALYSIS AND CLASSIFICATION	49
3.3.1.	Sampling and Data Collection	49
3.3.2.	Random Selection and Defining Labelled and Unlabelled Data	50
3.3.3.	Classification	50
3.3.4.	Machine Learning	50
3.3.5.	Background of the SDA Algorithm	55
3.3.6.	Model Accuracy	57
3.4.	SUMMARY	58
<b>CHAPTER 4 INVESTIGATING THE EFFECT OF BONDING PARAMETERS ON THE RELIABILITY OF AL WIRE</b>		
4.1.	WIRE BONDING PROCESS PARAMETER SETTING	59
4.2.	EXPERIMENTAL PROCEDURE	60
4.2.1.	Signal Acquisition Setting	61
4.2.2.	Wire Bonding Layout	62
4.3.	RESULTS AND DISCUSSIONS	62
4.3.1.	Relation of Different Designs and Bonds Bonded Area	62
4.3.2.	Relationship of Different Designs and Bond Electrical Signals	68
4.4.	SUMMARY	75
<b>CHAPTER 5 ESTABLISHING THE LINK BETWEEN ELECTRICAL SIGNATURE AND BOND QUALITY FOR LIFETIME PREDICTION OF WIRE BONDS</b>		
5.1.	EXPERIMENTAL PROCEDURE	77

5.1.1.	Sample Size .....	77
5.1.2.	Bond Parameter Settings.....	78
5.1.3.	Signal Detection.....	79
5.1.4.	Description of Samples for the Semi-Supervised Algorithm .....	80
5.2.	RELIABILITY TESTS AND VISUAL OBSERVATION FOR BONDED WIRES	80
5.2.1.	3D X-ray Tomography .....	80
5.2.2.	Passive Thermal Cycling .....	80
5.2.3.	Tweezer Tests .....	81
5.3.	RESULTS AND DISCUSSIONS.....	81
5.3.1.	Prediction of Bonds' Classes .....	84
5.3.2.	Setting Target for On-Line Monitoring Assessment .....	86
5.3.3.	Model Performance Evaluation .....	87
5.3.4.	Estimating Die/Substrate/Module Life from Wire Bond Process Classifier Data .....	90
5.3.5.	Determination of Degradation Rate.....	94
5.3.6.	Surface Treatment.....	99
5.4.	SUMMARY.....	104
<b>CHAPTER 6 CLASSIFIER PERFORMANCE FOR SAMPLES SUBJECTED TO ACTIVE POWER CYCLING .....106</b>		
6.1.	EXPERIMENTAL PROCEDURE .....	107
6.1.1.	Active Power Cycling Set-up .....	107
6.1.2.	Sample Preparation.....	108
6.1.3.	Bond Parameter Setting .....	109
6.1.4.	Signal Detection.....	109
6.1.5.	Description of Samples for the SDA Algorithm.....	110
6.1.6.	3D X-ray Tomography .....	110
6.2.	RESULTS AND DISCUSSIONS.....	110
6.2.1.	Determination of Degradation Rate.....	112
6.2.2.	Estimation of Lifetime.....	118
6.3.	SUMMARY.....	121
<b>CHAPTER 7 CONCLUSIONS AND RECOMMENDATIONS FOR FUTURE WORK.....122</b>		

7.1. CONCLUSIONS .....	122
7.2. FUTURE WORK.....	124
<b>Appendix I.....</b>	<b>126</b>
<b>Appendix II.....</b>	<b>127</b>
<b>Appendix III.....</b>	<b>133</b>
<b>References.....</b>	<b>134</b>

## List of Figures

Figure 1.1: World total primary energy supply of fuels in 2012 [2] .....	2
Figure 1.2: Different type of IGBT modules.....	3
Figure 1.3: A typical IGBT module with baseplate.....	4
Figure 1.4: Cross-section view of power IGBT module package .....	5
Figure 1.5: Aluminium (Al) thick wire bonds on IGBT and diode in a power module .....	6
Figure 1.6: A cross-section view of Al wire showing cracks propagation during cycling.....	7
Figure 1.7: Lifetime variation of wire bonds subjected to passive thermal cycling.....	8
Figure 2.1: Ultrasonic wedge-wedge wire bonder.....	14
Figure 2.2: Ultrasonic wedge bonding process a) the starting point and bonding first bond, b) wire bond looping process c) end of looping process, d) the ending point and bonding second bond .....	15
Figure 2.3: Schematic diagram of Al wire bond experiencing different stress during operation.....	17
Figure 2.4: Cross-section of Al wire bond showing crack grows 10-20 $\mu\text{m}$ above the bond interface[34] .....	18
Figure 2.5: SEM image of Al wire lift-off a) remain Al wire on bond pad, b) Al wire [40].....	19
Figure 2.6: EBSD images of Al wire bond in a) as-bonded condition and b) after 1000hr at 135°C[36].....	19
Figure 2.7: Heel crack in heavy Al wire bonding 1) SEM image of observed heel crack after active power cycling 2) Heel crack through bonded wires [34] .....	20
Figure 2.8: wire bond pull test.....	23
Figure 2.9: Wire bond shear test steps.....	24
Figure 2.10: Schematic illustration of X-ray tomography.....	26
Figure 2.11: Virtual cross-sections in the X-Y plane of the Al wire bond interface in (a) initial bonded condition (b) 105 cycles, (c) 215 cycles, (d) 517 cycles and (e) 867 cycles [9] .....	27

Figure 2.12: Amplitude of 2 <sup>nd</sup> harmonic of signal in different bonding conditions [29] .....	29
Figure 2.13: Predicted shear strength using the ratio of the steady-state amplitude to the peak value of 2 <sup>nd</sup> harmonic [11] .....	29
Figure 2.14: Work flow diagram of feature selection method used by Feng et al. [12].....	32
Figure 2.15: Artificial neural networks predicted shear test [12].....	33
Figure 2.16: Predicted shear strength vs. measured shear strength [76] .....	34
Figure 3.1: Wire bonding signal detecting principle .....	37
Figure 3.2: Details of signal detection tools .....	38
Figure 3.3: A typical signature of bond signals, a) current and b) voltage.....	39
Figure 3.4: A typical signature of bond current signal and its corresponding envelope.....	40
Figure 3.5: Test set-up for passive thermal cycling.....	42
Figure 3.6: A snapshots of temperature profile of thermal cycling test .....	43
Figure 3.7: Temperature distribution of the chip in thermal equilibrium [97] .	44
Figure 3.8: Image of power cycling rig .....	45
Figure 3.9: A snapshot of temperature profile.....	46
Figure 3.10: 3D X-ray tomography .....	47
Figure 3.11: Overview scan of bonded wires, a) Virtual cross-sections in X-Y plane of the wire bonds interface, b) Virtual cross-sections in Y-Z, c) Virtual cross-sections in X-Z plane, d) Volume rendered image of bonded wires.....	48
Figure 3.12: Procedures for a semi-supervised learning algorithm[125] .....	53
Figure 3.13: Performance comparison of different algorithms, Baseline, Eigenface [132], Laplacianface[133], consistency [121], LapSVM[120], LapRLS [120] and SDA .....	54
Figure 3.14: The on-line assessment technique flowchart.....	57
Figure 4.1: Aluminium wires bonded onto silicon dies.....	62
Figure 4.2: X-ray tomography virtual cross-sectional image in different plane view showing the bonded area of Design 1 .....	63
Figure 4.3: Bond bonded area for different parameter designs (0 cycles).....	64
Figure 4.4: Result of bond lifetime after thermal cycling for the different parameter designs .....	65

Figure 4.5: X-ray tomography images of design 1 and 15 in X-Y plane in as-bonded condition and after 700 cycles .....	66
Figure 4.6: X-ray tomography images of design 4 and 7 in the X-Y plane in as-bonded condition and after 700 cycles .....	67
Figure 4.7: Current envelope of bonding signals for designs 1 to 5.....	69
Figure 4.8: Current envelope of bonding signals for designs 1 and 4 (weakest design compare strongest design).....	70
Figure 4.9: Current envelope of bonding signals for the most reliable designs	71
Figure 4.10: Current envelope of bonding signals for the less reliable designs .....	72
Figure 4.11: Current envelope of bonding signals for designs 14 and 12 .....	73
Figure 4.12: Current envelope of bonding signals for the designs 17 .....	74
Figure 5.1: Layout for soldering silicon dies on substrate .....	77
Figure 5.2: Aluminium wires bonded onto silicon dies.....	79
Figure 5.3: Current envelope of 24 selected bonds .....	81
Figure 5.4: Variation in bonded area in the as-bonded condition measured by ImageJ software .....	82
Figure 5.5: Virtual cross-sectional images in the X-Y plane of classified signals in the as-bonded condition.....	83
Figure 5.6: Labelled signals according to measured bonded area .....	83
Figure 5.7: Average lifetime of predicted classes .....	84
Figure 5.8: Cumulative frequency curve of three classes.....	85
Figure 5.9: Using arbitrary limits for the on-line process monitoring technique .....	87
Figure 5.10: a) A typical substrate tile, b) cumulative frequency curve.....	93
Figure 5.11: Virtual cross-section images of two bonds in class “C” in X–Y plane in as-bonded condition, 700 cycles and 1400 cycles .....	96
Figure 5.12: Virtual cross-section images of two bonds in class “A” in X–Y plane in as-bonded condition, 700 cycles and 1400 cycles .....	97
Figure 5.13: Bonds degradation rate in class “A” and “C” .....	98
Figure 5.14: Envelope of current signals of plasma cleaned sample (condition “i”) .....	99
Figure 5.15: Envelope of current signals of freshly manufactured sample without plasma cleaning (condition “ii”).....	100



Figure 5.16: Envelope of current signals of manufactured dies which were kept in argon purged cabinet for 4 days (condition “iii”).....	101
Figure 5.17: Classification results in a) using fresh and plasma cleaned dies, b) fresh and without plasma cleaning c) old dies (stored for 4 days in purged cabinet) and without plasma cleaning.....	103
Figure 5.18: Average lifetime of wire bonds in different bond pad conditions .....	104
Figure 6.1: Fixing the sample on cold plate with copper plates .....	107
Figure 6.2: Substrate preparation for wire bonding.....	108
Figure 6.3: Aluminium wires bonded onto silicon dies for active power cycling test.....	109
Figure 6.4: Current envelopes of the eight bonds on a freshly manufactured die .....	111
Figure 6.5: Current envelope of the 8 bonds on a die which were kept in an argon- purged cabinet for seven days .....	111
Figure 6.6: An overview of sample for active power cycling test, a) 3D rendered view, b) Selected wires in X-Y plane .....	112
Figure 6.7: Virtual cross-sections with different Z height in the X-Y planes and Y-Z plane, bond no. 8, condition “1”, Class “A” .....	114
Figure 6.8: Virtual cross-sections with different X position in the, X-Y plane and X-Z planes, bond no. 8, condition “1”, Class “A” .....	115
Figure 6.9: Virtual cross-sections with different Z height in the X-Y planes and Y-Z plane, bond no. 8, condition “2”, Class “C” .....	116
Figure 6.10: Virtual cross-sections with different X position in the, X-Y plane and X-Z planes, bond no. 8, condition “2”, Class “C” .....	117
Figure 6.11: Region of stress in Al wire during active power cycling [150] .	118
Figure 6.12: Bonds degradation rate in class “A” and “C” (active power cycling) .....	119
Figure 6.13: Comparing the results of lifetime with a) Ramminger et al. [41]and b) Held et al. [57]lifetime curve .....	120

## List of Tables

Table 3.1: Details of 3D X-ray tomography imaging parameters .....	47
Table 3.2: Table of the terminology used in this thesis .....	49
Table 4.1: Bonding parameters designs for reliability test .....	61
Table 4.2: Bonding parameters selected for on-line quality assessment .....	74
Table 5.1: Optimized bond parameter settings .....	78
Table 5.2: Loop parameters setting .....	79
Table 5.3: Detailed information of the data used for the algorithm .....	80
Table 5.4: One-way ANOVA for wire bonds lifetime data.....	85
Table 5.5: Individual 95% confidence interval for mean of wire bonds lifetime data.....	86
Table 5.6: The error matrix of the bond quality classifier .....	88
Table 5.7: Precision value for each class.....	89
Table 5.8: Recall value for each class .....	89
Table 5.9 : Example of probabilities of failure for eight wires mix of class “A” and class “C” .....	93
Table 5.10: Example of probabilities of failure for eight wires mix of class “A” and class “B” .....	94
Table 5.11: Details of actual and lifetime values for class “A” and “C” .....	98
Table 6.1: The predicted class of bonds for active power cycling .....	112

## Abbreviations

BJT	Bipolar Junction Transistor
MOSFET	Metal-Oxide Semiconductor Field-Effect Transistor
IGBT	Insulated Gate Bipolar Transistor
CTE	Thermal Expansion Coefficient
DBC	Direct Diffusion Bonding of Copper
Al	Aluminium
EBSD	Electron Backscatter Diffraction
MTBF	Mean Time between Failures
POF	Physics of Failure
CT	Computed Tomography
PZT	Lead Zirconate Titanate
FFT	Fast Fourier Transform
PCA	Principal Component Analysis
ANN	Artificial Neural Network
PLL	Phase Locked Loop
RMS	Root Mean Square
LDA	Linear Discriminant Analysis
SVM	Support Vector Machines
TSVMs	Transductive Support Vector Machines
EM	Expectation-Maximization
SDA	Semi-supervised Discriminant Analysis
US	Ultrasonic
TD	Touch-Down
NCTF	Number of Cycle to Failure
ANOVA	Analysis of Variance
SEM	Scanning Electron Microscope
IR	Infrared
$d_f$	Degree of freedom
SS	Sum of squares
MS	Mean squares
F-ratio	A ratio of mean squares
P-value	Probability more than F-value

## Nomenclature

$X$	Labelled samples
$Y$	Unlabelled samples
$m_i$	Label
$K$	Dimension of feature vectors
$w^*$	Optimum projection vector
$w$	Projection vector
$C_b$	Between-class scatter matrix
$C_w$	Within-class scatter matrix
$C_t$	Total scatter matrix
$\lambda$	Eigenvalue
$W$	Weight matrix
$X_{m_i}$	Number of labelled samples in class $m_i$
$Y_p(n_i)$	The set of $p$ nearest neighbours of $n_i$
$J(w)$	Regularizer
$L$	Laplacian matrix
$D$	Diagonal matrix
$\alpha$	Parameter that controls the trade-off between model complexity and empirical loss
$n_0$	Minimum sample size
$Z$	The abscissa of the normal curve
$p$	Maximum variability
$d$	Margin of error
$N$	Total number of bonds
$n_A$	Number of bonds in class “A”
$n_B$	Number of bonds in class “B”
$n_C$	Number of bonds in class “C”
$P_A$	Probabilities of failure for each bond in class “A”
$P_B$	Probabilities of failure for each bond in class “B”
$P_C$	Probabilities of failure for each bond in class “C”

# **Chapter 1      Introduction**

This chapter presents a brief introduction to power electronic modules and their important role in a wide range of applications such as transport and renewable power generation and transmission. Then, the assembly structure and important packaging materials of a typical power electronic module is described. Thermomechanical fatigue is identified as a key driver for module failure and in particular the bond wires responsible for electrical interconnect to the top surface of the semiconductor dies. Variability in the quality of the wire bonding process is identified as a major concern as it will lead to variable product life. Techniques for determining the quality of bonded wires during bonding are discussed and the importance of being able to generate on-line, non-destructive predictions of individual wire bond life identified. Then, the contributions objectives of this thesis are discussed and finally the contents of each chapter are summarised.

## **1.1.   Overview and Motivation**

Global energy generation has increased significantly over recent decades [1]. According to a recent global status report, fossil fuels are the

world's major energy source (82%) (see Fig. 1.1)[2]. However, over-reliance of fossil fuels in order to meet the demand for energy leads to serious environmental and human health concerns. Furthermore, fossil fuels are not renewable and will run out one day. Therefore, future energy generation will progress with growing use of alternative energy resources such as wind, wave, solar, biomass, etc. which are renewable, free and environmentally friendly [3].

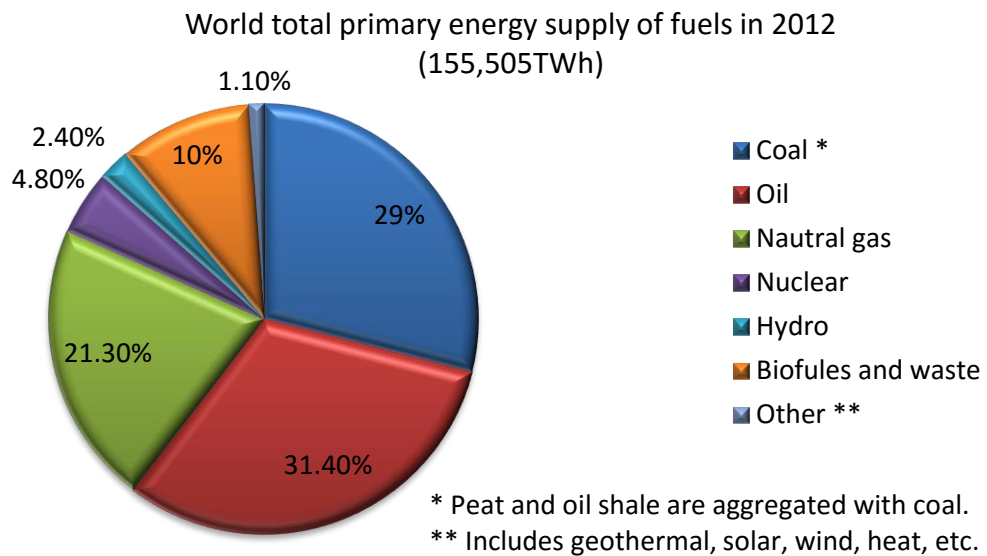


Figure 1.1: World total primary energy supply of fuels in 2012 [2]

The electricity generated from the majority of renewable energy resources cannot be connected directly to the power network [4] and typically, requires power electronics to convert the generated electricity into a form suitable for the grid connection [5]. Power electronics is a fundamental technology in alternative energy resources. Apart from its essential role in renewable energy, power electronics underpins many low-carbon transport and energy technologies, including hybrid and electric, railways and aircraft.

In the last four decades, power electronics has made remarkable progress towards the efficient conversion and more flexible control of energy. However, recent developments in the application of power electronics have highlighted the need for increased reliability in order to have high availability, longer

lifetimes and lower maintenance costs under long time operations and harsh environments.

A key enabling technology for power electronics are power semiconductor devices. Typical power electronic devices can be divided into two groups: 1) two terminal devices such as PiN diodes and Schottky diodes; 2) three terminal devices-switches such as bipolar junction transistor (BJT), metal-oxide semiconductor field-effect transistor (MOSFET), insulated gate bipolar transistor (IGBT) and thyristors. These devices have different voltage and current ratings and switching frequencies. Among these devices the IGBT power module is preferred for many applications as it offers the best compromise between cost, ease of application and performance [6]. Some example of packages is shown in Fig. 1.2).



Figure 1.2: Different type of IGBT modules.

In power IGBT modules various components of different materials with different thermal expansion coefficient (CTE) are connected together. Fig. 1.3 shows an opened module and Fig. 1.4 illustrates a cross-section view of a power electronic module.

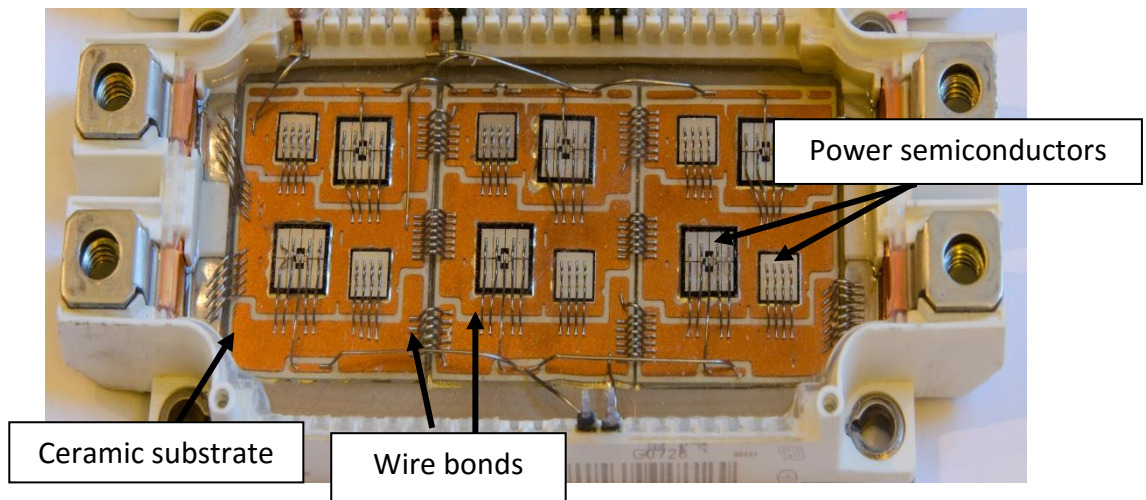


Figure 1.3: A typical IGBT module with baseplate

The main components are copper base plate, ceramic substrate, conductors, semi-conductors and the wire bonds. The entire module is encapsulated with silicone gel, closed with a lid and finally screwed to a heat sink. For better thermal transfer from the module to the heat sink a thin layer of thermal interface material is used (see Fig. 1.4). The manufacturing line of power electronic modules requires different assembly processes such as soldering, ultrasonic wire bonding, direct, diffusion-bonding of copper (DBC).



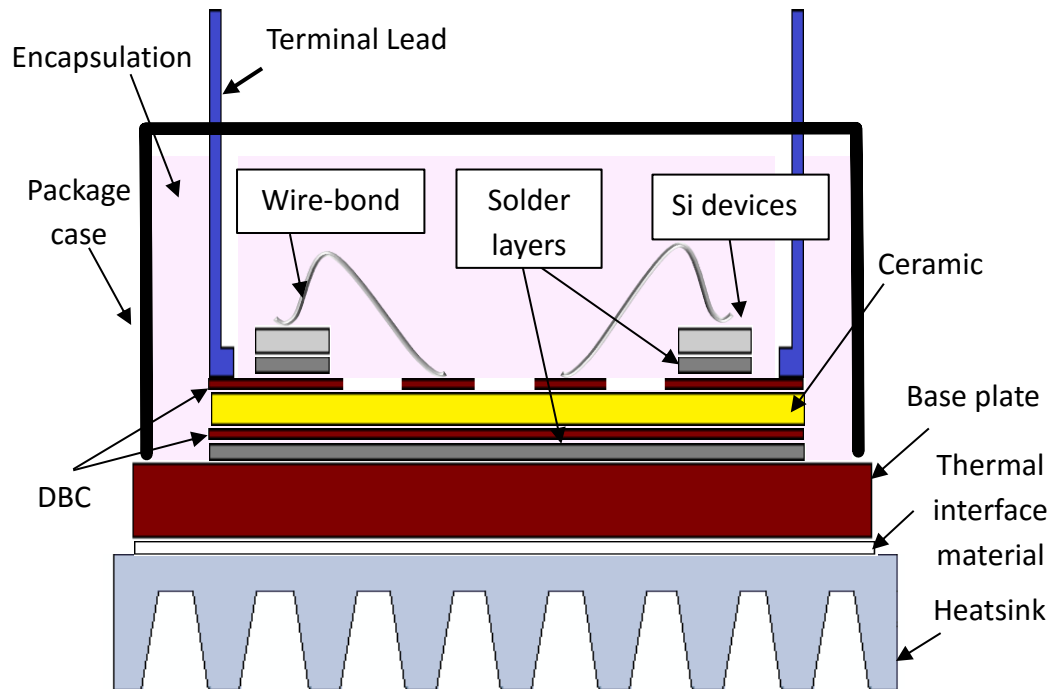


Figure 1.4: Cross-section view of power IGBT module package

Under operational conditions, power electronic modules dissipate heat and this result in variations in temperature in the various material layers. Differences in thermal expansion coefficients of the different constituents cause the materials to expand and contract at different rates leading to the generation of mechanical stresses [7]. Thermomechanical load cycles can lead to degradation and failure of the interconnections such as the wire bonds and solder joints and finally whole modules. For a high service life of the module, the connections within the modules must be robust and reliable. Therefore it is important for power electronic packaging manufacturers to address the reliability issues at the design stage and on the manufacturing line [8].

Wire bond lift-off and bond heel cracking are often considered the most important factors in power electronic module reliability. Wire bonding is a standard technology that provides electrical contact for the power semiconductor devices. In this process, in order to facilitate uniform current

distribution in the power semiconductor devices and so as not exceed the current carrying capacity of the wire, a number of wires are bonded in parallel (see Fig. 1.5).

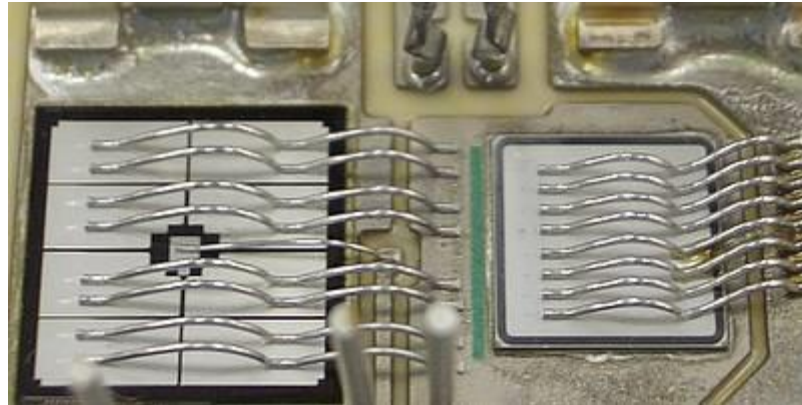


Figure 1.5: Aluminium (Al) thick wire bonds on IGBT and diode in a power module

Power semiconductor devices function as switches. During operation, these devices switch on and off in milliseconds causing losses which are generated by switching and conduction. These losses produce heat; therefore, wire bonds are subjected to temperature swings as they are on the active area of the Si devices. Cracks initiate at the boundaries of bonded area (extreme edges) due to thermo-mechanical stress then develop towards the bond centre (see Fig. 1.6). When the cracks reach the centre the bond lifts off, and the current density of the remaining attached wires increases. Changes in current density of the wires may cause a non-uniform current distribution within the chip leading to a change in temperature distribution. The rate of degradation mechanisms may subsequently increase because of the change in temperature distribution. Therefore, the quality of each single wire bond is important, since a single defect in one of the wire bonds might result in rapid failure of the device, the power module and the whole system.

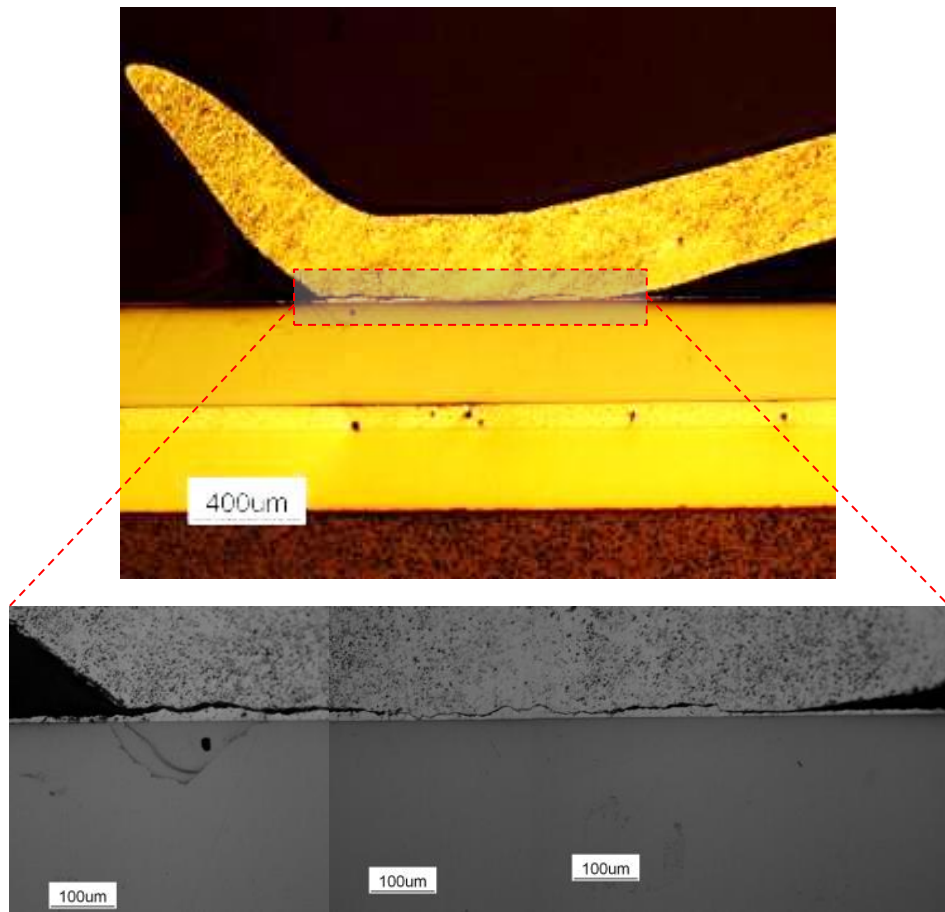


Figure 1.6: A cross-section view of Al wire showing cracks propagation during cycling

On the manufacturing line, the strength of wire bonds is usually evaluated by shear and pull tests, normally as a pre-treatment method at the start-up of production. The average value of the bond strength of a small number of sacrificial bonds indicates that the process can be started or needs further actions. However, both shear and pull test are reported as not being able to adequately judge bond strength efficiently can be more an indication of the mechanical properties of wires rather than the quality of bonded wire [9]. Furthermore, both tests are destructive and the scarified bonds cannot be evaluated over their entire lifetime. For example, a sample tile taken from the manufacturing line and subjected to thermal cycling test from  $-55$  to  $+125^{\circ}\text{C}$  may typically show a variation in wire bond lifetime from 1000 cycles to 2200 cycles as illustrated in Fig. 1.7.

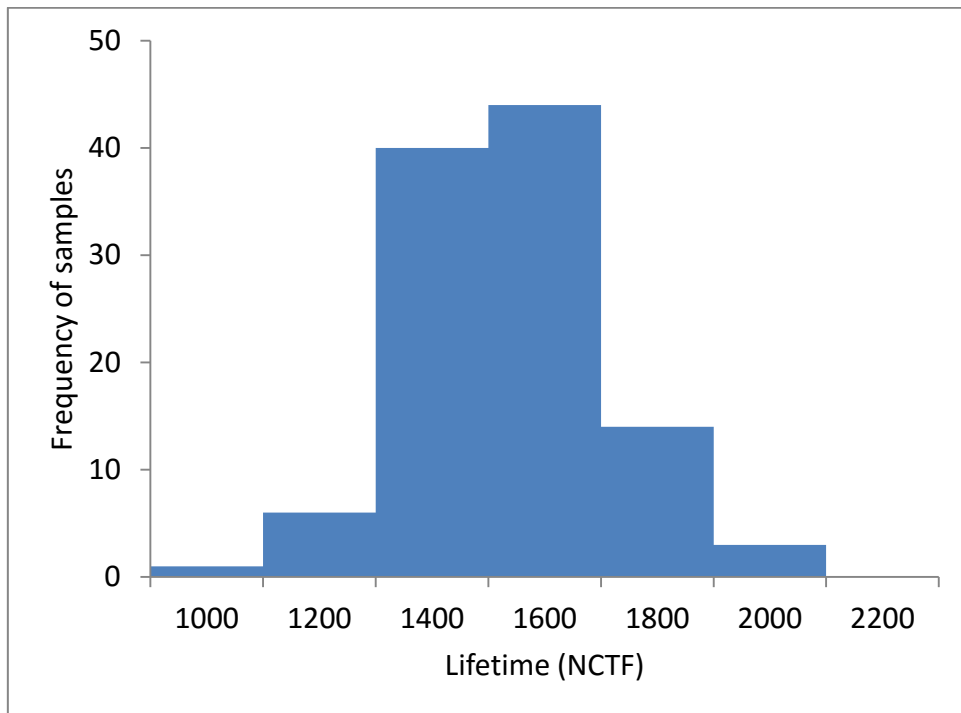


Figure 1.7: Lifetime variation of wire bonds subjected to passive thermal cycling

Consequently, the development and improvement of techniques for the on-line evaluation of bond quality and early detection of defects has been a topic of interest for many years.

## 1.2. Contributions

In general, the need to extract reliable, real-time information and analysis during the wire bonding process can be summarized as follows: 1) It can be used as a pre-treatment method in the start-up of production, so that faults or abnormalities in the wire bonding process can be detected at the onset; 2) The production line can be optimized through on-line analysis. If the wire bonding system makes weak bonds continuously then the operator can detect the abnormality and stop the production. 3) Production processes can be streamlined to identify varying bond quality to efficiently screen substrates and modules.

So far, there have been several attempts by researchers to obtain quality information without sacrificing wires and with different degrees of success. These include characterization of bond signals obtained from the ultrasonic generator [10, 11] and measurement of bond tool tip vibration with a laser vibro-meter and or sensor attached to the transducer [12-14]. Although a number of these methods are able to discriminate bond quality (i.e. “strong” and “weak” bonds) [12, 15], none have shown the ability to resolve subtle quality differences as might happen within a production batch as a result of wear-out in bonding tools, calibration issues, human factors, environmental factors, bond surface quality in terms of cleanliness, etc. Furthermore, none of these have shown capable of predicting the resulting individual wire bond lifetime.

The purpose of this research project has therefore been to develop and improve existing methods for on-line assessment of bond quality with the target of being able to predict wire bond lifetime from its initial condition and in real time.

The research objectives are detailed as follows:

1. To develop a methodology for detecting subtle quality differences in bond quality using signals obtained from ultrasonic generator and directly links there quality with actual lifetimes.
2. To improve understanding of wire bonding process by observing the effect of the complex interaction of bonding parameters.
3. To evaluate the initial bond quality and through its lifetime using a non-destructive tool instead of destructive characterization methods such as shear test.
4. To estimate module lifetime from wire bond process data.
5. To improve understanding of the effect of substrate/ Silicon device cleanliness prior wire bonding.
6. To provide uncertainty information in development of wire bond lifetime models to address some user needs.

### **1.3. Thesis Structure**

The thesis is organized as follows:

Chapter 2 reports on background studies for this thesis. The bonding process is briefly introduced. Then, failure mechanism and a review of wire bond evaluation techniques is presented. This chapter ends with details of previous works on on-line wire bond quality monitoring techniques.

In Chapter 3, the non-destructive technique for on-line quality assessment of the wire bonding process is presented. This chapter is divided into three sections. In the first section, the wire bonding equipment used in this work is introduced. Then, in the second section, the non-destructive method of observing Al wire bonds in initial condition and over its lifetime by 3D x-ray tomography is given. Finally, the details background of the semi-supervised algorithm used in this thesis is described.

In Chapter 4, the importance of optimization of the wire bonding process parameters prior to wire bonding is studied. Five important process parameters are selected at five levels and the reliability of the bended wires is investigated under passive thermal cycling. In addition, the change in electrical signals obtained from the ultrasonic generator is observed as a result of changes in the bonding parameters.

In Chapter 5, the technique presented in Chapter 3 is employed for predicting the in-service life-time of bonded wires by using samples produced using the optimized bonding parameter described in Chapter 4. The quality of bonded wire is predicted, and then the predicted result is compared with the actual lifetime data. Finally, the bond degradation rate and model performance for different surface treatments is given.

In Chapter 6, the model classifier that is built in Chapter 5 is used for predicting class of a few samples which are subjected to active power cycling tests. The predicted results are compared with actual lifetime data.

In Chapter 7, conclusions and future works for the on-line assessment technique are discussed.

#### 1.4. List of Publications

A list of publications arise from this work is provided below.

- **E. Arjmand**, P. A. Agyakwa, Martin R Corfield, Jianfeng Li, C. M.Johnson, Predicting lifetime of thick Al wire bonds using signals obtained from ultrasonic generator, IEEE transactions on Components, Packaging and Manufacturing Technology, 2016.
- **E. Arjmand**, P. A. Agyakwa, Martin R Corfield, Jianfeng Li, Bassem Mouawad, C.M.Johnson, A thermal cycling reliability study of ultrasonically bonded copper wires, Microelectronic Reliability( special issue), 2016.
- P. A. Agyakwa, Li Yang, **E. Arjmand**, Paul Evans, Martin R Corfield, C.M.Johnson, Damage evolution in Al wire bonds subjected to a small-scale junction temperature fluctuation of 30 K, Journal of Electronic Materials, 2016.
- **E. Arjmand**, P. A. Agyakwa, C. M.Johnson, Reliability of thick Al wire: A study of the effects of wire bonding parameters on thermal cycling degradation rate using non-destructive methods, Microelectronic Reliability, 2014.
- **E. Arjmand**, C.M.Johnson, P. A. Agyakwa, Methodology for Identifying Wire Bond Process Quality Variation Using Ultrasonic Current Frequency Spectrum, “15th European Conference on Power Electronics and Applications” France, 2013.

# **Chapter 2      Background and Literature Review**

This chapter describes the background studies for this thesis. Firstly, a detailed description of the wire bonding process is presented. Then, wire bond failure mechanisms and the evaluation techniques for the wire bonding process are reviewed, including details on on-line quality monitoring techniques.

## **2.1.    Wire Bonding Technology**

Wire bonding is a standard technology for providing electrical interconnection between semiconductor chips and relative metal pads on substrates or lead frames [16]. Literally billions of wires are bonded every year for use in electronic devices, including power electronic modules. Aluminium (Al) wedge bonding is typically used in power modules.



The purpose of the wire bonding process is to make a continuous metallurgical attachment between the wire and bonding surface. According to the energy source and force used during bonding, the wire bonding technology can be divided into three categories: 1) thermo-compression ball bonding, 2) thermo-sonic ball bonding and 3) ultrasonic wedge bonding. Thermo-compression and thermo-sonic ball bonding are not related here as this work is concerned with ultrasonic wedge bonding.

## **2.2. Ultrasonic Wedge Bonding**

Ultrasonic bonding is the most common technology used for Al wire and is the most commonly used technique for making electrical contacts on the semiconductor chip in power electronics applications.

### **2.2.1. Ultrasonic Wedge Wire Bonder**

A typical ultrasonic wedge bonder consists of an ultrasonic generator and a bond-head. The main constituents of the bond-head are a transducer (piezoelectric driver), which converts the ultrasonic signals into mechanical oscillation, a voice coil motor, the bond tool (wedge), a touch-down sensor, a wire guide and cutter (see Fig. 2.1).

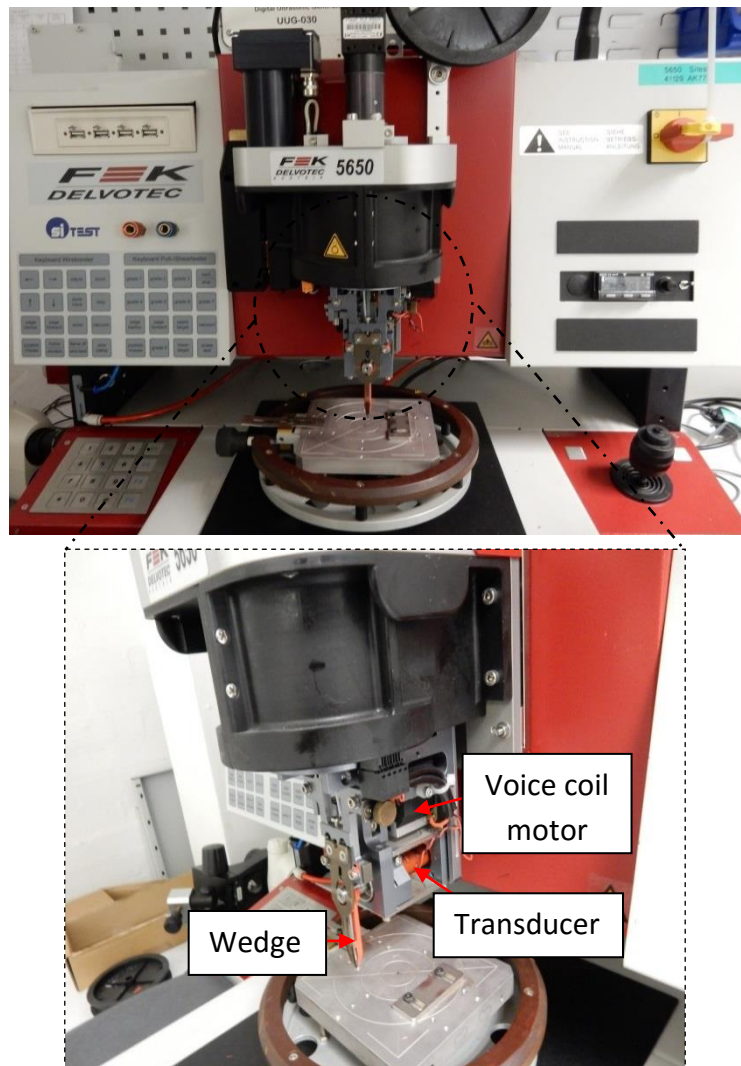


Figure 2.1: Ultrasonic wedge-wedge wire bonder

### 2.2.2. Ultrasonic Wedge Wire Bonding Process

Fig. 2.2 illustrates the steps in wedge-wedge ultrasonic bonding. In the first bond, bonding tool moves down to the programmed bond position in contact with silicon device. Bond forces coupled with ultrasonic waves are applied during bonding time through the bonding tool. During the bonding process, bond wire is attached to the bond pad by interfacial motion (scrubbing) upon first application of ultrasonic energy that results some cleaning action [17]. The scrubbing motion breaks up surface oxide, exposes a fresh surface and promotes intimate contact between the pad and bonding wire. Non-optimum

bonding parameters may however leave residual surface oxide [18, 19]. The ultrasonic energy absorbed by the wire significantly reduces its deformation stress, allowing plastic flow to occur at the interfaces and a metallurgical bond to form [20]; the softening achieved can be equivalent to that achievable by heating the wire to several hundreds of degrees Celsius [20-22]. After creating the first bond between the wire and pad/substrate, then the tool moves the wire to form a loop, ending at the next bond pad. In this step, the bond head again brings the wire into contact with defined force, and ultrasonically welds the second bond onto the surface. Finally the bond head moves up slightly to cut the wire.

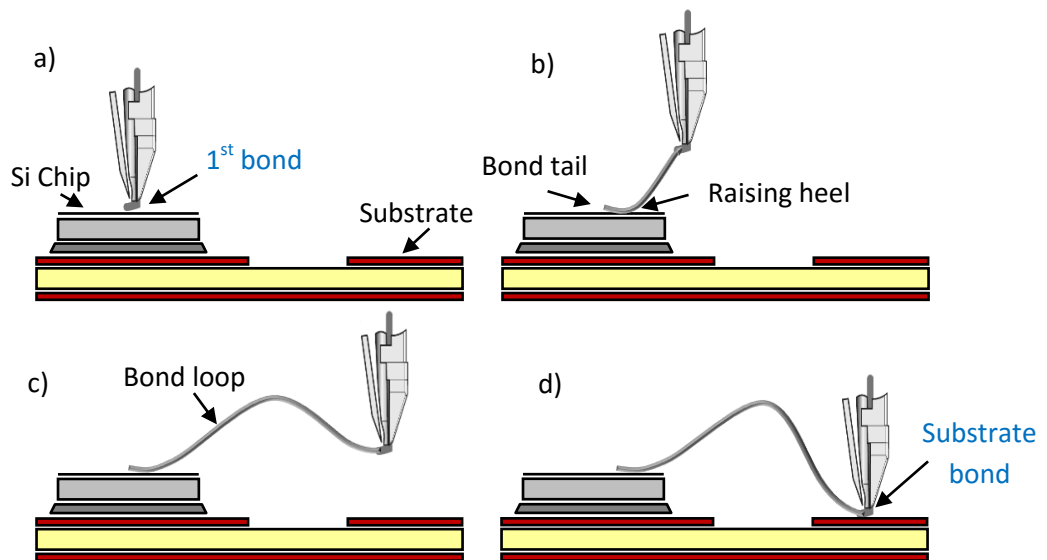


Figure 2.2: Ultrasonic wedge bonding process a) the starting point and bonding first bond, b) wire bond looping process c) end of looping process, d) the ending point and bonding second bond

In the ultrasonic wedge bonding process, ultrasonic power is an important factor. During the formation of a bond, the piezoelectric driver converts electrical signal into mechanical oscillation/vibration. The vibration is amplified to a larger value at the tip. This results in an oscillatory motion and force parallel to the bond pad and the bond interface.

### **2.3. Wire Bonding Process Variation and Process Parameters Optimization**

The quality/strength of a bond depends on various parameters, such as the capability of wire bonder, wear-out of bonding tools, calibration issues, human factors, environmental factors, wire bonding set-up parameters, bonding temperature and bond pad cleanliness. These above factors can directly impact on ultimate quality of each single bond[23].

Assuming that the wire bonder is capable of make reliable bonds repeatedly, and that there are no calibration issues, no wear-out in bonding tools, no human errors or environmental issues, it is still important to use optimised bonding process parameters, as they control bond wire quality and reliability [24-26]. A number of studies have found that inappropriate bonding parameters can deform the bonds extensively resulting very thin and weak heels that can be broken easily [27]. Poor loop settings and bond head movements can subject the wire to excessive stresses resulting heel cracks and weakly adhered bonds [27]. According to Schafer et al. [28], Pufall [29] and Satianrangsarith et al .[24], ultrasonic power, bonding force and time are key bonding process parameters. Several attempts have been made to optimize these parameters to reduce wire bonding process variation and improve the quality of the wire bonding process. One popular methodology often used is Design of Experiments (DoE) [24, 26, 30-32]. However, these have not investigated in sufficient details considering the complex interaction between parameters. In addition, even if the bonding parameters are identical and optimized the bond quality could considerably vary due to other source of variation that cannot be recognize so easily.

### **2.4. Wire bonding Failure Mechanisms**

In power electronic modules reliability, understanding the wire bonding process and reliability and robustness of wire bonds is an important issue for

development of power electronic technology and manufacturing line optimization.

As mentioned earlier, the degradation of the bond interface occurs due to repeated heating and cooling during switching of the devices results in thermo-mechanical strains because of the mismatch of thermal expansion coefficients (CTE) between the Al bonding wire and the silicon chip at the interface (see Fig. 2.3). This thermo-mechanical loading leads to the initiation of cracks and the propagation of new and pre-existing micro cracks.

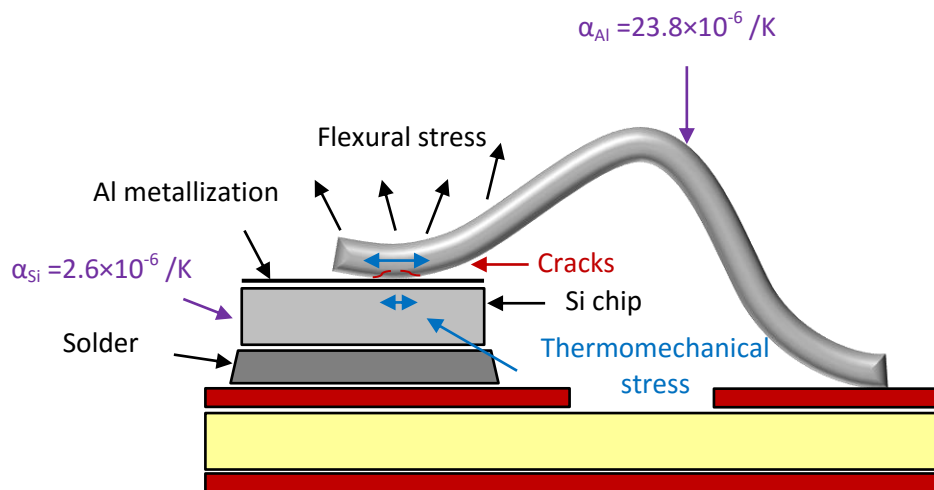


Figure 2.3: Schematic diagram of Al wire bond experiencing different stress during operation

The cracks/ micro voids propagate from the bond heel and toe towards middle of bonds until complete wire lift-off. The cracks and voids usually occur at the interface, and may be brought about by the presence of extraneous particles and oxides. [33]. The crack paths are typically 10-20 $\mu$ m above the interface. Microstructure analysis of bonded wire shows small Al grains just above interface and large grain of Al within the bulk wire. The fine grain layer is harder than large grain layer, so the weakest region may be at the boundary between these two grain sizes (see Fig. 2.4) [34].

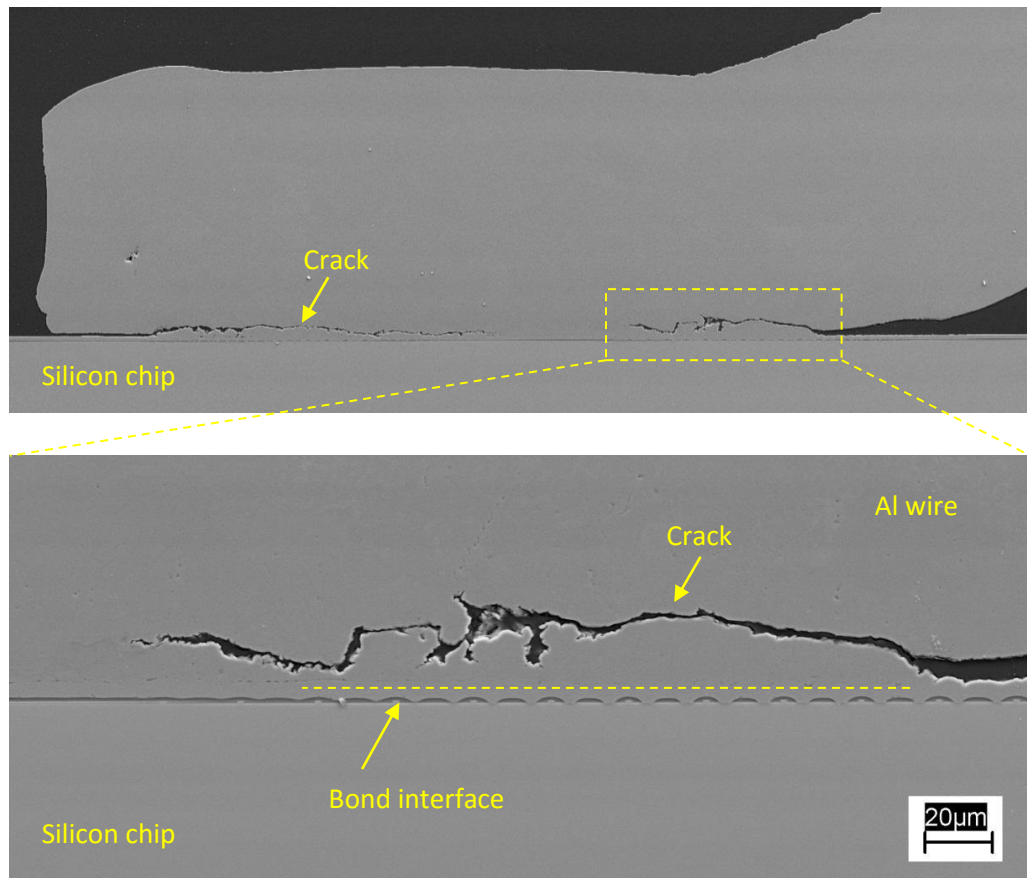


Figure 2.4: Cross-section of Al wire bond showing crack grows 10-20  $\mu\text{m}$  above the bond interface[34]

A footprint study of lifted wires confirmed that the weakest part of the interface is between grain sizes, as layers of Al remained on the bond pad [17] (see Fig. 2.5). This has also been confirmed by hardness and electron backscatter diffraction (EBSD) investigations by [35, 36]. The EBSD images revealed that recrystallization and grain growth continue during thermal cycling (see Fig. 2.6). In the as-bonded condition (zero cycles), the Al wire bonds show fine grained and highly deformed structure, but after thermal treatment, the grains coarsen considerably [36-39].



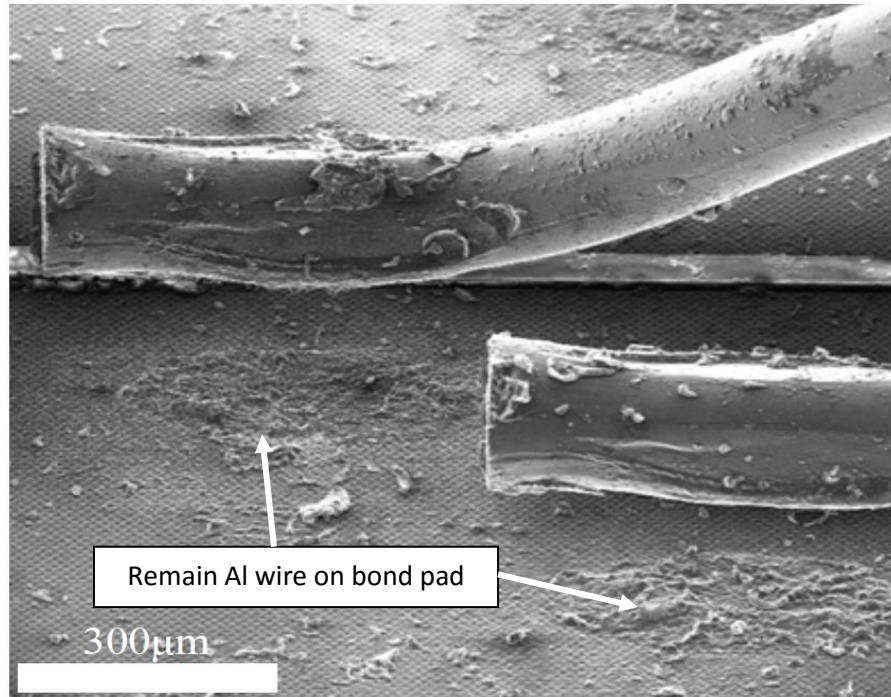


Figure 2.5: SEM image of Al wire lift-off a) remain Al wire on bond pad, b) Al wire [40]

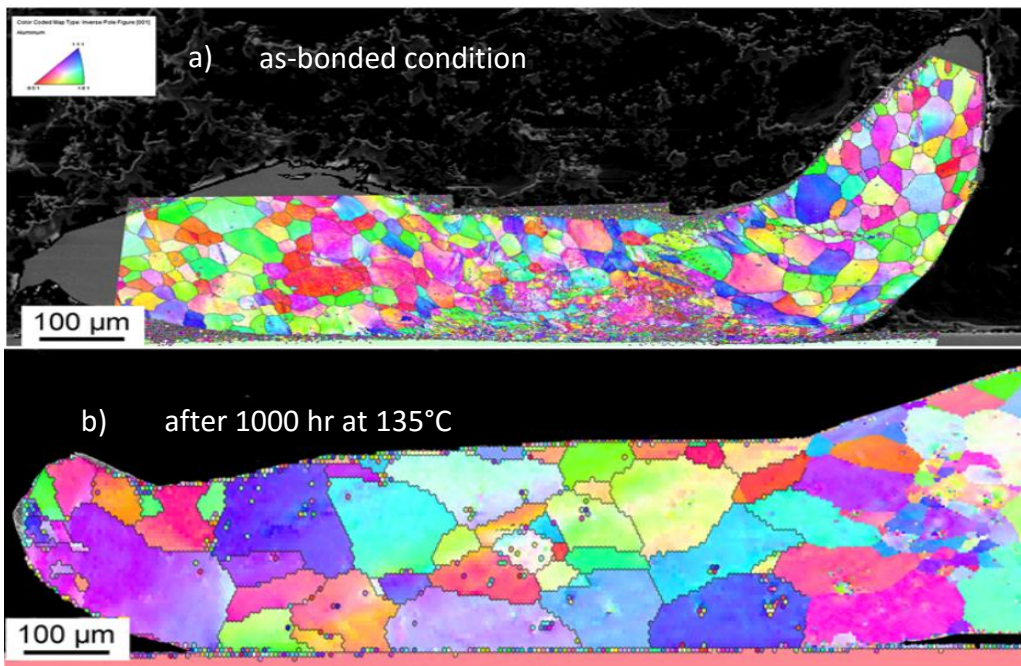


Figure 2.6: EBSD images of Al wire bond in a) as-bonded condition and b) after 1000hr at 135°C[36]

Compared to wire bond lift-off, heel cracking rarely occurs in power electronic modules. When it does occur, it is often under harsh operation conditions especially where the bond loop geometry has not been optimized [41]. Heel cracking is caused by mechanical bending stress where the bond wire expands and contracts in a cyclical way during operation. The temperature fluctuation generates displacement at the upper side of bond wire in the heel which leads mechanical bending stress at this region [22, 35, 41] (see Fig. 2.7).

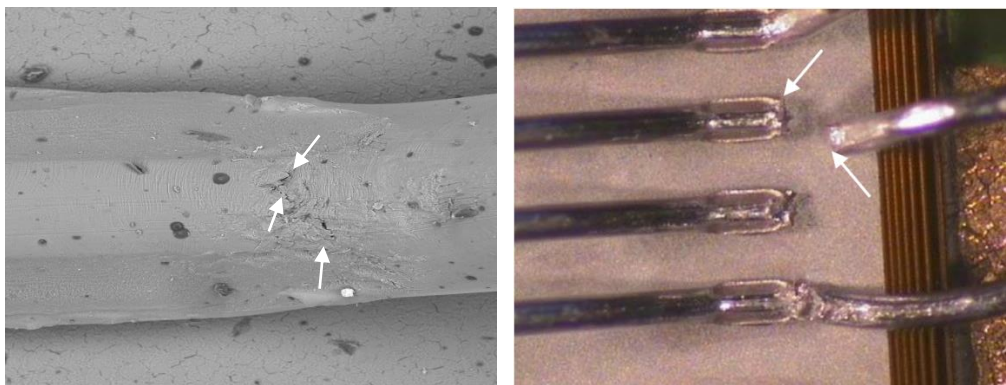


Figure 2.7: Heel crack in heavy Al wire bonding 1) SEM image of observed heel crack after active power cycling 2) Heel crack through bonded wires [34]

The lifetime of Al wire bonds can be enhanced by increasing the Al grain size above bond interface by annealing [33, 38]. The other solution is to provide clean bond pad surface and remove any contamination prior to wire bonding. Using plasma cleaning before bonding provides the best wire bond quality in order to achieve highest reliability [42-45].

Another solution is using an organic coating onto the wire intended to promote better contact even with large cracks [25, 46]. A few studies suggest that using glop-top can reduce the stress in wire bonds and improve the reliability [47, 48].



## 2.5. Wire Bond Reliability Assessment and Lifetime Prediction

Reliability assessment and lifetime prediction of power electronic modules have long been a concern, in order to produce reliable and competitive product and reduce maintenance costs. US MIL-HDBK-217 [49], Bellcore TR-NWT-000332 [50] and Siemens Standard SN29500 [51] are traditionally used to predict the reliability of components/devices [52]. Among these, US MIL-HDBK-217 is the most commonly used handbook for estimating reliability of semiconductor devices, and is based on determining the mean time between failures (MTBF). MTBF measures the operating time, typically years or hours, until a device fails. These methods, however, suffer from a number of serious flaws. These are based on statistical analysis of historical failure data and the actual cause of failures is unknown [35, 53].

In contrast to these traditional lifetime prediction methods, physics of failure (PoF) methods offer better accuracy as they are based on understanding the critical failure modes [54]. The aim of PoF methods is to understand and identify the cause and mechanism of failure at an accelerated rate. This approach provides more realistic estimation of reliability compared to traditional predictive methods and requires less time [55].

One of the common lifetime prediction models for wire bonds is the Coffin-Manson model. The basic form of the model is based only on the temperature swing  $\Delta T_j$  (see Eq. 2.1) and does not consider important parameters such as frequency of cycles, heating and cooling times, etc. [56]. Another form of the Coffin-Manson model deals with these parameters by incorporating the mean temperature  $T_m$  using Arrhenius term (see Eq. 2.2) [57, 58].

$$N_f = \beta (\Delta T)^\alpha \tag{2.1}$$

$$N_f = \beta (\Delta T)^\alpha \exp\left\{\frac{E_A}{K_B T_m}\right\} \tag{2.2}$$

Where,  $N_f$  is number of cycle to failure,  $\alpha$  and  $\beta$  are fitting parameters and  $E_A$  is activation energy. The model parameters are often estimated by numerical simulation. However, they are provided by experimental measurements on thermal or power cycling accelerated tests. Other modifications of the Coffin-Manson based include the Norris-Landzberg model [59, 60] and the Bayerer model [61].

The above models have been shown to represent wire bond degradation behaviour under certain conditions. However, still there are some issues with using these models in prediction of wire bonds lifetime:

- Most of models do not consider the effect of different materials with different geometry such as wire type and wire diameter. It has been demonstrated that different wire diameter results different bond bonded area which directly effect on the bond lifetime [40, 62].
- The value of  $\Delta T$  is regardless of the temperature range, while the degradation behaviour in wire bonds are reported to be different in different temperature range with the same  $\Delta T$  [63].
- Most models are based on deterministic data; however, failure is probabilistic and uncertainty arises from the inherent quality differences which exist in a normal wire bonding process [57].
- The experimental data from which the models are derived are based measuring shear/pull strength, as these decrease with decreasing the bond bonded area during accelerated cycling test. However, the change in bond strength may also because of the change in the yield strength of materials [64].

So far, this indicates a need to find a way to address these issues and uncertainties to include into the model. In next part, a background of wire bond's quality evaluation methods is discussed.

## 2.6. Wire Bonding Characterization/Evaluation

The standard for wire bonding evaluation varies depending on the application specifications. Assessing the quality of bonded wires can be grouped into two categories of visual test and random sampling mechanical tests for evaluating bond strength. In next sub-sections, a brief review of bond evaluation techniques is given.

### 2.6.1. Wire Bond Pull Test

The pull test is a common method for determining wire bonding quality. Several papers have been proposed on this subject and test methods and validation are given [65-67].

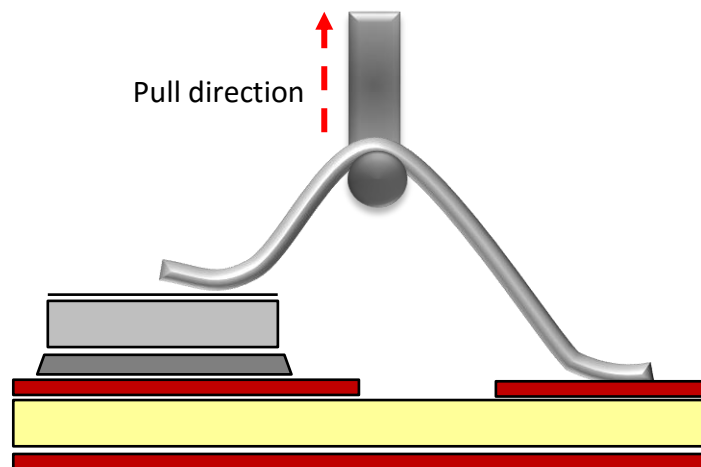


Figure 2.8: wire bond pull test

Basically, the pull test consists of pulling on the loop of the wire with a hook by increasing the force until it breaks. It can be performed non-destructively only on wedge bonds (see Fig. 2.8). In this case, the maximum applied force is limited and can be done for all bonded wires but it is important to note that it will remove weak bonds. Several studies have reported that there are some issues with using pull test for evaluating bond quality [66, 68-70]. Herman et

al. has indicated that the result of a pull test is depended on the position of hook and the pull angle [68]. Sundararaman et al. reported the stress distribution under the bond pad is depended on the angle of the pull hook [69]. Herman et al. and Petch et al. have observed that the elongation of the wire has an impact on the result of pull test [70]. Also, it has been suggested that the common pull test is incapable of determining the true value of bond strength as the bonded wire breaks at a weak point [22] and it may also merely give a measure of the mechanical properties of the wire, which may not be related to the actual strength of the bond being evaluated [71].

### 2.6.2. Wire Bond Shear Test

The shear test uses a probe which applies a horizontal force to the wire bond to push it off. Fig. 2.9 shows a schematic of the wedge wire shear test steps. The bond shear test was first introduced by Gill et al. [72, 73]. Then after almost 10 years it was considered by Jellison [74]. The test method and control guidelines for the shear test can be found in MIL-STD-883 [75]. Almost all previous studies that have been written on optimizing process parameters of wire bonding process [24, 26, 30-32], monitoring bond quality [10-12, 14, 29, 76] and reliability assessment and lifetime models[34, 35, 40] used shear test to measure the strength of bonded wires.

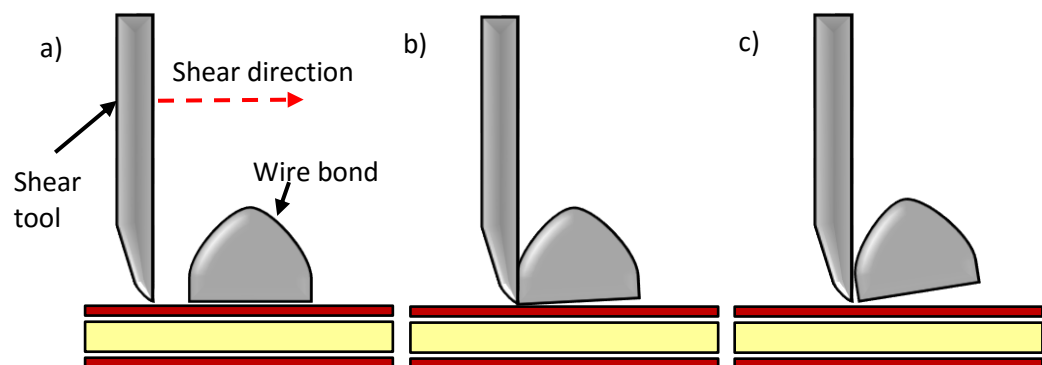


Figure 2.9: Wire bond shear test steps

The reason for using shear tests is that the shear force is a measure of the bonded area and reduces during aging as a result of crack propagation. However, this might not be accurate since the reduction in shear force might be because of a change in yield strength of the wire [9, 63]. Furthermore, the sensitivity of shear testing is very low, therefore, small defects in bond quality differences may not be detected. In addition, incorrect positioning of the shear tool is one of the most pervasive practical problems with shear tests [27].

### **2.6.3. 3D X-Ray Tomography**

X-ray Computed Tomography (CT) is a non-destructive technique for visualising internal features within solid objects and for obtaining 3D measurements of structure. It can be used for a wide range of materials, such as rock, metals, bone, ceramic and also soft tissue. An X-ray tomography microscope consists of an X-ray source, a series of detectors which measure X-ray intensity reduction along multiple beam paths and a rotational sample stage. The X-ray source produces a conic beam of electrons which goes through the sample to be analysed, and then digital signals produce a radiograph image by 2D detector. The object on the stage rotates and images are acquired by the detector at a number of displacements in equally spaced angles. The scan typically covers a rotational span of 360 degrees, but for different applications or sample geometries, the span might be limited. The series of 2D projection images are then reconstructed mathematically to produce a 3D map of the sample (see Fig. 2.10).

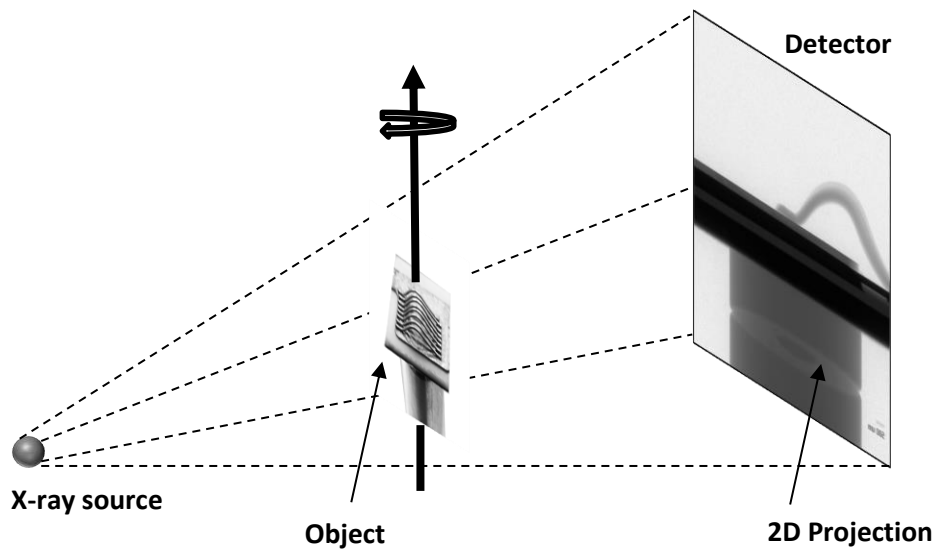


Figure 2.10: Schematic illustration of X-ray tomography

Consequently, it has become a great tool for non-destructive study of a specific sample over its lifetime [77-79]. A recent study by Agyakwa et al. has, for the first time, studied crack development of Al wire bonds during thermal cycling using X-ray tomography [9]. In this study, the condition of an Al wire bond in its initial bonded condition (as-bonded) and at various extents of thermal cycling exposure has been observed three-dimensionally and provides multiple virtual cross-sections a unique view of damage evolution (see Fig. 2.11) [9]. However, it should be noted that only a limited number of bonds can be imaged since it is expensive and time consuming. Secondly, there are some issues and difficulties in imaging of fine features such as crack and voids (1-3 $\mu$ m) in large samples. This is because achieving high resolution images is dependent on the optimal source-sample and detector-sample distances [9].

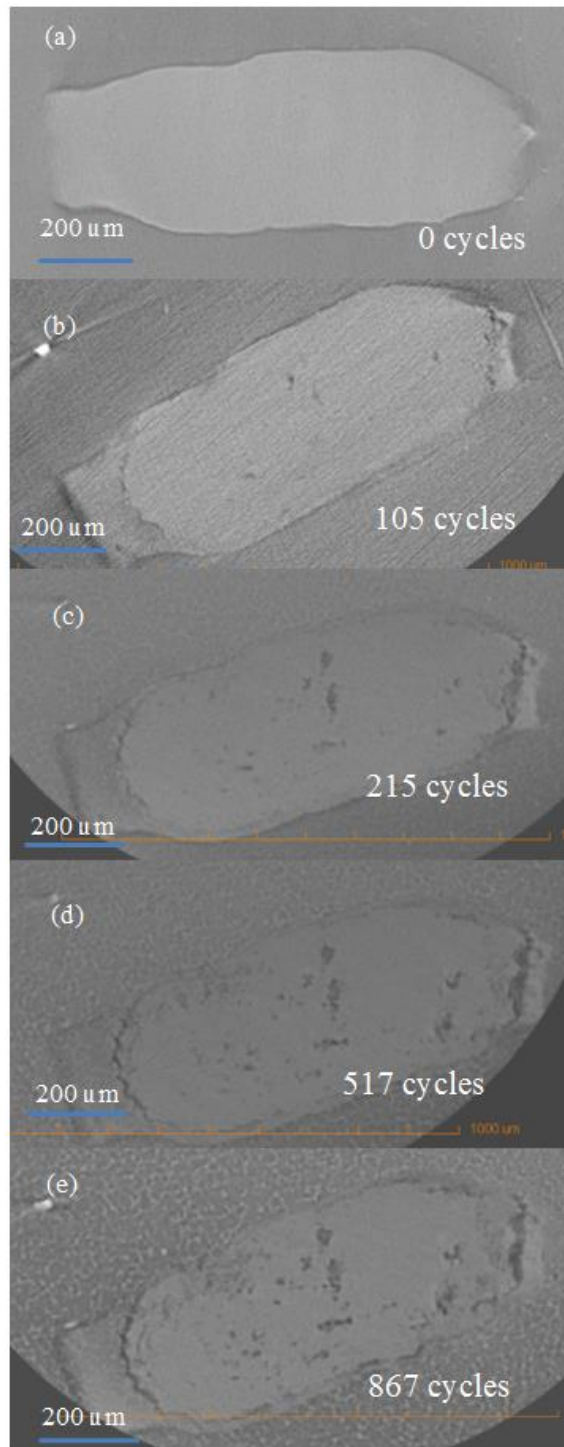


Figure 2.11: Virtual cross-sections in the X-Y plane of the Al wire bond interface in (a) initial bonded condition (b) 105 cycles, (c) 215 cycles, (d) 517 cycles and (e) 867 cycles [9]

## **2.6.4. On-Line Wire Bonding Process Monitoring**

In theory, during the formation of a bond, the electrical impedance and resonant frequency of the ultrasonic system are affected by the condition of the wire bond interface. Therefore, any changes in boundary condition at the tip, such as changes in the mechanical properties of the material at the interface, lead to change in the electrical signals of the ultrasonic generator. The signal at the transducer will directly reflect this change by the electromechanical coupling effect [12, 13]. In other words, bond quality information is inherent within the signals. To date, several approaches have been applied to extract this inherent quality information. These methodologies can be categorized into three major groups based on the principle of monitoring as follows:

### **2.6.4.1. Measuring Vibration by Attaching Additional Piezoelectric (PZT) Sensor**

Over the years, a number of researchers have measured the vibration amplitude of the tip during wire bonding by attaching an additional PZT sensor. Pufall [29] attached a piezo-ceramic sensor to the horn of the bond arm to measure the amplitude of the ultrasound. The presented work identified patterns in the 2<sup>nd</sup> harmonic signals using Fast Fourier transform (FFT) analysis. As it can be seen in Fig. 2.12, the good bond waveform is more stable in receiving power than the poor quality bond and/ or the non-sticking bond. He reported that the 2<sup>nd</sup> harmonic of the horn vibration could be monitored as an indicator of bond quality. However, this work investigated only extremes of bond quality, i.e. different surfaces and has not yet been investigated for normal wire bonding conditions.



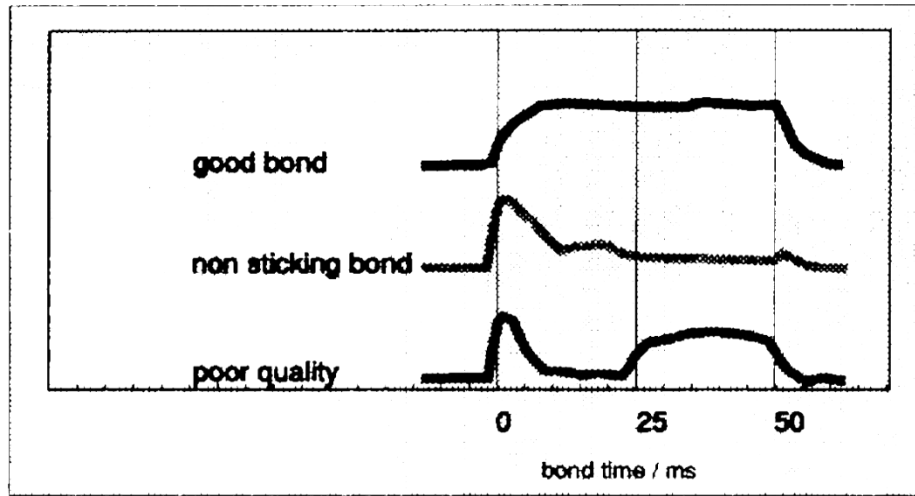


Figure 2.12: Amplitude of 2<sup>nd</sup> harmonic of signal in different bonding conditions [29]

Or et al. [10, 11] also measured the mechanical vibrations of bonder horn and observed the 2<sup>nd</sup> harmonic of ultrasonic (US) signal via a piezoelectric sensor on transducer. They discovered a linear correlation between shear strength and the ratio of the steady-state amplitude to the peak value of 2<sup>nd</sup> harmonic (see Fig. 2.13), thus, allowing shear strength to be predicted from the above signal characteristics. However, further development of this approach to minimize the spread in predicted shear force values would be beneficial.

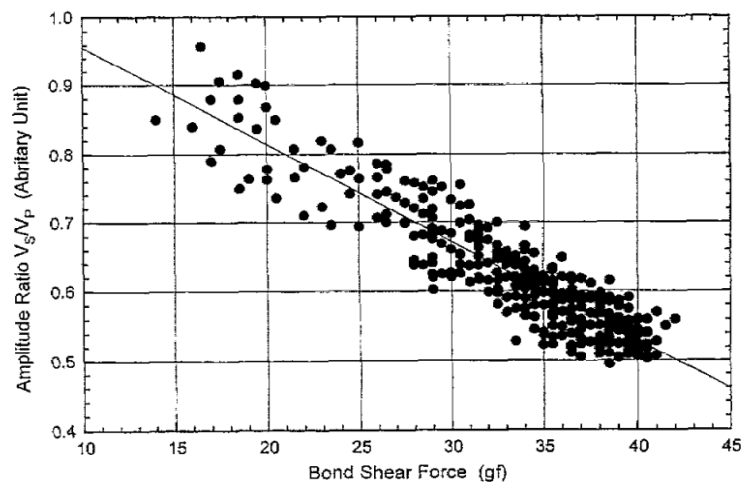


Figure 2.13: Predicted shear strength using the ratio of the steady-state amplitude to the peak value of 2<sup>nd</sup> harmonic [11]

Later, Chu et al. [80] placed a PZT ring in the middle of driver of a wire bonder transducer to monitor bond quality during wire bonding. They made different type of bonds, such as good bonds, peeled-off bonds, non-stick bonds and bonding without wire. The normalized sensor signal clearly showed differences for the different conditions. However, this method has not yet been properly validated under normal bonding conditions.

All these sensor-based studies so far, however, are not suitable for on-line monitoring as the properties of the transducer are altered by the attached sensors [76].

#### **2.6.4.2. Measuring Vibration Amplitude by Using Vibro-meter**

As mentioned earlier, the vibrational amplitude of the wedge tip corresponds directly with the bonding process. Zhong et al. [81] and Gaul et al. [82] have measured this signal using laser interferometry, to observe any slight changes in the resonant frequency of the system.

However, this approach suffers from a couple of limitations. One is that it requires additional space and it is sensitive to external disturbance. Furthermore, it is not cost effective.

#### **2.6.4.3. Measuring Signal Obtained from Ultrasonic Generator**

J. L. Landes [83] evaluated the amount of energy passing through the package by measuring electrical impedance of the transducer. The method is able to turn the bonding tool on or off based on the second derivatives of the impedance. Perhaps one of the disadvantages of the presented method is that it is just sensitive to determine two bonding conditions, first when there is no wire and second when the tool is not in contact with the wire.

In 1982, Chan et al. [84] measured the current envelope of ultrasonic signals. They used a rule-based analysis of some parameters of the current envelope to control power of ultrasonic transducer for the automatic evaluation of bonded

wires, and were able to discriminate between ‘good’ and ‘bad’ bonds. One of the weaknesses of this method, however, is the limited number of rules which might not be accurate/ appropriate over a wider range of bonding conditions.

Broekelmann et al. [85] used two sensing techniques for evaluating wire bonding process. The presented process feedback at the wedge tip showed that good sensing technique can be achieved by either signals obtained from ultrasonic generator and integrated sensor within transducer. However, further works required to investigations the potential of monitoring in real time under normal operating conditions.

Recently, in order to determine the link between obtained ultrasonic signals and wire bond quality, Feng et al. [12, 14] have presented a sensor-less technique for on-line quality detection of wire bonding process. This involved the extraction of waveform features from the electrical signals of the ultrasonic generator. During the bonding process, a measuring circuit was set up to record both current and voltage of bonds of different qualities, and features were extracted from three phase of the signals’ envelopes, after which the bonded wires were sheared (see Fig. 2.14).

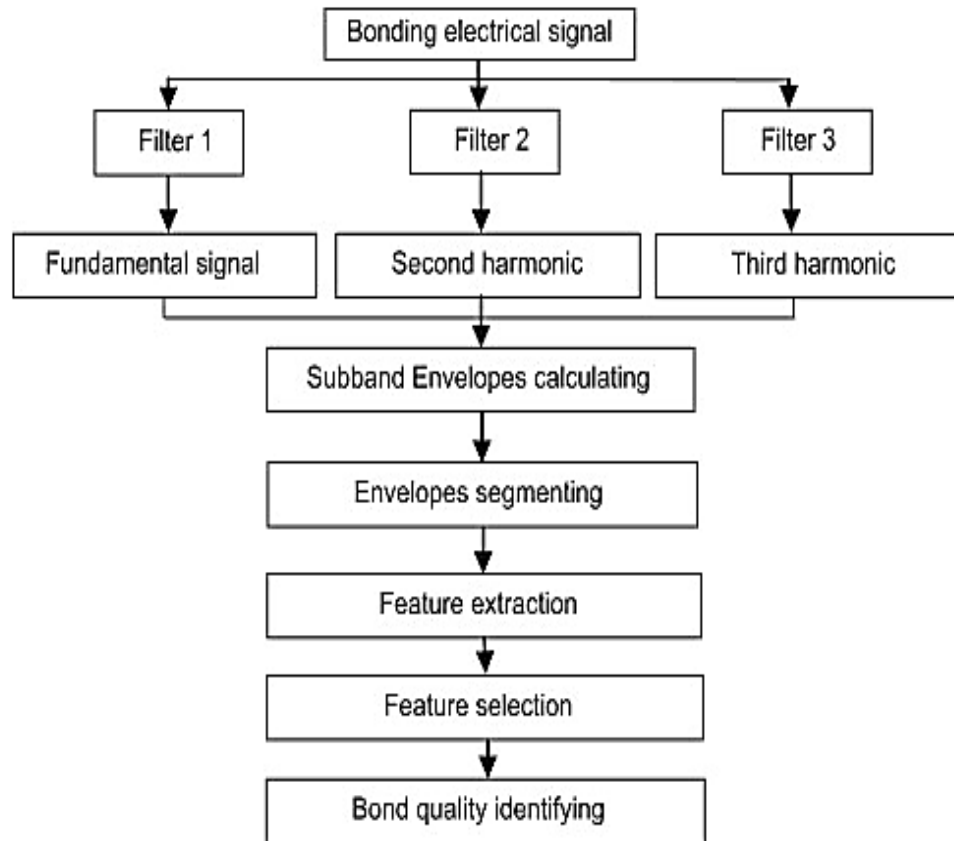


Figure 2.14: Work flow diagram of feature selection method used by Feng et al. [12]

With the extracted features, principal component analysis (PCA) was applied to reduce dimensionality of feature variables. Finally, an artificial neural network (ANN) was used to predict the strength of bonds. Results showed that it could be a reasonably useful method in predicting shear strength (see Fig. 2.15).

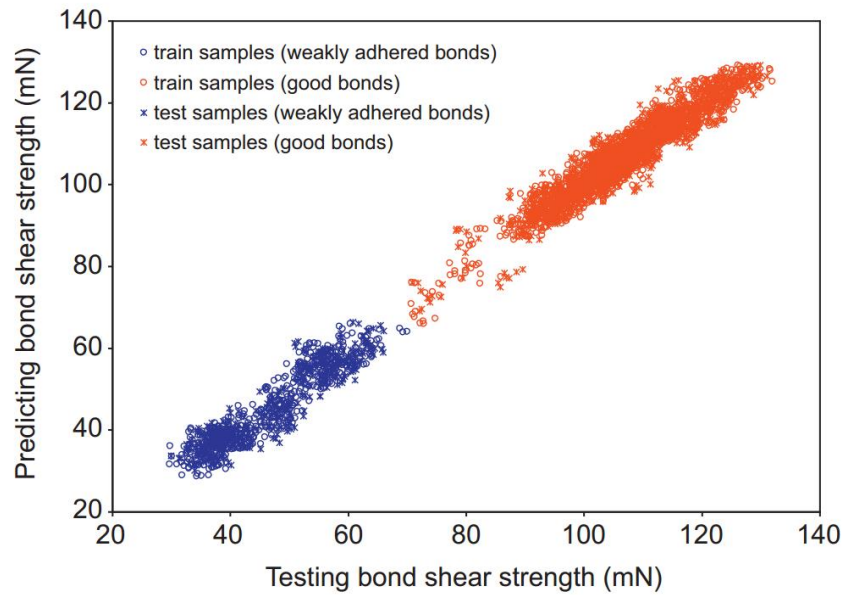


Figure 2.15: Artificial neural networks predicted shear test [12]

A year later, they used the impedance during bonding to evaluate bond quality. Five features were selected from the impedance data and then neural networks used to predict bonds strength. The result showed a good correlation between predicted bond strength and real shear strength [13].

Wang et al. [76] predicted the wedge bond strength using current signal obtained from ultrasonic generator and an artificial neural network. The bonded wires were mixture of weak and strong bonds. They have taken seven characteristics of frequency component of current signal to determine the shear strength. Fig. 2.16 shows predicted shear strength vs. measured shear strength.

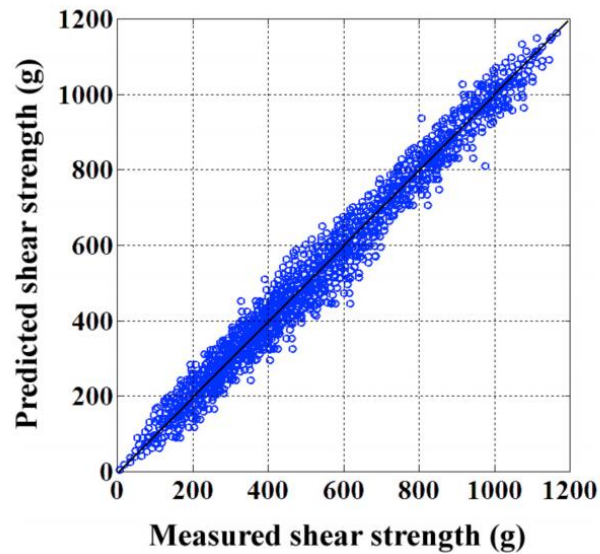


Figure 2.16: Predicted shear strength vs. measured shear strength [76]

Together, the evidence presented in the above studies of on-line techniques have shown that variations are detectable from the electrical signals obtained from ultrasonic generator, as these are inherently linked to bond quality, and this approach may be preferable to those involving the incorporation of a vibro-meter or an additional piezo-sensor.

From these above studies, none have shown the ability of their method to resolve quality differences that might occur in normal production.

## 2.7. Summary

Some novel applications requires power electronic modules to be able to perform reliably in harsh operating conditions; therefore power electronic modules must be designed and manufactured robustly with small variation in lifetime degradation. That makes the quality control of every process of manufacturing power electronic modules more important and demands the investigation of fast and reliable quality tools.

Wire bonding is the most common interconnect technology in power electronics. A single fault in one of the bonded wires might result in failure in

the whole module. Consequently, the effective detection of imperfections and determination of reasonable bond quality during the manufacturing process has been a concern for many years.

However, a serious weakness with most of the works on on-line monitoring of wire bonding methodologies is that they have been shown to work for simulated, extreme conditions (e.g. stick or non-stick, different bond pad surfaces, etc.). In the reality, bond quality under such extreme conditions can often be obvious by visual inspection even without the application of sophisticated sensing techniques. Together, these studies outline the need for further research to be able to distinguish quality differences within a normal batch, so that inferences about life prediction model uncertainty can be made.

Another problem with previous research into the on-line monitoring of wire bonding process is that they have been evaluated by shear and pull tests. This means that valuable information regarding reliability and lifetime is lost. In addition, no attempt was made on the accuracy of the monitoring technique since the bonds sacrifices and further evaluation over their entire life is impossible.

Overall, these studies highlight the need for characterizing the influence of such a slight quality change on the spread in predicted lifetimes. Therefore, it would be really be more useful to link the quality of wire bonds in as-bonded condition with lifetime performance. This can only be done using a non-destructive technique without scarifying bonds with shear and pull test.

Therefore, this is important to establish a practical non-destructive technique for detecting bond quality in normal process condition and predicting useful service life.

# **Chapter 3      Experimental Method for On-line Quality Assessment of Wire Bonding Process**

This chapter describes a non-destructive technique for on-line quality assessment of the wire bonding process. The chapter is divided into three sections. In the first section, a brief introduction to the wire bonding equipment and process is given. Then, a non-destructive observation of damage evaluation in the Al wire bonds in their initial condition and under subsequent accelerated lifetime test is given. Finally, the non-destructive technique for wire bond lifetime prediction is introduced and the detail and background of the algorithms employed in this method are described.

## **3.1. Non-Destructive Wire Bond Lifetime Prediction Technique**

As mentioned earlier, analysing the electrical signals obtained from the ultrasonic generator is one of the more practical ways of on-line monitoring of the wire bonding process. In order to describe the non-destructive, on-line



quality assessment and lifetime prediction technique, firstly the wedge-wedge wire bonder that is used in this study is introduced.

The wire bonder was manufactured by F&K Delvotec and operates at a signal frequency of about 58 kHz. The ultrasonic generator of the wire bonder has a phase locked loop (PLL) controller which adjusts the output frequency to the resonant frequency of the mechanical system including the transducer, tool and sample. The generator runs in constant-voltage mode, so the current signal varies according to the mechanical impedance presented to the transducer and it is this signal that is therefore acquired.

### 3.1.1. Signal Detection Principle and Set-up

Fig. 3.1 shows the wire bonding signal detecting principle used in this work. It consists of a measuring circuit between the ultrasonic generator and transducer, an oscilloscope as a data acquisition unit and a computer for data analysis.

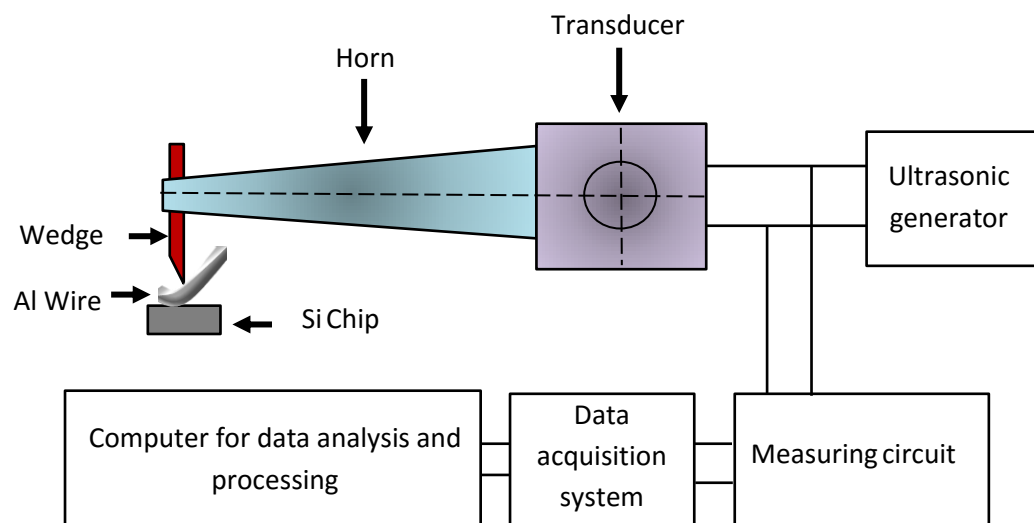


Figure 3.1: Wire bonding signal detecting principle

The current signals of the first bonds made on silicon dies were collected. The reason for choosing the bonds on the silicon device is that wire lifts usually occur on the die before the substrate [86-88].

The sampling rate was set to 12.5 MHz in order to ensure that the signals collected could resolve the variations anticipated. The experimental set-up showing the current probe and oscilloscope is shown in Fig. 3.2. Fig. 3.3 shows a typical signature of bond signal for both current and voltage.

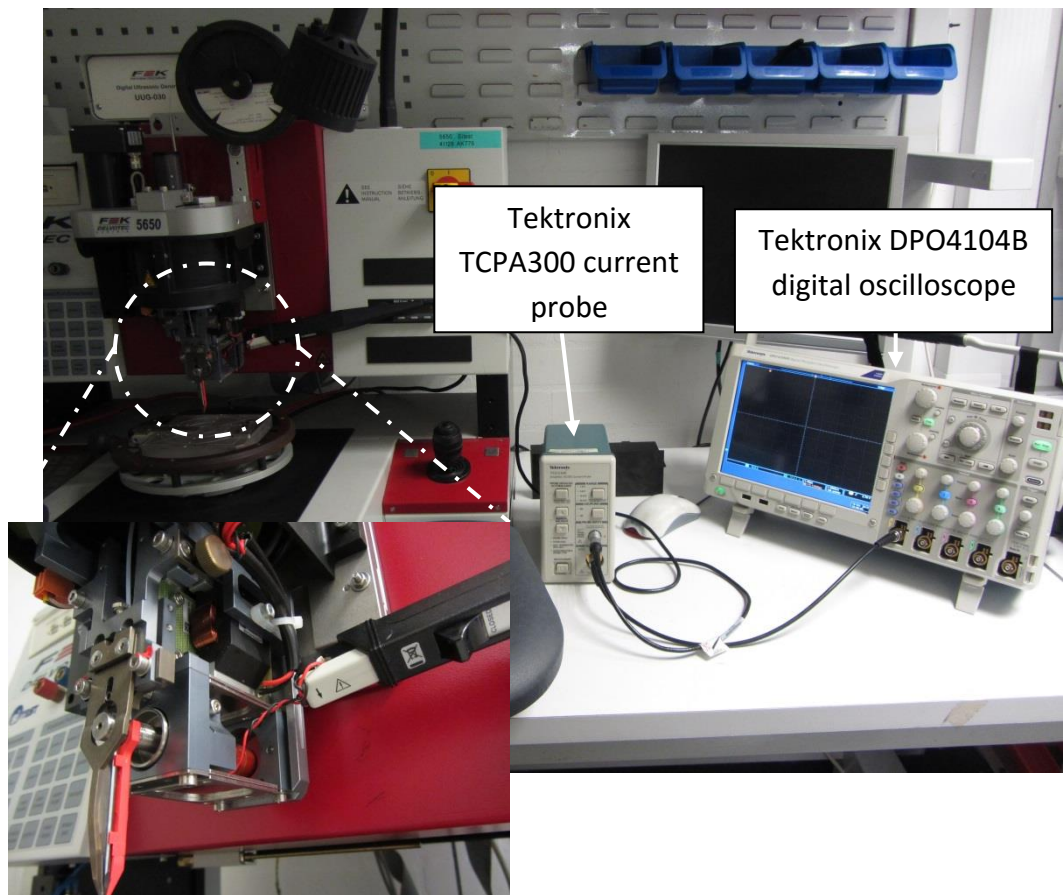


Figure 3.2: Details of signal detection tools

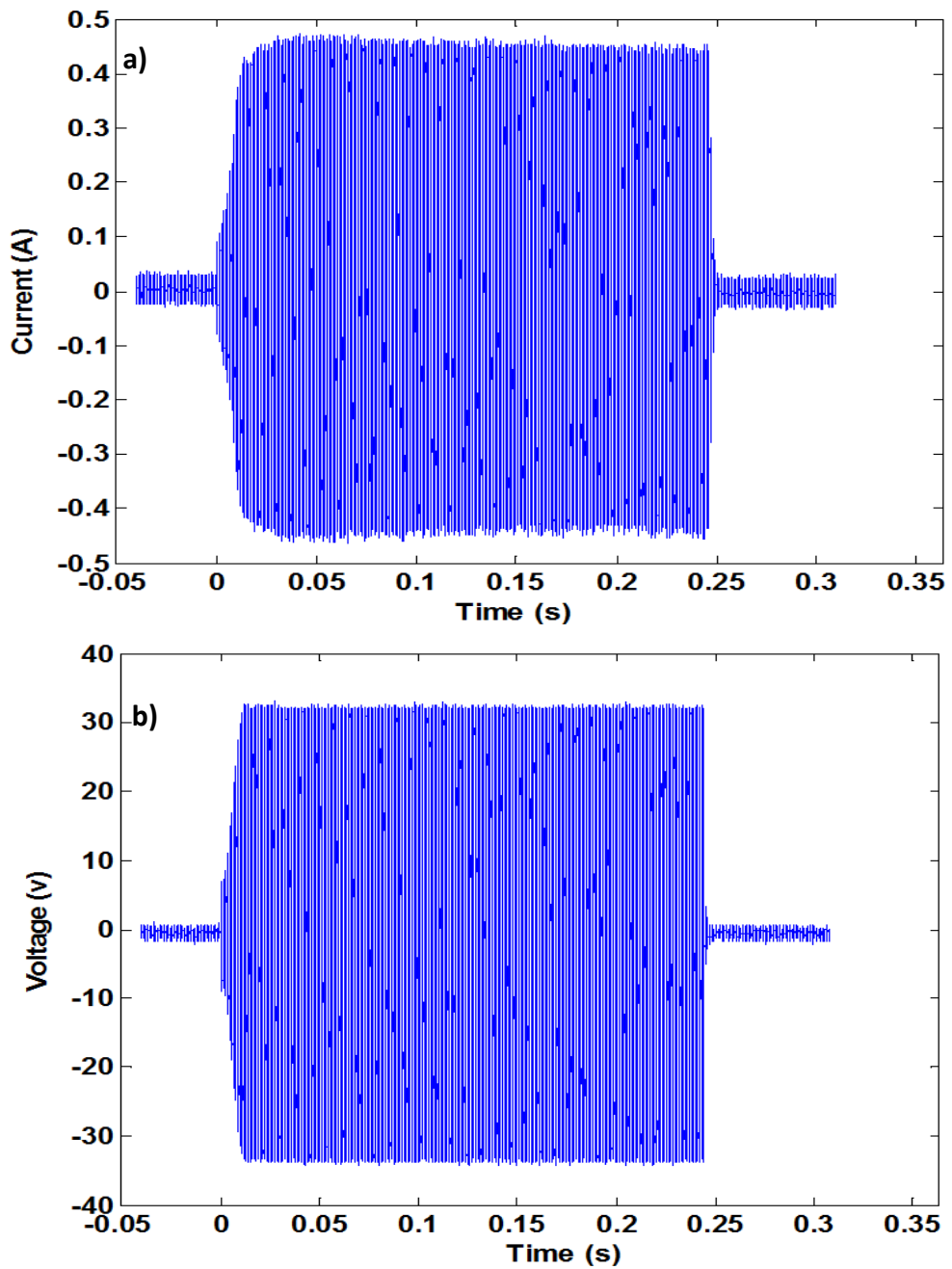


Figure 3.3: A typical signature of bond signals, a) current and b) voltage

### 3.1.2. Signal Pre-processing

To date, various approaches have been employed to analyse bond signals, such as measuring power, system impedance, looking at patterns in the second harmonics of the current signals by Fast Fourier Transforms (FFT) and looking

at the envelope of the current signals [12, 14, 29, 84]. For this study, the envelope of current signals was determined to extract the features which are related to the bond quality. Therefore, for each single wire bonded onto the dies in this research, the envelope of signal was computed using MATLAB code (Appendix I) as follows: firstly, the bond signals were divided into 1000 intervals, and then FFT analysis was performed for each interval and the root mean square (RMS) of the FFT magnitude was calculated at the frequency of interest and used as the value of current for the corresponding interval. Fig. 3.4 shows a typical signature of a bond current signal and its corresponding envelope.

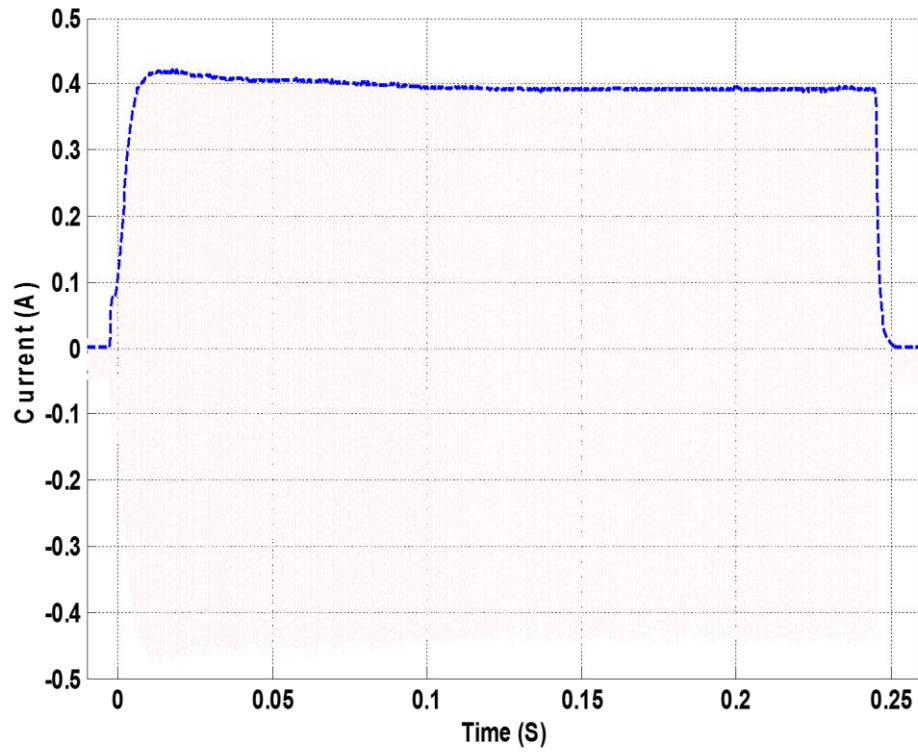


Figure 3.4: A typical signature of bond current signal and its corresponding envelope

## **3.2. Technique of Non-destructive Analysis and Visual Observation of Degradation**

### **3.2.1. Process Parameters Optimization**

The wire bonding process is influenced by a variety of factors. Some of the most important factors are: the properties of the wire itself, substrate cleanliness, bonding parameters (e.g. force, ultrasonic power, time, etc.) and wire loop parameters. More importantly the capability of the wire bonder to produce reliable bonds repeatedly with optimized bond and loop parameter settings is critical. Therefore, in the present study, a newly serviced and calibrated machine was employed and a new wedge tool was fitted. The effect of bonding parameters on lifetime of Al wire is investigated in Chapter 4 and selected bond process parameters used for this research is given.

### **3.2.2. Passive Thermal Cycling**

As shown in Chapter 2, the primary failure mechanism in power module packaging is thermomechanical in nature. One of the most common reliability test methods used in semi-conductor industries is passive thermal cycling. In this technique, the sample/specimen is subjected to rapid temperature cycles in an environmental chamber to simulate the thermomechanical stresses which occur in power modules under operation. During thermal cycling, the temperature of the several layers within the sample fluctuates over time (see Fig. 1.4 in Chapter 1). Differences in the thermal expansion coefficients of the layers cause the materials to expand and contract at different rates [89]. The stress and strain which build up as a result lead to degradation and failure of the interconnections such as wire bonds. In this work, the Al wire bonds for the experiments described in Chapter 4 and 5 were subjected to passive thermal cycling from -55 to +125 °C (See Fig. 3.5). Each cycle was about 30 minutes long and the temperature amplitude was approximately 180K (see Fig. 3.6).

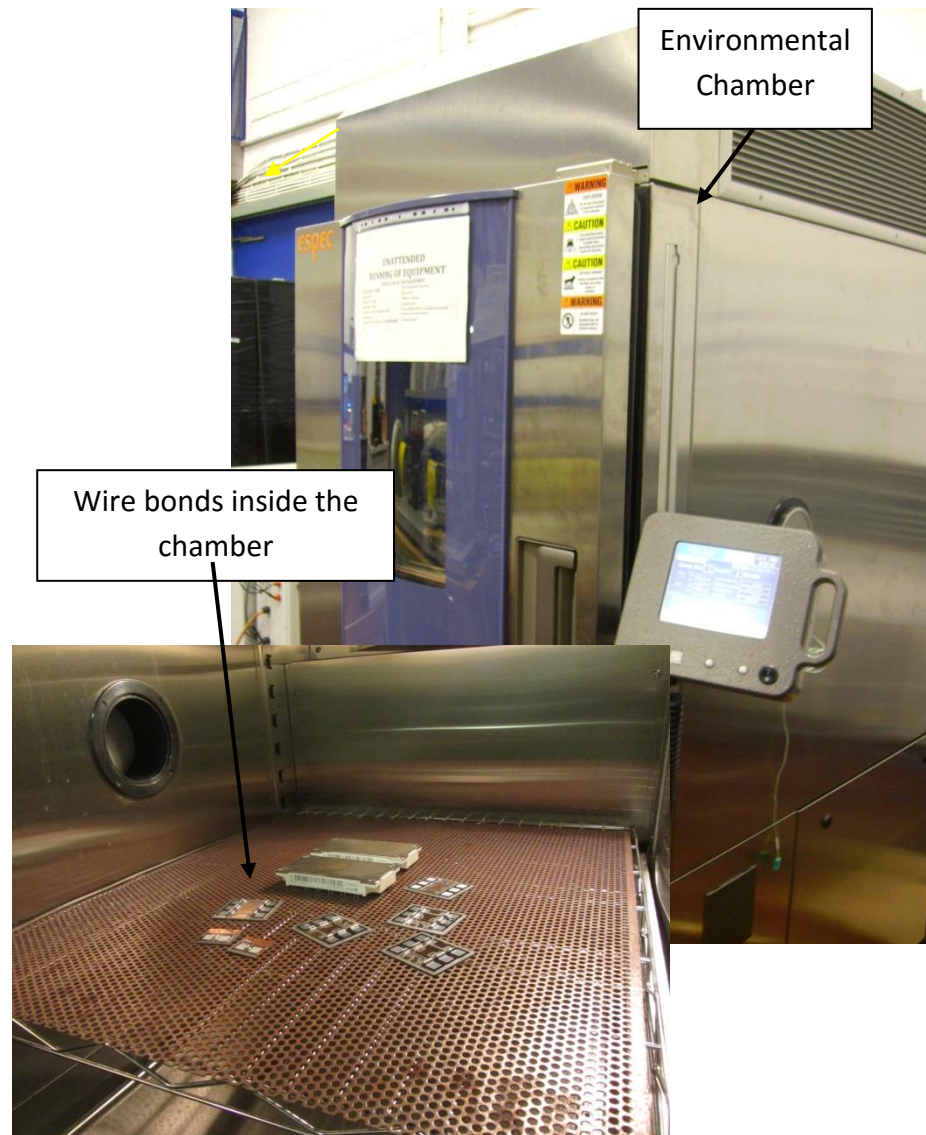


Figure 3.5: Test set-up for passive thermal cycling

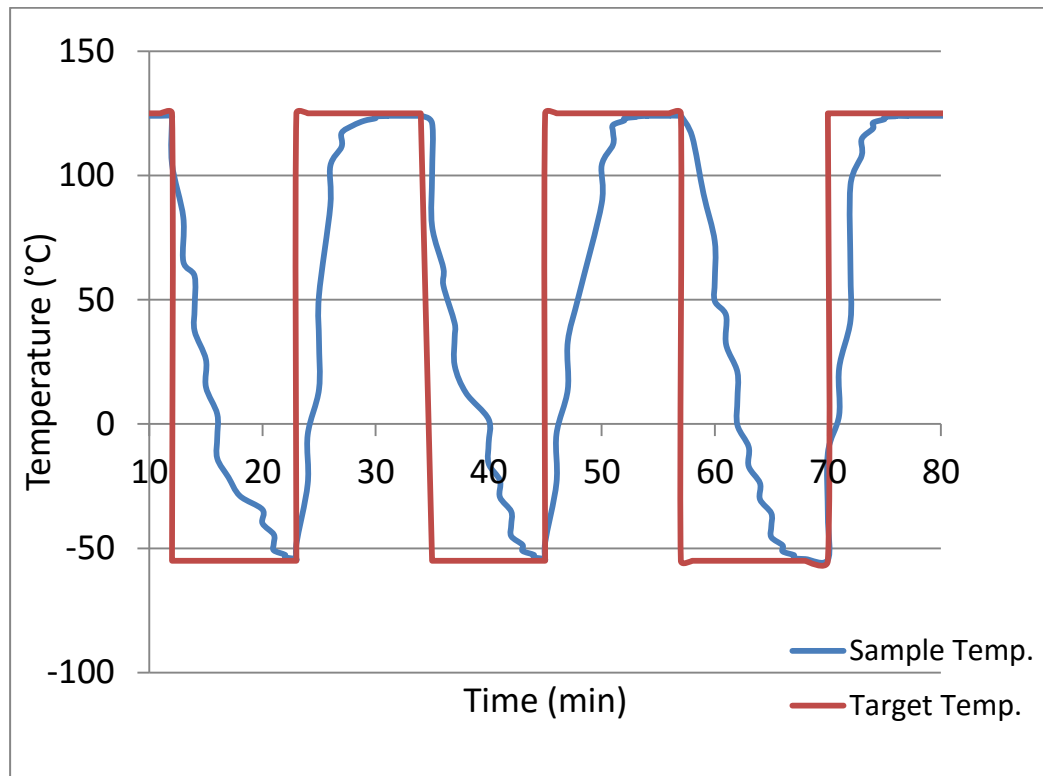


Figure 3.6: A snapshots of temperature profile of thermal cycling test

### 3.2.3. Active Power Cycling Test

Power cycling tests are also widely used for determining the lifetime of the power module [57, 90, 91]. A typical power cycling test applies a constant direct current (DC) pulse for a programmed time followed by a cool down period [88, 92-94]. During the power cycling test, a load current is conducted by the power chips and the power losses heat up the chip. When the chip reaches the target maximum temperature, or after a pre-set time, depending on the adopted control method, the load current is switched off and the chip cools down to its target minimum temperature. The next cycle is begun by applying the load current again. The thermal stress from the repeated heating and cooling leads to fatigue at the components and interconnections [95]. In comparison to thermal cycling, power cycling generates more stress on the device [96]. The temperature distribution of the silicon device during power cycling has been widely investigated in several studies [97-101]. The analysis



of temperature profiles reveal that the maximum temperature is close to the centre of the silicon device (see Fig. 3.7).

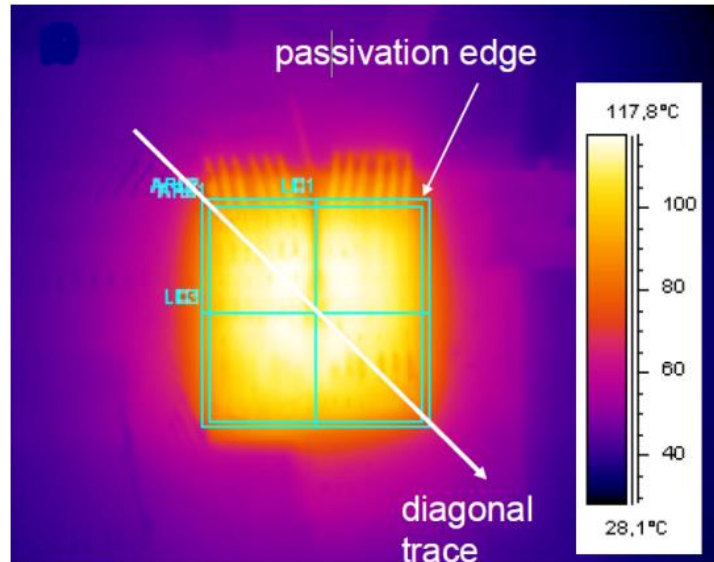


Figure 3.7: Temperature distribution of the chip in thermal equilibrium [97]

In this research, the Al wire bonds used for experiments in Chapter 6 were subjected to active power cycling from 40°C to 120°C. The power cycling rig applied a constant current of about 70 A and the die temperature controlled directly using feedback from an infra-red sensor. Each cycle (heating and cooling) was about 8 seconds (in total) and temperature amplitude was controlled to be 80K at the centre of the die. The power cycling rig and a snapshot of the temperature profile are given in Fig. 3.8 and 3.9 respectively.

It should be noted that substrate delamination and solder joint failure have been tested prior the passive and active cycling tests in order to eliminate the effect of these failures on the wire bond life-off results.



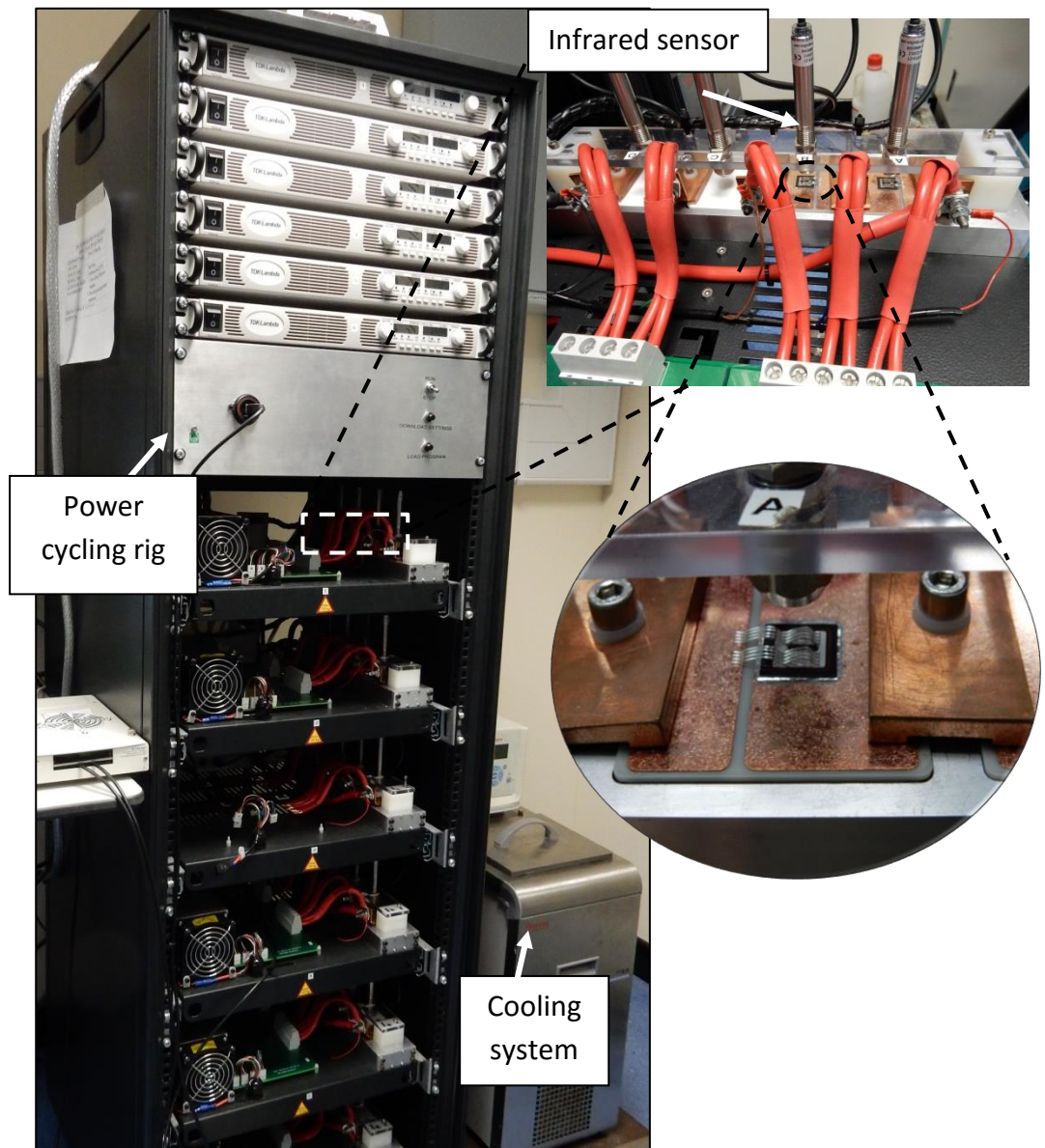


Figure 3.8: Image of power cycling rig

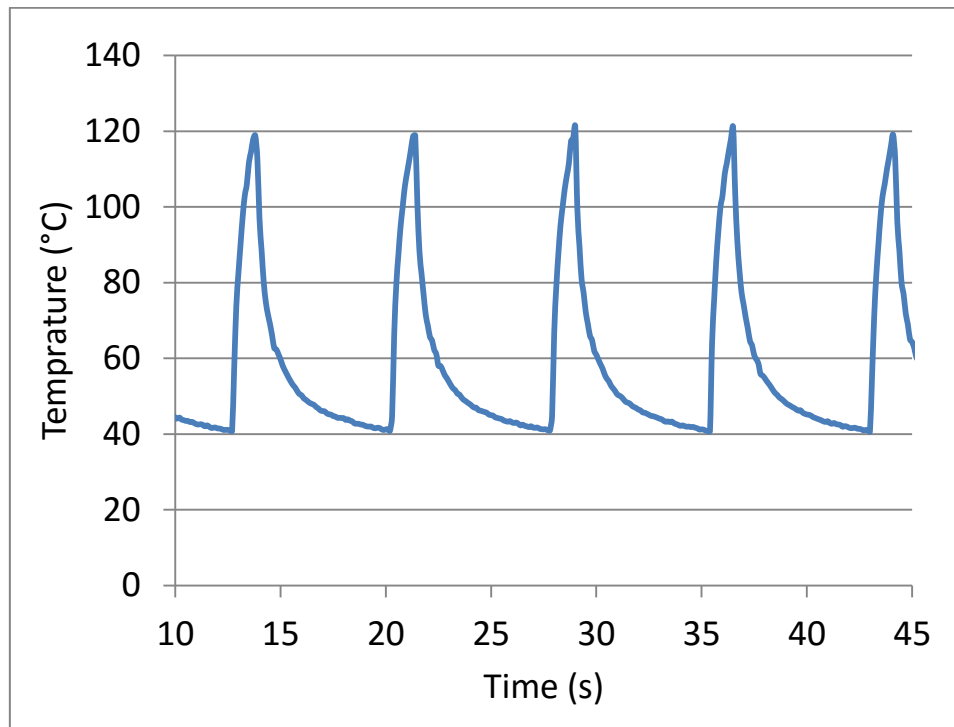


Figure 3.9: A snapshot of temperature profile

### 3.2.4. 3D X-ray Tomography

X-ray computed tomography (CT) is a well-known non-destructive testing method which has seen growing interest in the last decade [102]. It allows reliable quality control by means of three-dimensional defect detection [102]. The machine consists of an x-ray source and a detector. Several projections of samples are obtained by a detector at multiple rotational angles, which are then mathematically reconstructed to make a three-dimensional model of the sample. The main advantage of X-ray CT for wire bond quality monitoring is the possibility of observing the bond interface and tracking damage evaluation during reliability tests. A Versa-XRM 500 machine supplied by Carl Zeiss X-ray Microscopy was used for this work in order to observe the relationship between the as-bonded condition and performance under loading of wire bonds, as demonstrated in [9]. Details of imaging parameters used for tomography are given in table below.

Table 3.1: Details of 3D X-ray tomography imaging parameters

Imaging parameters	Value
Voltage	80-90kV
Camera binning mode	2×2
Detector	4X objective lens
Exposure time	18 to 22 s
Pixel size	~1.60μm
Total projections	2401
Rotation span	180°
Sample-source distance	-25 to -46 mm
Sample-detector distance	72.5 to 136 mm

It should be noted that the substrates of the randomly selected samples were cut to a smaller size in order to reduce tomography imaging time and increase the resolution. In addition, an appropriate filter was applied in order to reduce beam hardening effects. Fig. 3.10 shows the 3D X-ray tomography machine.

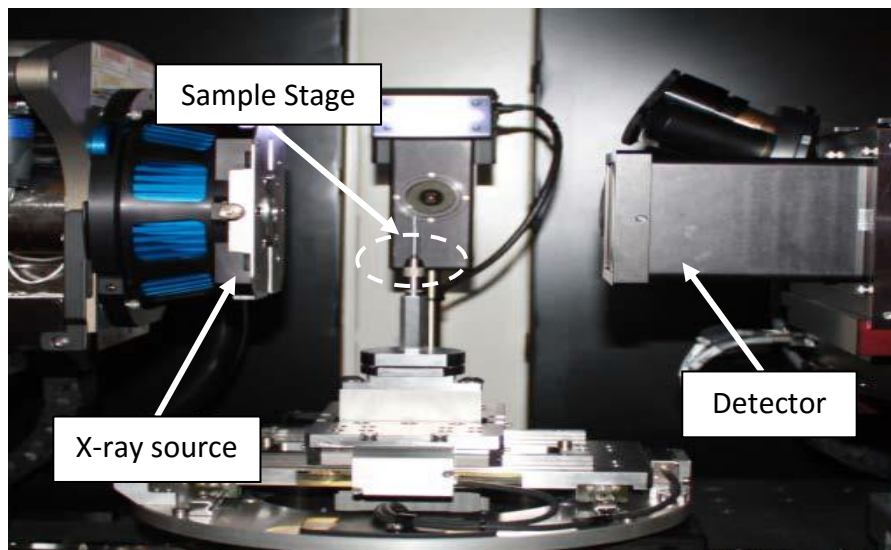


Figure 3.10: 3D X-ray tomography

Virtual cross-sections in different planes and a volume rendered image of a sample are given in Fig. 3.11. The X-Y plane cross-section is parallel to the

interface of the bonded wires and bond interface can be seen in this plane. Additional virtual cross-sections are the cross-sections made along Y-Z (indicated by red -dashed lines) and X-Z planes (indicated by yellow- long dashed lines).

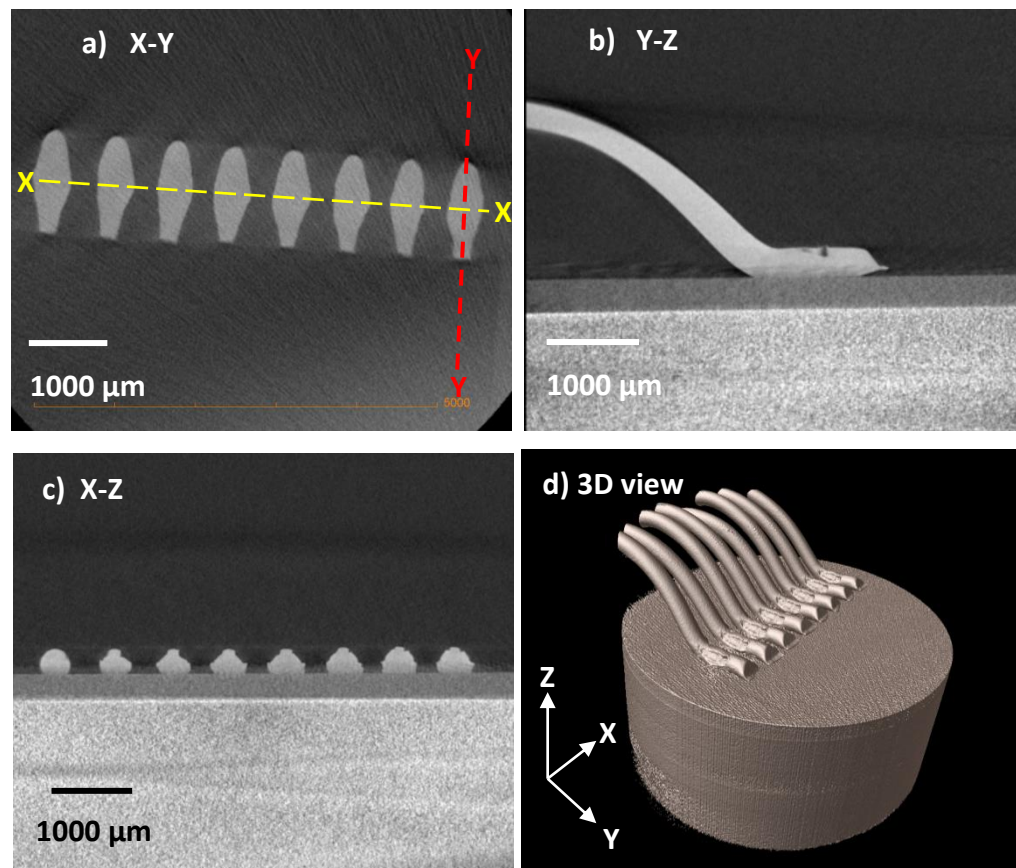


Figure 3.11: Overview scan of bonded wires, a) Virtual cross-sections in X-Y plane of the wire bonds interface, b) Virtual cross-sections in Y-Z, c) Virtual cross-sections in X-Z plane, d) Volume rendered image of bonded wires

The X-Y plane presents a view of bond footprints and bonded area. Any voids, pre-cracks, cracks and/ or damage can usually be seen in this plane view. For the purpose of this research, the initial bond quality is assessed based on the bonded area at the interface in the X-Y plane in as-bonded condition (zero cycles). To quantify the degradation of bonded wires following accelerated tests, reduction in the X-Y plane was measured using the polygon tool in ImageJ software. The other plane views were used for further observation.

### 3.2.5. Tweezer Test

Any lift-offs or failures of wire bonds are usually hard to detect visually without physically manipulating the wires to some degree. Therefore, in this research, in order to record lifetime of each single bonded wire, they were gently prodded with tweezers after every 100 cycles.

## 3.3. Technique for Data Analysis and Classification

This section focuses on techniques that can be applied to automatically predict bond quality. Analysis of the changes in the ultrasonic bonder current envelope provides a mechanism for dividing the bonds into discrete classes which reflect the bond quality and can ultimately be related to bond life. The table below is introduced to clarify the terminology most frequently used in this thesis.

Table 3.2: Table of the terminology used in this thesis

Sample	Bonded wires
Bond quality	Bond strength
Data	Obtained signal (current) from ultrasonic generator
Unlabelled data	Data/signals that can be obtained during bonding
Labelled data	Labelled data takes a set of unlabelled data that can be expensive to obtain. In our case, random signals that selected for 3D tomography imaging has labelled/classified according their bonding condition at the bond interface
Features	Useful part of data that contains information

### 3.3.1. Sampling and Data Collection

Once the wire bonder set-up and bonding parameters are optimized, the bonding process is ready and collection of the current signals during bonding can commence. Details of the number of samples acquired and the sampling method are given in the subsequent chapters.

### **3.3.2. Random Selection and Defining Labelled and Unlabelled Data**

3D x-ray tomography imaging can be considered as the best and most reliable method for non-destructive quality evaluation of bonded wires and hence for the generation of labelled data. However, this method is time consuming and expensive to use for all the bonded wires. Therefore, with aid of this method, a limited number of bonds can be randomly selected for non-destructive evaluation in the as-bonded condition and then at other stages of life. These bonds then form the labelled data and the remaining bonded wires can be logged as the unlabelled data.

### **3.3.3. Classification**

Both the labelled and the unlabelled data can be processed by a machine learning algorithm to evaluate the correlation between the acquired electrical signatures and the bond quality. Knowledge of the correlation can then be exploited to build a model classifier which can be used to predict bond quality from the electrical signature.

### **3.3.4. Machine Learning**

In the manufacturing process, a wide range of factors can effects on the quality of final product. The destructive nature of traditional methods for wire bond quality based on shear and pull tests are not suitable for detecting the quality differences in individual as-bonded wires and for the same reason cannot be used for lifetime prediction. Therefore, there is a need for new techniques that are able to monitor process data without interfering with the wire bonding process. Modern machine learning techniques have been shown to be promising tools for quality monitoring in other areas and we seek to build on these techniques to establish their effectiveness for wire bond quality monitoring[103].

As mentioned earlier, signals obtained from the ultrasonic generator contain quality information. Therefore, by comparing ultrasonic signals during bonding, the condition of bonds can be discerned. Analysing and processing of these signals can provide important information about the wire bonds. However, the extraction of features from the ultrasonic signals is not straightforward. Some features might be highly sensitive to bond failure and they can indicate damage in very early stage of bonding, while some features may not be as sensitive.

#### **3.3.4.1. Feature Reduction**

In many cases the input data is represented by a very large number of features and/ or variables where many of these features are not needed for the learning model [104]. Moreover, with increase in the number of features, the computational complexity of the algorithm for process monitoring and cost increases [105-108]. There are two ways of reducing the dimensionality in a dataset: choosing a small subset of features or deriving a set of new artificial features that is smaller than the original features [109]. Both methods can be used as a pre-processing step from a large data set before it is fed into learning algorithms [110]. As a result, the learning algorithms can be operated faster and more effectively.

#### **3.3.4.2. Machine Learning Algorithms**

Modern industrial processes require stability of production in order to meet customer requirements. Obviously, unexpected failures are costly. Therefore, on-line process monitoring techniques have been widely used in semiconductor manufacturing, chemical, polymer and biology industries [111]. One of the most popular methods that have been developed is principal component analysis (PCA) and its extensions[112]. PCA is an unsupervised statistical algorithm that ignores class labels and its goal is to find patterns of variations within a dataset. It performs dimensionality reduction by projecting the

original n-dimensional data onto a new m-dimensional space which are identified as the principal components (PCs). PCs are eigenvectors which are orthogonal and the PCs preserve the majority of information from the data and explain the largest variations present in the data. PCA can detect the variations from process variables based on a predefined model from a pure normal operating condition [113]. The performance of PCA would be less sensitive there is a small variation between quality classes and where there is noisy data [114]. For effective quality monitoring, the detection model should be based on both process and quality variables.

An alternative to PCA, linear discriminant analysis (LDA) is a popular linear and supervised classifier that tries to separate different classes. Linear discriminants represent the planes that maximize the separation between multiple classes. Both PCA and LDA have been widely applied in past decades. However, typically they are not capable of dealing with complex datasets which are highly dimensional and noisy [115]. In this situation, a possible solution is to use a supervised and or semi-supervised learning algorithm.

In supervised learning techniques, a classifier model predicts the class of the product based on both labelled and unlabelled data. Support vector machines (SVM) and neural networks are the most popular algorithms in supervised learning. Recently, semi-supervised learning methods have gained attention in the area of large datasets with very few labelled data [116], as they require less human effort and give high accuracy. A semi-supervised approach is appropriate in our case because a small quantity of labelled data (imaged bonded area by 3D X-ray tomography) is available while unlabelled data is abundant. Semi-supervised learning is of practical value as it requires less training data than a fully supervised method and is preferable to an unsupervised approach in terms of accuracy [117].

Semi-supervised learning theory and practical applications are available in Zhu's work [118]. Some of the most popular semi-supervised learning methods are: 1) Expectation Maximization (EM) with generative mixture



models, 2) self-training, 3) co-training, 4) data based methods, 5) Transductive Support Vector Machines (TSVMs) and 6) graph-based methods [119].

Recently, graph based semi-supervised techniques have attracted increasing amounts of interest and success [120-122]. This technique constructs a graph to connect similar data points in order to classify them into a class/label. Compared with other semi-supervised learning methods, graph based methods make better use of data distributions revealed by unlabelled data [123]. Graph based, semi-supervised learning has been a powerful tool in data mining in many applications, such as medical image segmentation, classification of hand-written digits, image retrieval, etc.[123, 124]. Fig. 3.12 shows typical procedures for a semi-supervised algorithm.

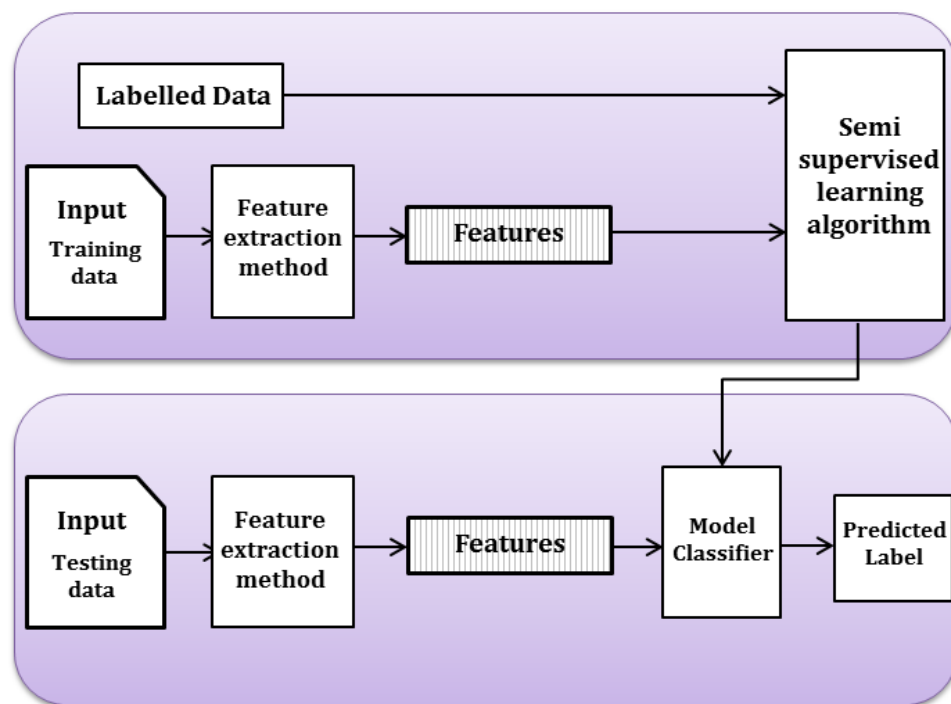


Figure 3.12: Procedures for a semi-supervised learning algorithm[125]

### 3.3.4.3. Semi-Supervised Discriminant Analysis (SDA)

The graph-based semi-supervised algorithms can generally be divided into transductive and inductive learning. Transductive learning produces labels only

for available unlabelled data. On the other hand, inductive learning produces labels not only for unlabelled data but also produces a classifier [126].

Inductive learning is mainly for classification-based feature learning from high dimensional data, such as [127-129]. Semi-supervised discriminant analysis (SDA) is one of the semi-supervised learning algorithm which is able to reduce the dimensionality of data in semi-supervised cases, achieving a much more efficient computation and has shown promising performance in a variety of applications [130]. The SDA algorithm has been tested on a dataset of images of faces, and its performance in face recognition has compared to that of other algorithms, see Fig. 3.13 [131]. The SDA performed the best as it faster than the other algorithms with smallest error rates. Therefore considered appropriate for this research.

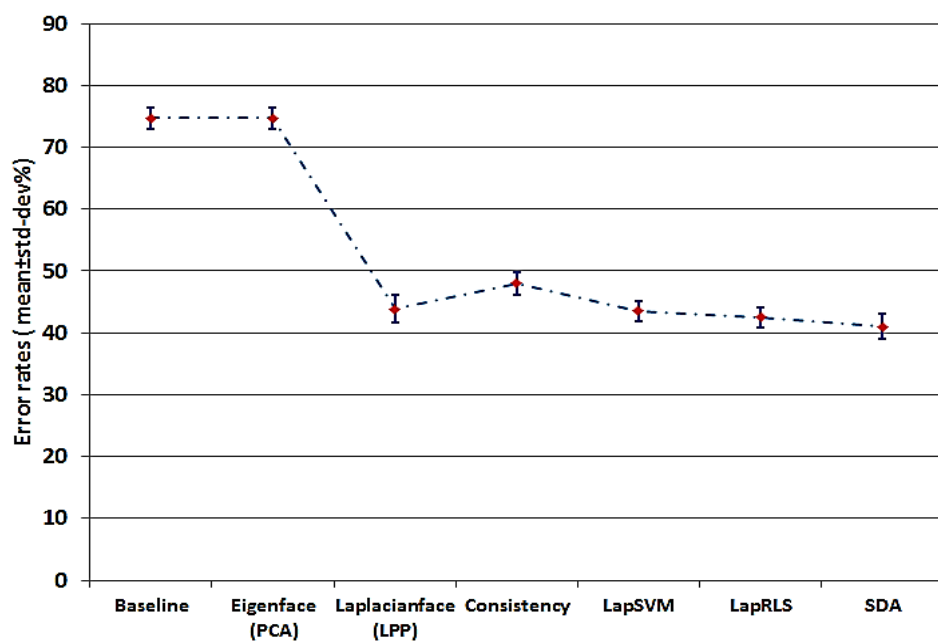


Figure 3.13: Performance comparison of different algorithms, Baseline, Eigenface [132], Laplacianface[133], consistency [121], LapSVM[120], LapRLS [120] and SDA

The SDA algorithm is described in detail in the next section, and comes from the source code provided (see Appendix II) by the authors of references [119, 134-136].

### 3.3.5. Background of the SDA Algorithm

SDA is extended from the LDA algorithm which is able to deal with a large set of unlabelled data [137, 138]. Therefore, firstly the LDA algorithm is presented.

Let  $X$  labelled training samples  $N_L = \{n_1, n_2, \dots, n_X\}$  and  $Y$  unlabelled samples  $N_U = \{n_{X+1}, n_{X+2}, \dots, n_{X+Y}\}$ .

$m_i$  is the label,  $m_i \in \{+1, -1\}$ ,  $1 \leq i \leq X$ .

Let  $N = N_L \cup N_U$  denote the set of all training samples.

$N \in \mathbb{R}^{K \times (X+Y)}$ ,  $K$  is the dimension of feature vectors. The objective function of Linear Discriminant Analysis (LDA) is to find the projection vector  $w^*$  which can maximize between class differences and minimize within-class differences [139]:

$$w^* = \arg \max \frac{w^T C_b w}{w^T C_w w} \quad (3.1)$$

where  $C_b$  is between-class scatter matrix and  $C_w$  is within-class scatter matrix. The total scatter matrix is  $C_t = C_b + C_w$ .

The objective function of LDA (3.1) can be cast as a generalized eigenvalue decomposition problem [119]:  $C_b w = \lambda C_t$ . The solutions are projection vector  $w$  and eigenvalue  $\lambda$ . From the view of manifold learning [133], the above relationship can be represented with matrixes. We can define matrix  $W$  as the weight of the edge  $(n_i, n_j)$ :

$$W_{i,j} = \begin{cases} \frac{1}{X_{m_i}} & \text{if } m_i = m_j \\ 0, & \text{if } m_i \neq m_j \end{cases} \quad (3.2)$$

where  $X_{m_i}$  denotes the number of labeled samples in class  $m_i$ . Based on  $W$ , we can obtain the following Laplacian matrices:

$$L^{C_w} = I - W, L^{C_b} = W - \frac{1}{M} e e^T \text{ and } L^{C_t} = I - \frac{1}{M} e e^T$$

and the corresponding

$$C_w = N_L L^{C_w} N_L^T, \quad C_b = N_L L^{C_b} N_L^T \quad \text{and} \quad C_w = N_L L^{C_t} N_L^T, \quad \text{where } e = (1, 1, \dots, 1)^T \text{ is a } X \text{ dimensional vector.}$$

In practice, when there is no sufficient number of training samples, the performance of the LDA tends to be degraded. In order to improve this issue, Deng Cai et. al [119] presented SDA to prevent overfitting of LDA with less labelled data. SDA applies  $p$ -nearest of each sample to model the relationships of all training samples including labelled and unlabelled training samples, forming a graph. The weight of the edge in the graph encodes this relationship, defined by matrix  $C$ :

$$C_{ij} = \begin{cases} 1, & \text{if } n_i \in Y_p(n_j) \text{ or } n_j \in Y_p(n_i) \\ 0, & \text{otherwise,} \end{cases} \quad (3.3)$$

where  $Y_p(n_i)$  denotes the set of  $p$ -nearest neighbours of  $n_i$ . SDA defines a regularizer  $J(w)$  as:

$$J(w) = \sum_{ij} (w^T n_i - w^T n_j)^2 \quad S_{ij} = w^T N L N^T w \quad (3.4)$$

$L = D - S$  is the Laplacian matrix [140].  $D$  is a diagonal matrix with  $D_{ii} = \sum_j S_{ij}$ . The underlying explanation is that if two samples are close, they are likely to be in the same class. The objective function of SDA is:

$$\max_w \frac{w^T C_b w}{w^T C_t w + \alpha J(w)} = \max_w \frac{w^T (N_L L^{C_b} N_L^T)}{w^T (N_L L^{C_t} N_L^T + \alpha N L N^T) w} \quad (3.5)$$

Parameter  $\alpha$  controls the trade-off between model complexity and empirical loss. It is clear that (3.5) is similar to (3.1) except  $C_w$  is replaced. Thus it can be solved in the same way as (3.1) [119]. With this regularizer, the output of SDA,  $w$  not only considers the discriminant power among labelled data but the intrinsic geometrical structure among all training samples.

### 3.3.6. Model Accuracy

In this step, the accuracy of model is checked against actual lifetime data from accelerated lifetime tests (see Section 3.2). Once the model classifier is accurate enough, the model can then be used for on-line monitoring of wire bond quality on the production line. Fig. 3.14 illustrates the block diagram of the non-destructive technique that follows in this thesis for on-line industrial quality monitoring based on MATLAB codes.

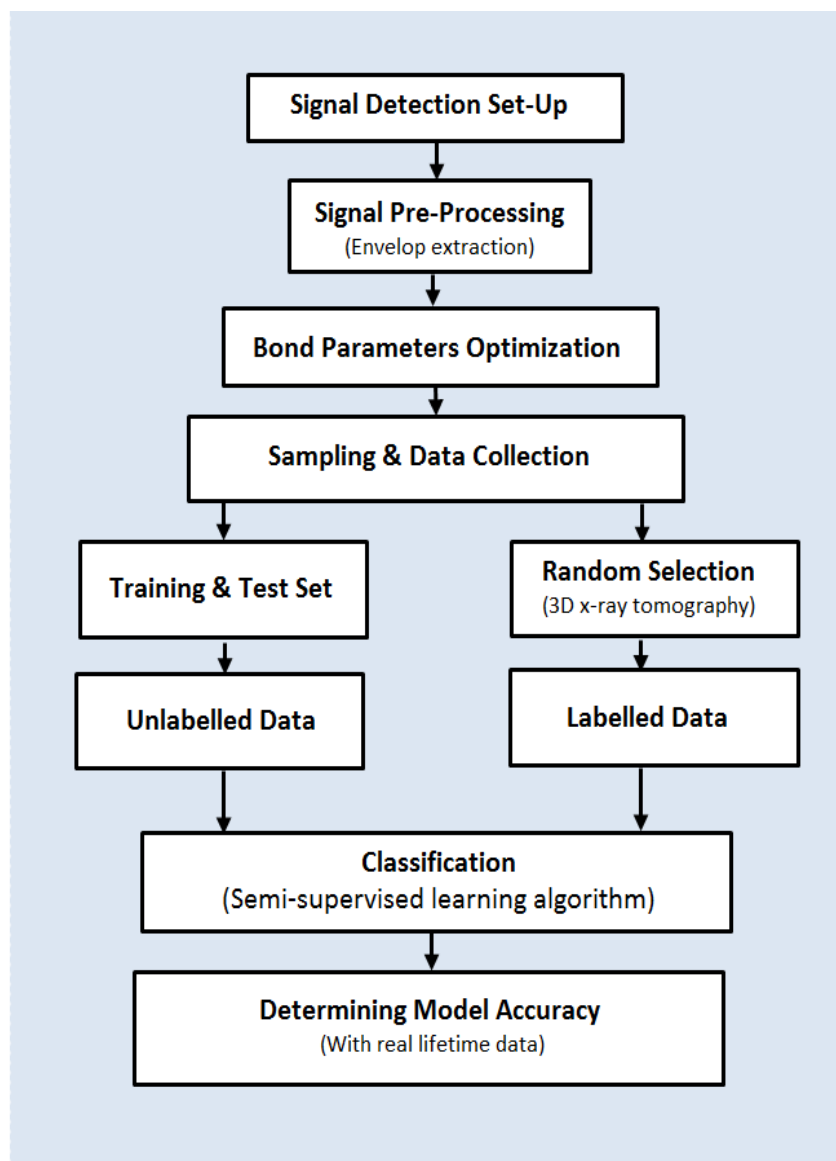


Figure 3.14: The on-line assessment technique flowchart

### **3.4. Summary**

Routine monitoring of the wire bonding process requires real-time evaluation and control of wire bond quality. This chapter introduced a new non-destructive method for predicting the in-service lifetime of wire bonds using current signals obtained from ultrasonic generator and a semi-supervised algorithm. 3D x-ray tomography is used as a non-destructive tool for evaluating the initial bond quality and its through-life degradation. The next chapter presents the process parameter optimization method employed in this research prior sampling for in-service lifetime prediction technique.

# **Chapter 4      Investigating the Effect of Bonding Parameters on the Reliability of Al Wire**

This chapter studies the importance of wire bonding process parameters optimization prior wire bonding. The effect of bonding parameters on the reliability of Al wire bond is investigated. Bonds were made in 25 different designs of bonding parameter settings. The bonds signals (current) were collected during bonding. 3D X-ray tomography was then used to evaluate bond quality during passive thermal cycling between -55 °C and +125 °C. In this chapter firstly, the experimental plan is given, and then the results and key findings are summarized.

## **4.1. Wire Bonding Process Parameter Setting**

As mentioned earlier, wire bond reliability strongly depends on bonding parameters such as time, ultrasonic power, force, etc. Over the last few years, there has been some work on the effect of bonding parameters on reliability of

heavy wire bonds [38, 141]; however, these have not been investigated in sufficient detail considering the complex interactions between important process parameters, and more importantly with a non-destructive methodology [9].

For the most appropriate process parameter setting, five important bond parameters such as time, ultrasonic power, begin-force, end-force and touch down steps (pre-compression) were selected with five levels using two analytical techniques and passive thermal cycling for determining the most appropriate bonding parameter settings for the proposed on-line quality monitoring. The analytical techniques included: monitoring bond quality using signals obtained from the ultrasonic bonding generator; a visual and semi-quantitative characterization of virtual bond cross-sections in terms of area and shape of the wire bonds and a tweezer test method to check bond lift-off rate.

## **4.2. Experimental Procedure**

25 designs were created to determine the best bonding process setting of five major bonding parameters in terms of bond quality: namely time, ultrasonic (US) power, begin force, end force and touch-down (TD) steps (pre-compression). The designs are based on five factors with five levels (Taguchi design)[142]. The experimental design is shown in Table 4.1. The experiment was repeated six times, making a total of 150 bonds.



Table 4.1: Bonding parameters designs for reliability test

Design ID	Time(ms)	US-Power(digits)	Begin-Force(cN)	End-Force (cN)	TD-Step (digits)
1	100	115	200	200	70
2	100	125	400	400	80
3	100	135	600	600	90
4	100	145	800	800	100
5	100	155	1000	1000	110
6	135	115	400	600	100
7	135	125	600	800	110
8	135	135	800	1000	70
9	135	145	1000	200	80
10	135	155	200	400	90
11	170	115	600	1000	80
12	170	125	800	200	90
13	170	135	1000	400	100
14	170	145	200	600	110
15	170	155	400	800	70
16	215	115	800	400	110
17	215	125	1000	600	70
18	215	135	200	800	80
19	215	145	400	1000	90
20	215	155	600	200	100
21	250	115	1000	800	90
22	250	125	200	1000	100
23	250	135	400	200	110
24	250	145	600	400	70
25	250	155	800	600	80

#### 4.2.1. Signal Acquisition Setting

The current signals of the bonds made on silicon dies (i.e. the ‘first’ bonds) were collected at a sampling rate of 12.5 MHz in order to ensure that the signals collected could resolve the variations anticipated by width. Current envelopes of signal were calculated according to the MATLAB code given in Appendix I. Details of current the probe and the oscilloscope are given in Chapter 3.

## 4.2.2. Wire Bonding Layout

The bond wires were 99.999% pure (5 N) aluminium wires, 375  $\mu\text{m}$  in diameter, and were ultrasonically bonded at room temperature onto silicon dies with a 5- $\mu\text{m}$ -thick aluminium top metallization with bellow layout (see Fig. 4.1). It should be noted that substrates and silicon dies are provided by Dynex Semiconductor Ltd.

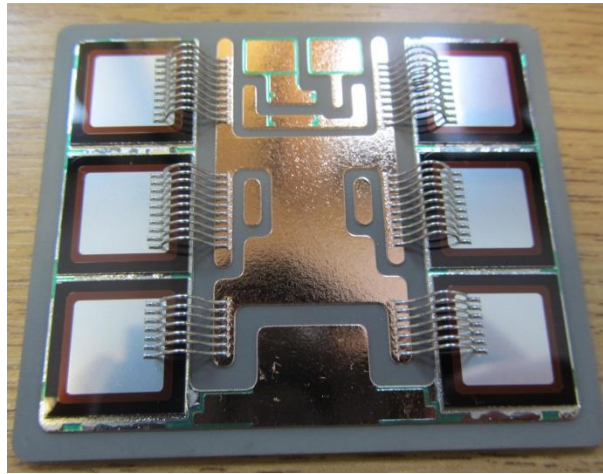


Figure 4.1: Aluminium wires bonded onto silicon dies

The bonds were subsequently subjected to passive thermal cycling from -55 to +125  $^{\circ}\text{C}$ . From the 150 bonds, 25 were randomly selected for X-ray tomography and imaged. The remaining 125 bonds were tweezer tested after every 100 cycles in order to detect any lift-offs or failures. Details of the thermal cycling, x-ray tomography and tweezer test experiments are given in the sections below.

## 4.3. Results and discussions

### 4.3.1. Relation of Different Designs and Bonds Bonded Area

The bonds that were selected for x-ray tomography were imaged in the as-bonded condition (zero cycles), after 700 cycles. Virtual cross-sections of the

bonds in different plane observed (e.g. see Fig. 4.2). From a virtual cross-section of bond interface in the X-Y plane the bond footprint, any damages and the bonded area can be seen. Some micro defects observed in X-Y plane which can be clearly seen in Y-Z Plane as two small pre-cracks that might be because of improper bonding parameters in Design 1. Bond bonded area in the as-bonded condition was measured using the polygon tool in ImageJ software. Results are given in Fig. 4.3.

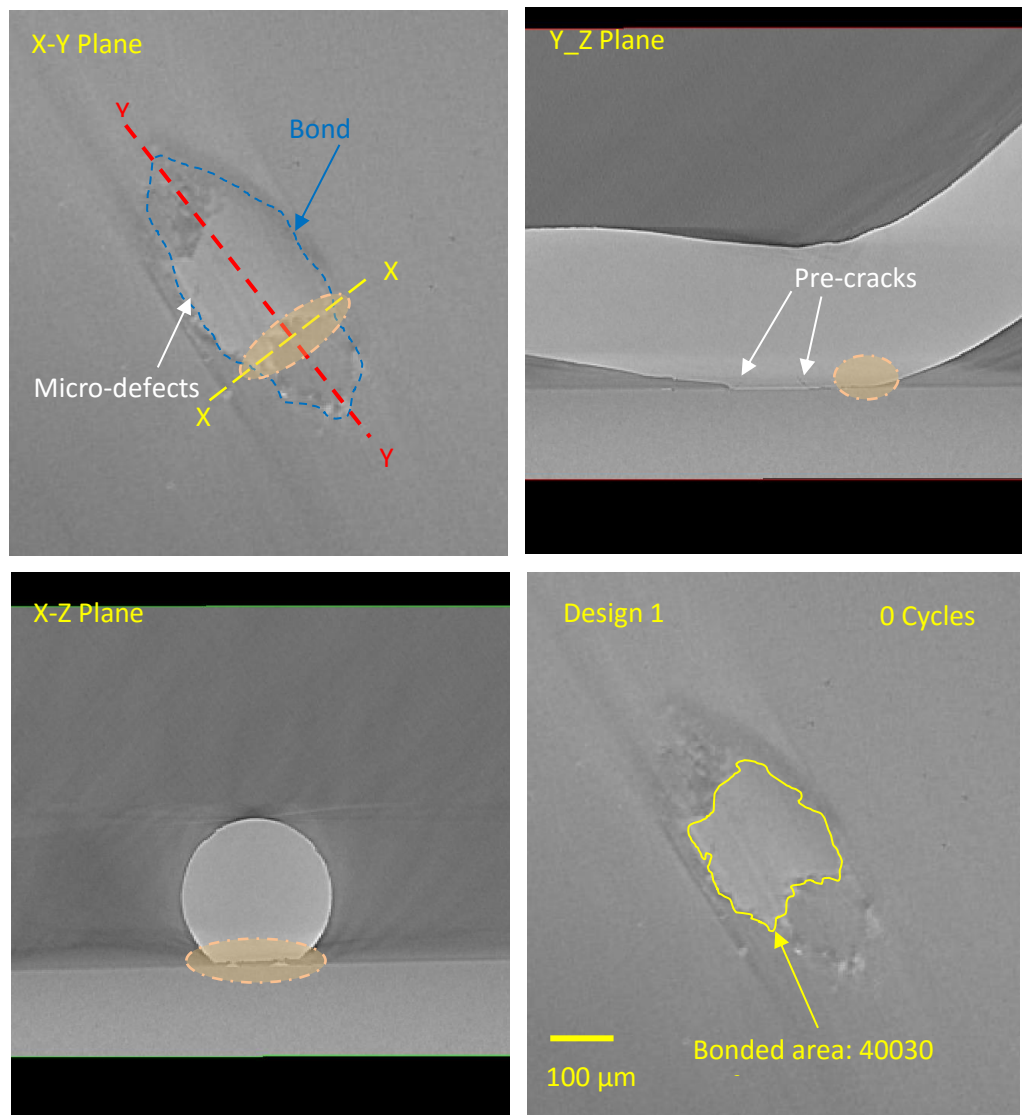


Figure 4.2: X-ray tomography virtual cross-sectional image in different plane view showing the bonded area of Design 1

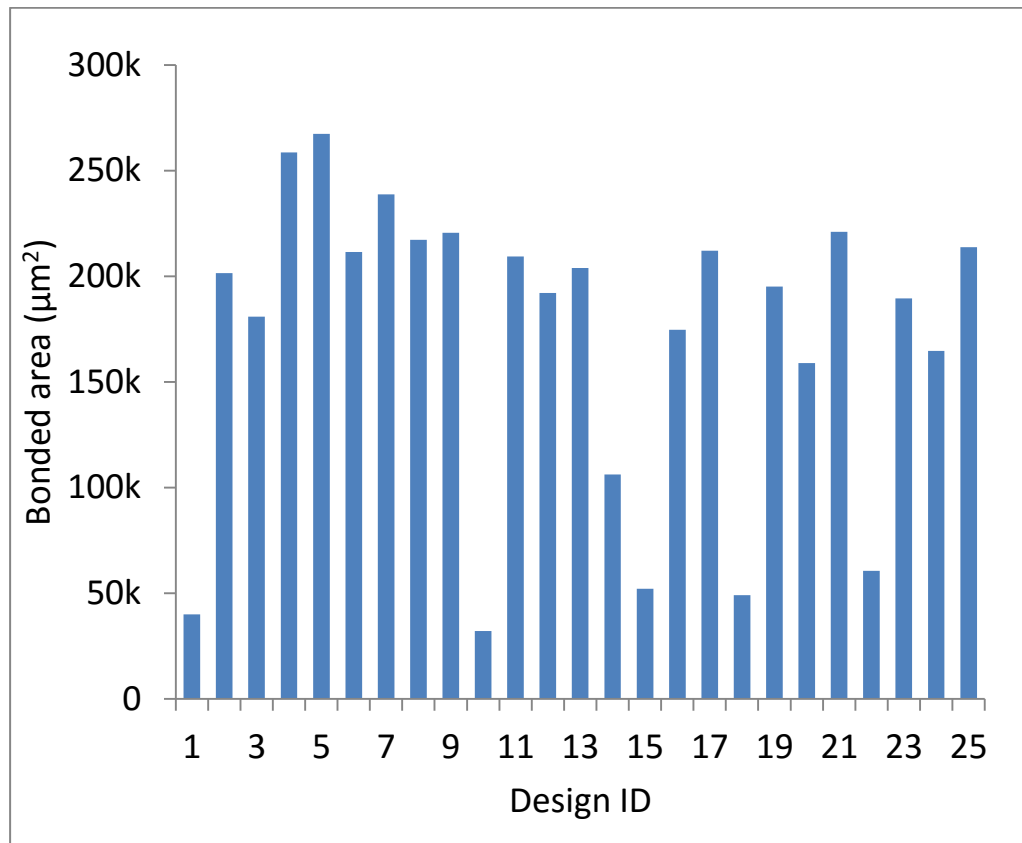


Figure 4.3: Bond bonded area for different parameter designs (0 cycles)

From the tomography images in the as-bonded condition, designs 10, 1, 18 and 15 have the least bonded area, and designs 5, 4, 7 and 21 have the largest bonded area. All the bonded wires were then subjected to thermal cycling from -55 to +125 °C. Tweezer test results of wires are given in Fig. 4.4.

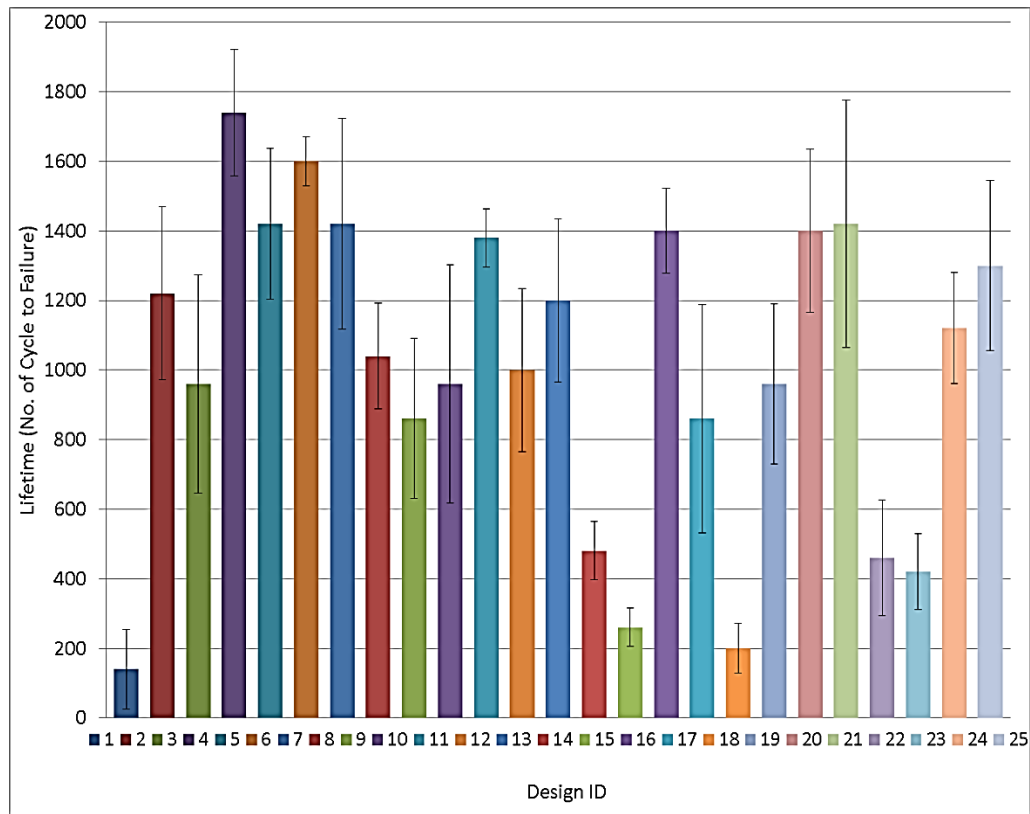


Figure 4.4: Result of bond lifetime after thermal cycling for the different parameter designs

Results of bond lift-off rate indicate that the bonds with least bonded area are less reliable i.e have less lifetimes, such as designs 1, 18 and 15, and bonds with largest bonded area are more reliable. From both the virtual x-ray tomography cross-sections and bond lift-off rates, the following observations were made:

1) Insufficient begin force and touch-down (pre-compression) steps result in poor bonded area and ultimately less reliable bonds, such as designs 1, 18, 22, and 15 (see Fig. 4.5). As can be seen in Fig. 4.5, in the as-bonded condition, the bonds attached from the middle with non-uniform shape and pre-cracks appear from both corners of the bonds. After 700 cycles the cracks started to grow from both corners and micro-voids and micro-cracks started to join together, and as shown in the X-Z plane image of design 1, the bond had almost lifted off.

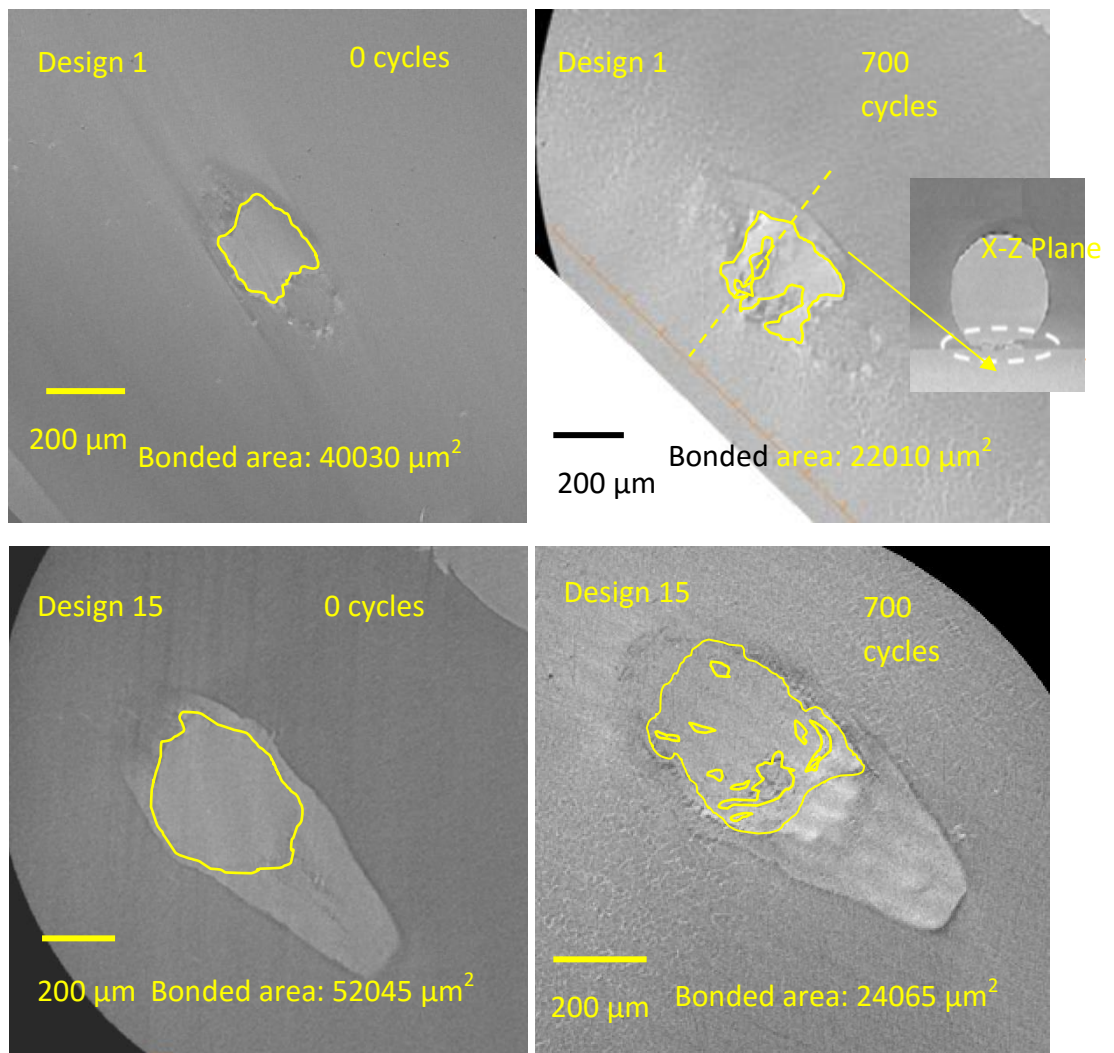


Figure 4.5: X-ray tomography images of design 1 and 15 in X-Y plane in as-bonded condition and after 700 cycles

2) Sufficient ultrasonic power and bond force create uniform bonded area and more reliable bonds such as designs 4, 6, 21, 7 and 5 (see Figs. 4.6 and 4.4).

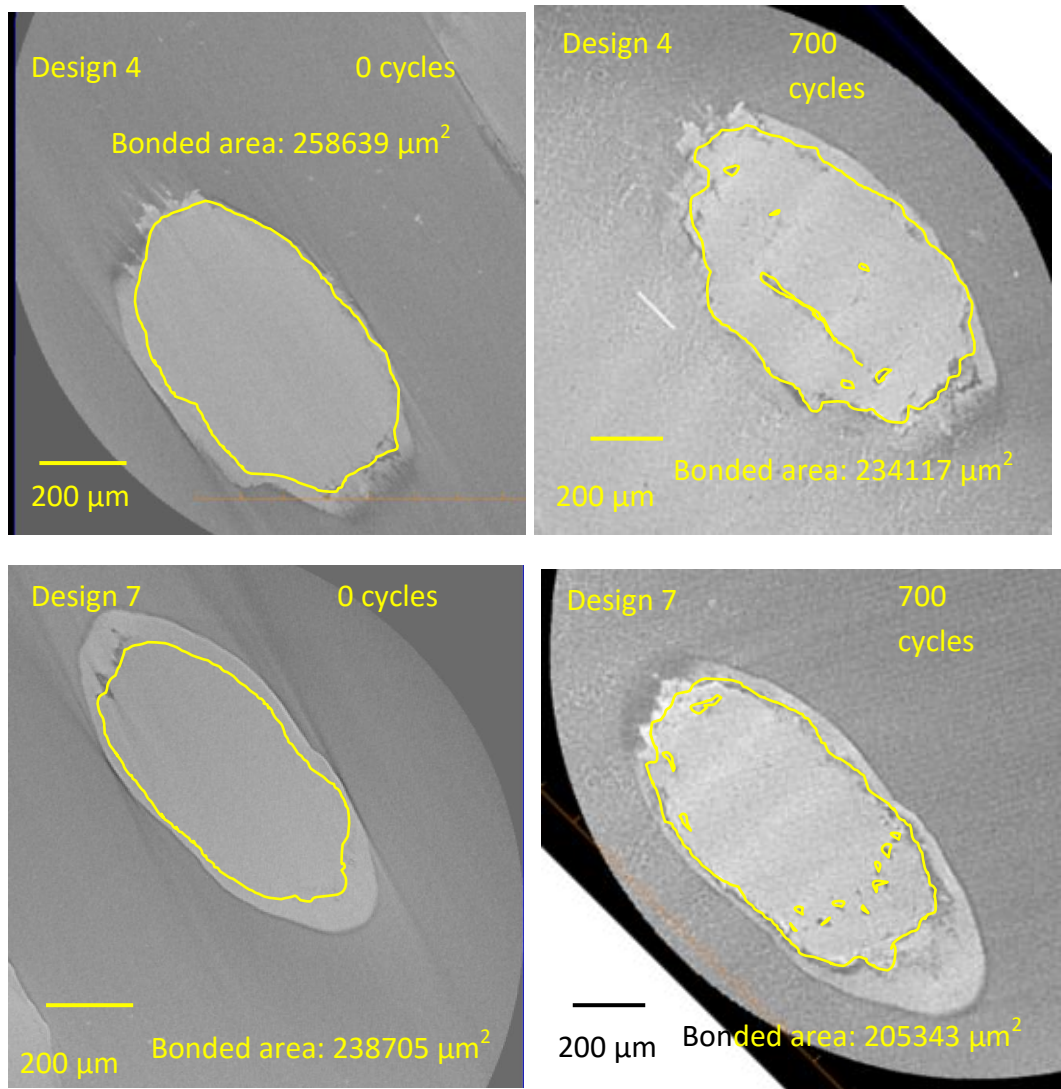


Figure 4.6: X-ray tomography images of design 4 and 7 in the X-Y plane in as-bonded condition and after 700 cycles

3) Results of designs 21 and 4 show that there is an inverse relationship between ultrasonic power and time. In other words it can be said that you can get well attached and reliable bonds with high power in low times or less

power with longer times. Thus the total energy is the important factor, rather than either power or time on their own.

#### **4.3.2. Relationship of Different Designs and Bond Electrical Signals**

From the above experiment, with its complexity of designs, it was seen that there are many poor bonding parameter settings that make the bonds less reliable, while there are few parameter combinations that make the bonds well attached and hence more reliable. It is therefore of interest for on-line quality monitoring to investigate the effect of changes in bonding parameter on the current signature of ultrasonic generator. For instance, as it can be seen in Fig. 4.7 that all current signals rise sharply for about 2 milliseconds at beginning of bonding before diverging. Different settings and combinations of parameters lead to differences in the rising characteristics and uniformity of the waveforms, the time they take to reach a steady state and the maximum current (see Fig. 4.7). These features allow potential correlations between the bond quality and current signal to be investigated.



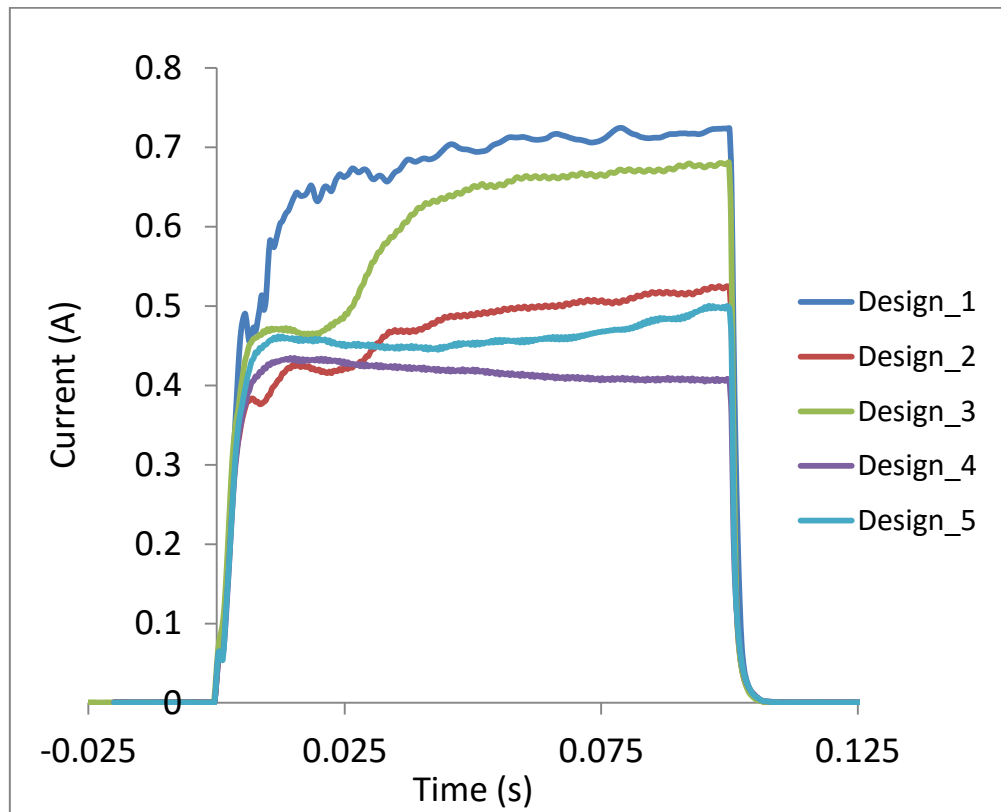


Figure 4.7: Current envelope of bonding signals for designs 1 to 5.

From the results of the bonding parameters designs that are shown in figures 4.3 and 4.4, the following remarks can be made:

- 1) For the bonding parameter designs that create less attached bonded area and ultimately shorter lifetimes, current signals reach a steady state at a higher value compared to the designs that have more bonded area and longer lifetime (see Fig. 4.8). Furthermore, the result obtained from signal analysis show the more reliable designs such as design 4 have a more uniform signal shape compared to less reliable designs such as design 1.

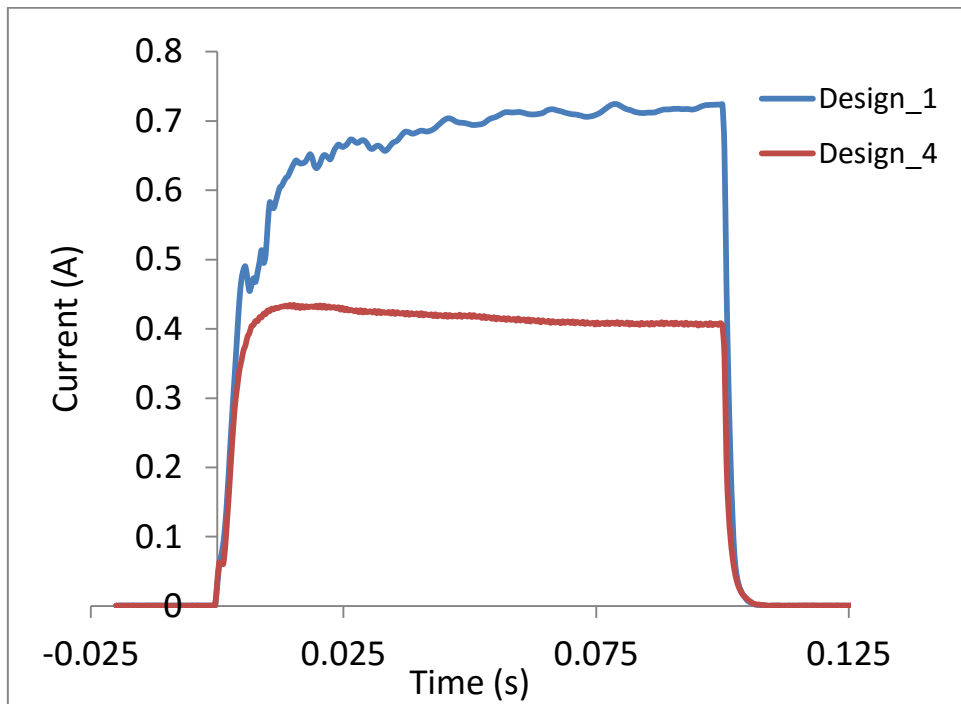


Figure 4.8: Current envelope of bonding signals for designs 1 and 4 (weakest design compare strongest design)

2) It can be said that the bonding parameter designs such as 4, 6, 21, 7 and 5 received a more constant level of power compared to the other designs (see Fig. 4.9), indicating consistent mechanical conditions at the bond foot. The x-ray tomography cross-sections and lift-off rates confirm that these are more reliable designs. Average lifetimes of the above designs were 1740, 1600, 1420, 1420 and 1420, respectively.

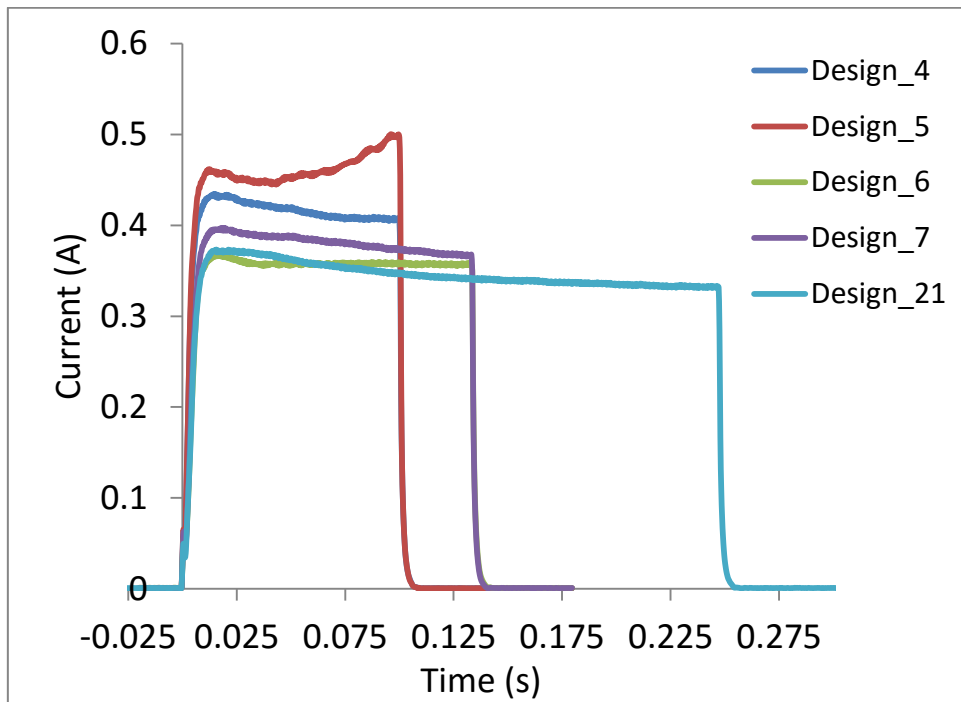


Figure 4.9: Current envelope of bonding signals for the most reliable designs

3) A number of designs such as 1, 18, 15, 23 and 22 have unstable signals during bonding. Such signal characteristics indicate inconsistent transfer of energy at the bond interface, probably resulting from changing mechanical conditions. This could be because of inappropriate levels of begin-force and touch down (pre-compression) steps. The lift-off rates during thermal cycling also confirm that the above designs are the weakest designs (see Fig. 4.10). Average lifetimes of the mentioned designs are 140, 200, 260, 420 and 460 cycles, respectively (see Fig. 4.4).

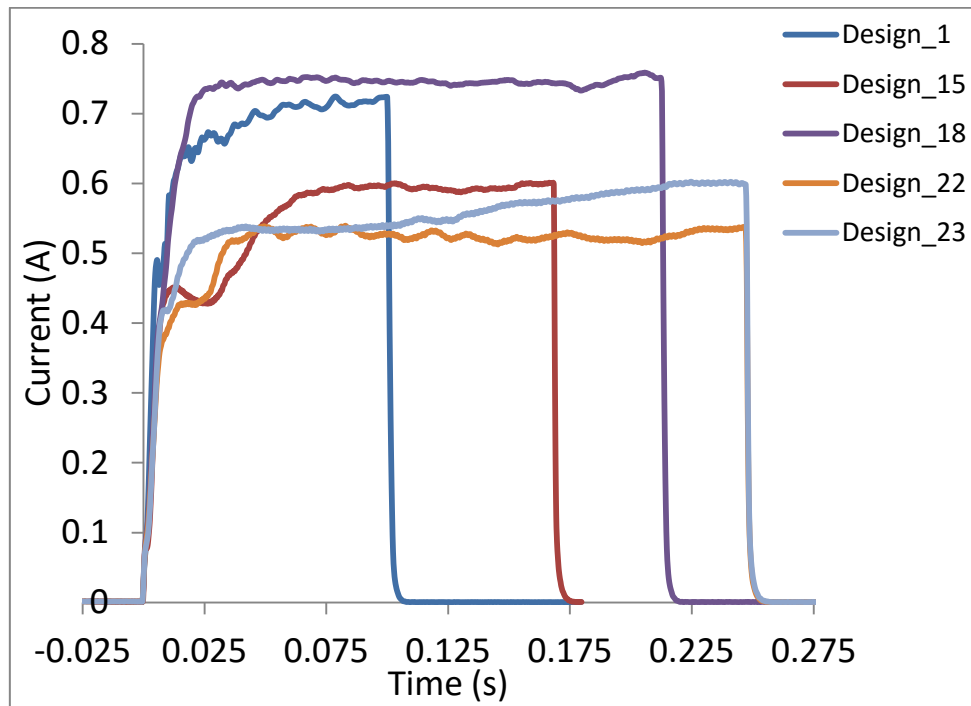


Figure 4.10: Current envelope of bonding signals for the less reliable designs

4) Interestingly, the correlation between begin-force and end-force with electrical signal can be seen clearly when begin-force value is lower than end-force, and vice versa (see Fig. 4.11). For instance, in design 14 the begin-force was set to a low value of 200 cN, the signal rose to a high level as for other weak designs, then slowly fell to a lower value and finally, after the higher end-force was applied, levelled off. This illustrates very clearly that the changing mechanical conditions at the bond foot are directly reflected in the current envelope. Results of thermal cycling and tomography confirm the importance of proper begin-force on reliability of wire bonds. As can be seen in Fig. 4.4, the bonds in designs 14 and 12 survived an average of 480 and 1000 cycles, respectively.

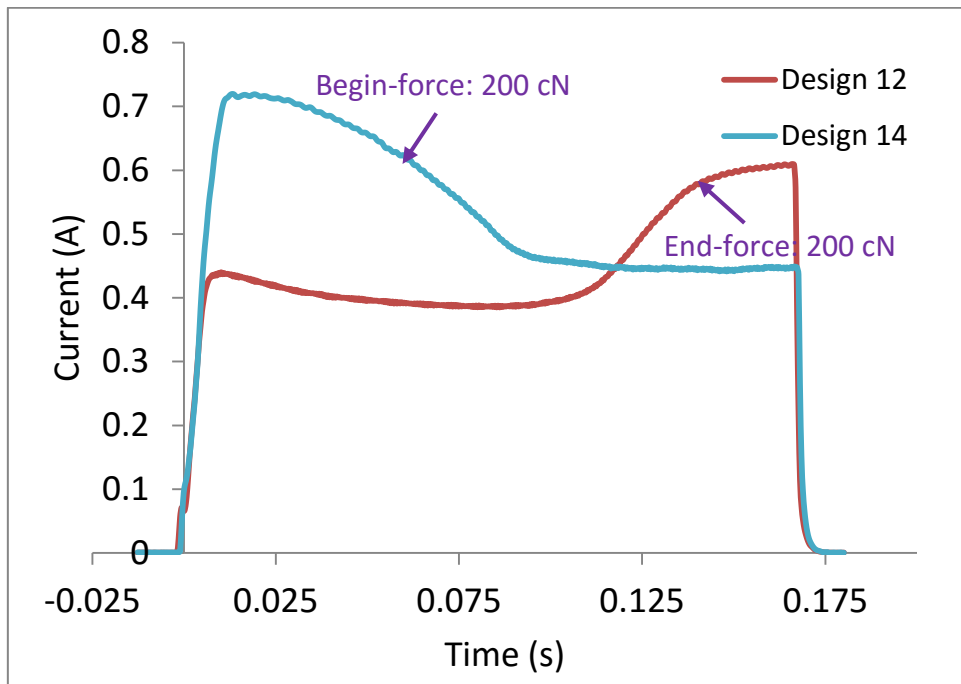


Figure 4.11: Current envelope of bonding signals for designs 14 and 12

5) Signal analysis also allows us to observe the repeatability of bonding of the different designs. For instance, as it can be seen in Fig. 4.12, design 17 shows different signals for each trial, which indicates the design is not repeatable. Entirely different lifetimes also resulted from this cohort (see Fig. 4.4). It is likely that this variability results from the low number of touch-down (TD) steps (pre-compression) used in this design.

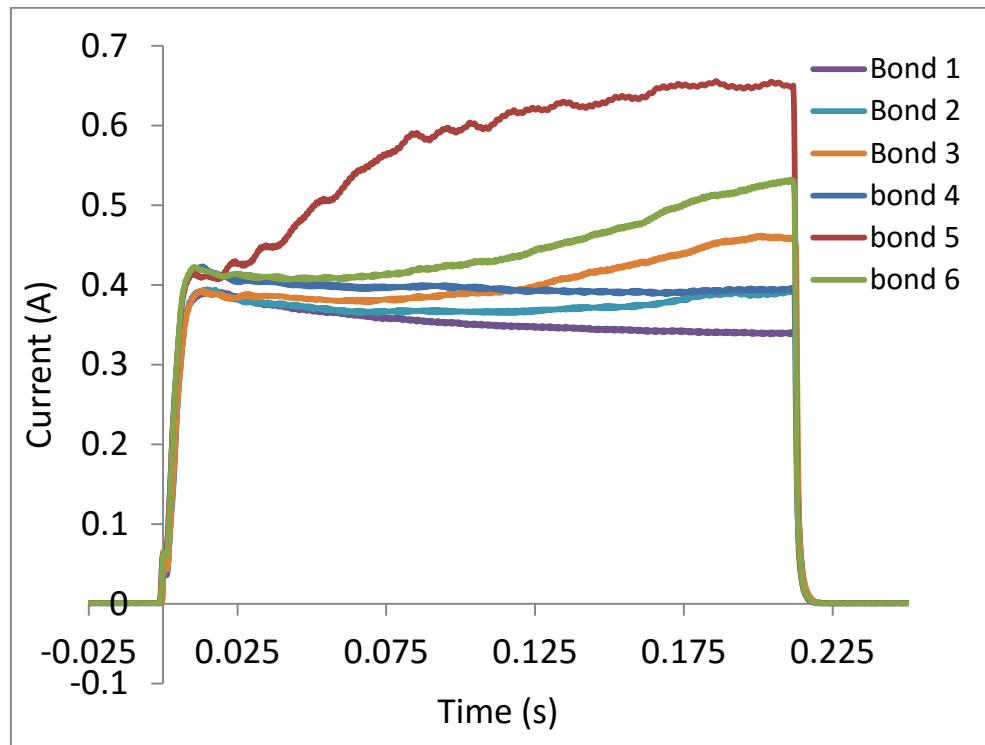


Figure 4.12: Current envelope of bonding signals for the designs 17

The above experiment has shown that bond signal analysis can facilitate the non-destructive evaluation of the effect of bonding process parameters on bonds quality. Furthermore, it allows selecting the most appropriate bonding parameter settings. For work in the subsequent chapters of this thesis, it has been decided to choose the bonding parameters that shown in Table 4.2.

Table 4.2: Bonding parameters selected for on-line quality assessment

<b>Time</b>	<b>US power</b>	<b>B-force</b>	<b>E-force</b>	<b>TD-steps</b>
250	145	400	900	100

The average predicted lifetime of these above parameters were calculated by MINITAB software (Predict Taguchi Results). The predicted value according to the lifetime results of each single design is 1604 number of cycle to failure (NCTF).

#### **4.4. Summary**

The results of X-ray tomography images of bonds indicate a strong correlation between the inferences of bond quality made from the bond signals and wire bond lifetime. In addition, the above experiments have shown that the variations in bond quality are detectable from the current envelope of ultrasonic signals. In the next chapter, the experimental procedure for on-line process monitoring using the selected bond parameter settings found in this chapter in order to establish a link between electrical signature and bond quality is described.

# **Chapter 5      Establishing the Link between Electrical Signature and Bond Quality for Lifetime Prediction of Wire Bonds**

In this chapter, the techniques for predicting the in-service lifetime of bonded wires, presented in Chapter 3 using the optimized bonding parameters described in Chapter 4. First, the quality of bonds are predicted using SDA algorithms based on signals obtained from the ultrasonic generator, then the predicted results are compared with the actual bond lifetimes under passive thermal cycling. Further, the degradation rates of two selected bond classes are investigated. Finally, the performance of the method is examined for different bond surface conditions. Details of the experimental work are given in section 5.1 and 5.2. The results and discussions are presented in section 5.3.



## 5.1. Experimental procedure

Similar to the experiments presented in Chapter 4, the substrates with solder-mounted and Silicon diode dies were supplied by Dynex Semiconductor Ltd as shown in Fig. 5.1.

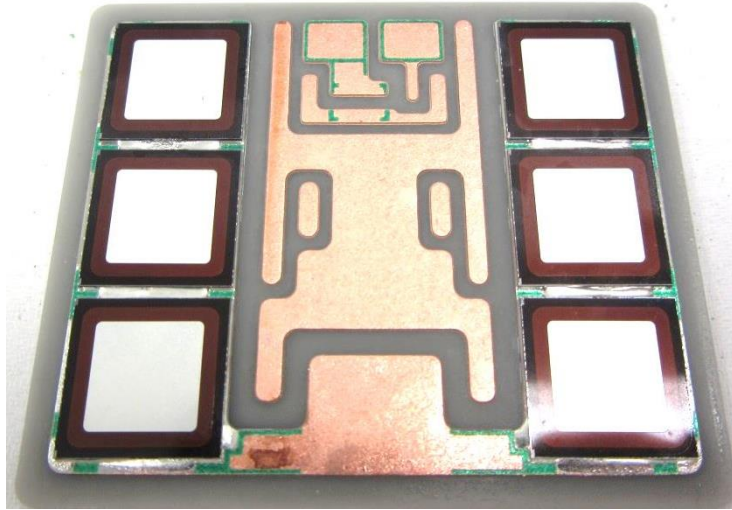


Figure 5.1: Layout for soldering silicon dies on substrate

### 5.1.1. Sample Size

For this work, the minimum sample size was determined by the Cochran method [143]. It should be noted that the formula is based on a normal approximation. Assuming the total number of bonds made on the manufacturing line in a single batch is relatively large, then:

$$n_0 = \frac{Z_{score}^2 \times (p) \times (1 - p)}{d^2} \quad (5.1)$$

Where  $n_0$  is the minimum sample size,  $Z_{score}$  is determined by the acceptable likelihood error (the abscissa of the normal curve). The value of  $Z_{score}$  is generally set to 1.96 representing a 5% level of error that gives minimum sample size with high accuracy.  $p$  is the expected prevalence or proportion (maximum variability) for a good estimation and according to Daniel et. al

[144], a good choice for  $p$  is 0.5.  $d$  is the margin of error (precision); it has been shown that if  $p$  is between 0.1 and 0.9 then  $d$  should be set to 0.05 [144].

$$n_0 = \frac{(1.96)^2 \times (0.5) \times (1 - 0.5)}{(0.05)^2} = 384.16 \sim 385$$

Therefore, the minimum sample size for the proposed method should not be less than 385 bonded wires.

### 5.1.2. Bond Parameter Settings

In total 513, 99.999% pure aluminium wires, 375  $\mu\text{m}$  in diameter, were ultrasonically bonded at room temperature onto silicon dies with a 5- $\mu\text{m}$ -thick aluminium top metallization with the selected bonding parameters described in Chapter 4 and shown in Table 5.1.

Table 5.1: Optimized bond parameter settings

<b>Time (ms)</b>	250
<b>Ultrasonic power (digits)</b>	145
<b>Bond force start (cN)</b>	400
<b>Bond force end (cN)</b>	900
<b>Touchdown steps (<math>\mu\text{m}</math>)</b>	100

Bonding loop parameters are given in Table 5.2. Bonding parameters and loop parameter settings were kept identical through all experiments.

Table 5.2: Loop parameters setting

<b>Loop mode</b>	No reverse
<b>Loop form</b>	Rectangular
<b>Z-Presign (%)</b>	45
<b>Loop Height (<math>\mu</math>)</b>	0
<b>LoopH-Fct (%)</b>	145
<b>XY LoopH-Fct (%)</b>	45

The bonds were made on substrates using the below layout shown in Fig. 5.2; a maximum 68 bonds could be made on each single substrate.

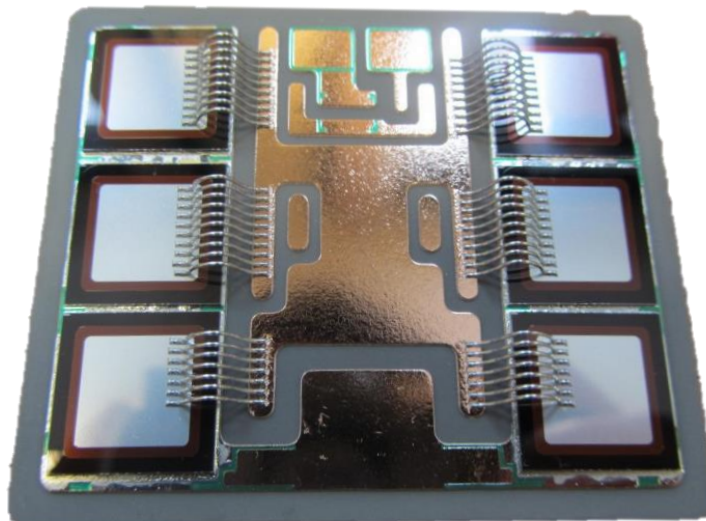


Figure 5.2: Aluminium wires bonded onto silicon dies

### 5.1.3. Signal Detection

Electrical signatures were recorded for each bond at a sampling rate of 12.5 MHz. Similar to the experiment in Chapter 4, the envelopes of the ultrasonic generator currents were computed using MATLAB codes available in Appendix I.

#### **5.1.4. Description of Samples for the Semi-Supervised Algorithm**

From the 513 bonds, 24 bonds were randomly selected for use as labelled data. 20% of all bond signals, with the exception of those used as labelled data, were randomly selected as a training set and the remaining bonds were selected for use as the test set for the SDA algorithm (see Table 5.3 for detailed information).

Table 5.3: Detailed information of the data used for the algorithm

	<b>Labelled data</b>	<b>Training set</b>	<b>Test set</b>
<b>No. of bonds</b>	24	98	391

## **5.2. Reliability Tests and Visual Observation for Bonded Wires**

The quality and lifetime of wire bonds under passive thermal cycling from -55 to +125 °C, were evaluated by means of 3D x-ray tomography and tweezer tests.

### **5.2.1. 3D X-ray Tomography**

The 24 bonds which were randomly selected for use as the labelled data were imaged in their as-bonded condition, and then after 700 cycles and 1400 cycles. It should be noted that the substrates onto which the randomly selected wires were sectioned in order to reduce their size so that tomography imaging time and resolution could be optimised.

### **5.2.2. Passive Thermal Cycling**

The samples were subjected to passive thermal cycling from -55 to +125 °C in an environmental chamber (see Figs. 3.5 & 3.6). The degradation behaviour of

the wire bonds was evaluated by measuring the reduction in bonded area using x-ray tomography virtual cross-sectional images of the same bonds in the as-bonded condition and then subsequently over their lifetime.

### 5.2.3. Tweezer Tests

The bonded wires were gently prodded with tweezers after every 100 cycles in order to detect any lift-offs and obtain a record of the lifetime of each single bonded wire.

## 5.3. Results and Discussions

The 24 bonds which were randomly selected for X-ray tomography imaging were analysed by estimating the bonded area from two dimensional virtual cross-sections of the interface in the X-Y plane. This was done using ImageJ software as described in Chapter 3. Fig. 5.3 and Fig. 5.4, respectively, show the variation in bond signal envelope of the imaged wire bonds and their bonded area, respectively.

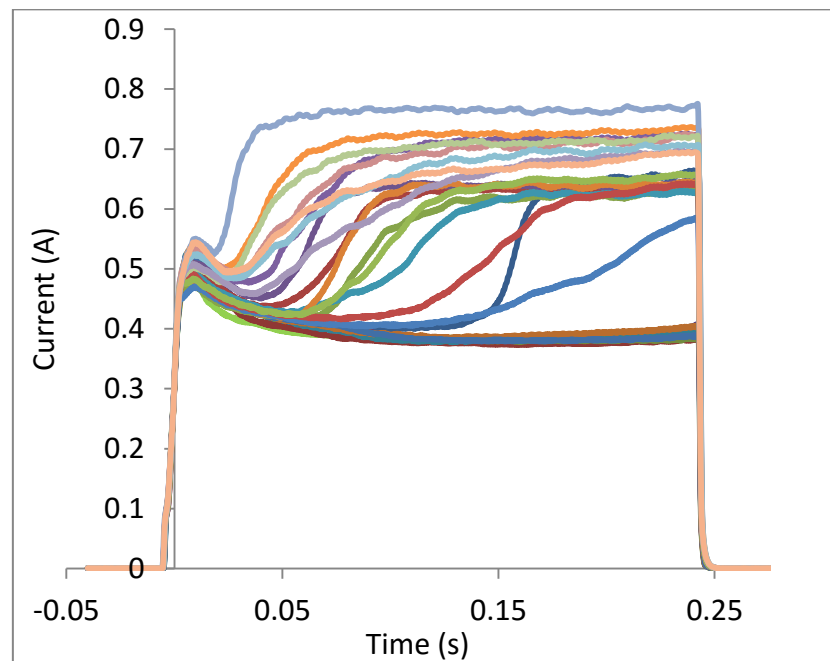


Figure 5.3: Current envelope of 24 selected bonds

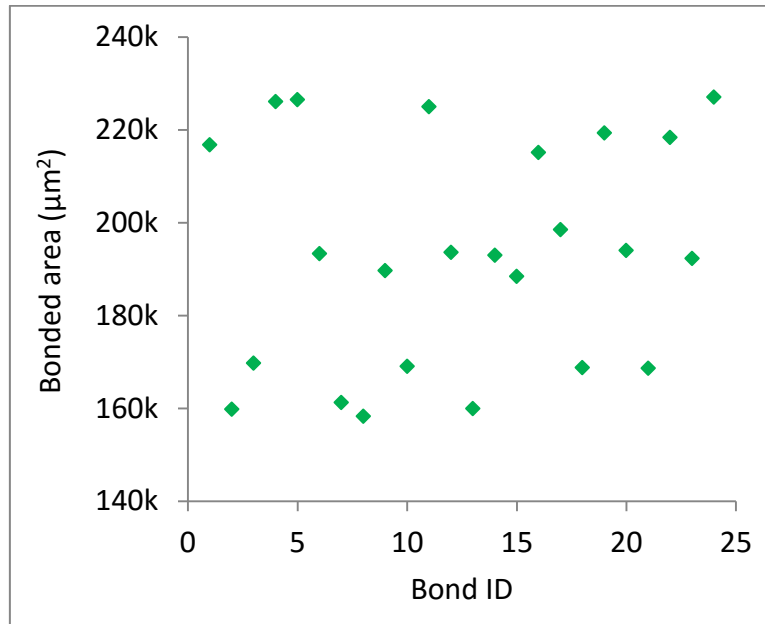


Figure 5.4: Variation in bonded area in the as-bonded condition measured by ImageJ software

According to the results of measured bonded area, the bonds' signals were classified into three classes "A", "B" and "C", and the classified signals were used as labelled signals for the semi-supervised algorithm.

- *Class A* > 20.5k bonded area (µm<sup>2</sup>)
- 17.5k bonded area (µm<sup>2</sup>) ≤ *Class B* ≤ 20.5k bonded area (µm<sup>2</sup>)
- *Class C* < 17.5k bonded area (µm<sup>2</sup>)

The bonds within class "A" had the largest bonded area and those within class "C" had the least bonded area. Fig.5.5 shows typical X-ray tomography images of the bonded area in each class. The labelled signals according to the measured bonded area are given in Fig. 5.6. As can be seen, the bonds with the largest bonded area (Class "A") have a more uniform signal shape and received a more constant level of power compared to the bonds with the least bonded area.

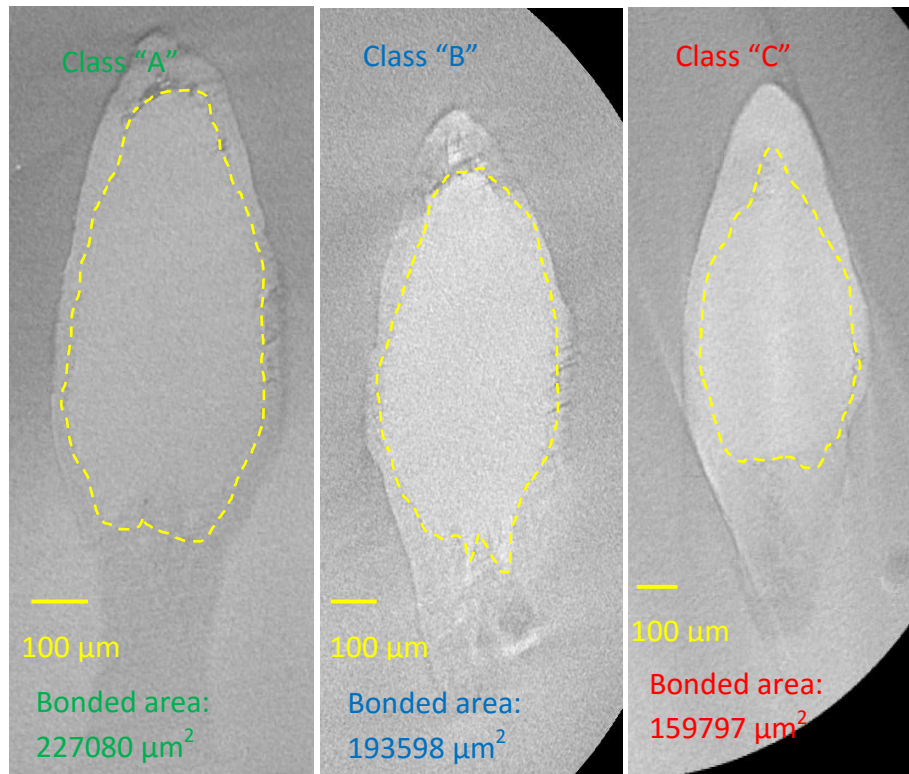


Figure 5.5: Virtual cross-sectional images in the X-Y plane of classified signals in the as-bonded condition

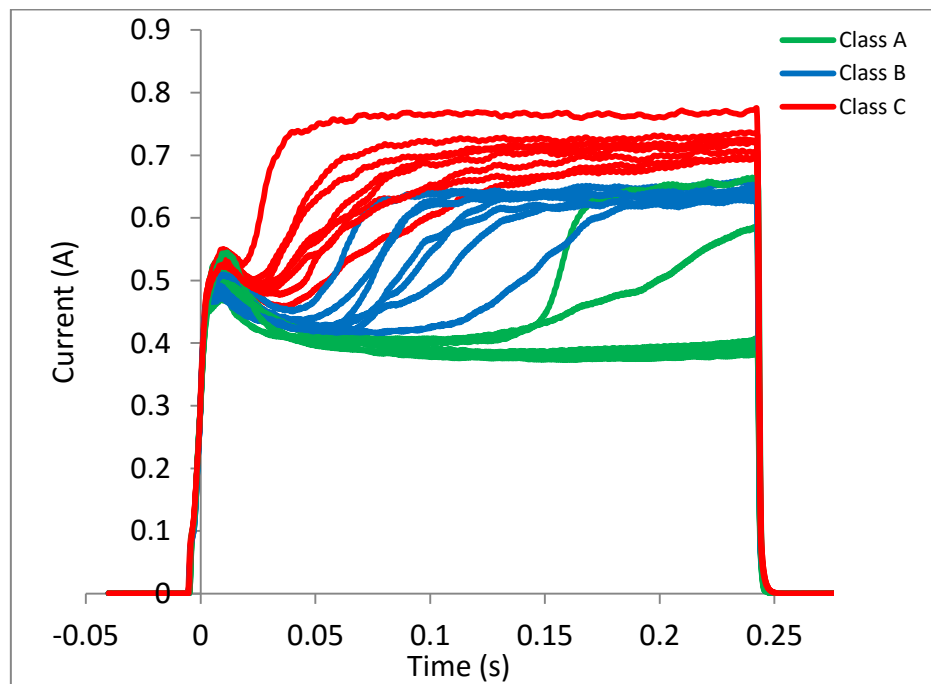


Figure 5.6: Labelled signals according to measured bonded area

### 5.3.1. Prediction of Bonds' Classes

20% of all bond signals, with the exception of those used as labelled data, were randomly selected as a training set and the remaining bonds were selected for the test set. The SDA algorithm [119] was used to predict the bonds' classes. Meanwhile all bonds were subjected to thermal cycling (-55 to +125 °C) and inspected for the occurrence of lift-offs at 100 cycle intervals. Fig. 5.7 shows that the average lifetime of the class 'A' bonds (with largest bonded area) is longer than either the class 'B' or class 'C' bonds. The results from the model classifier thus indicate a strong correlation between the inferences of bond quality made from the bond signals and wire bond lifetime.

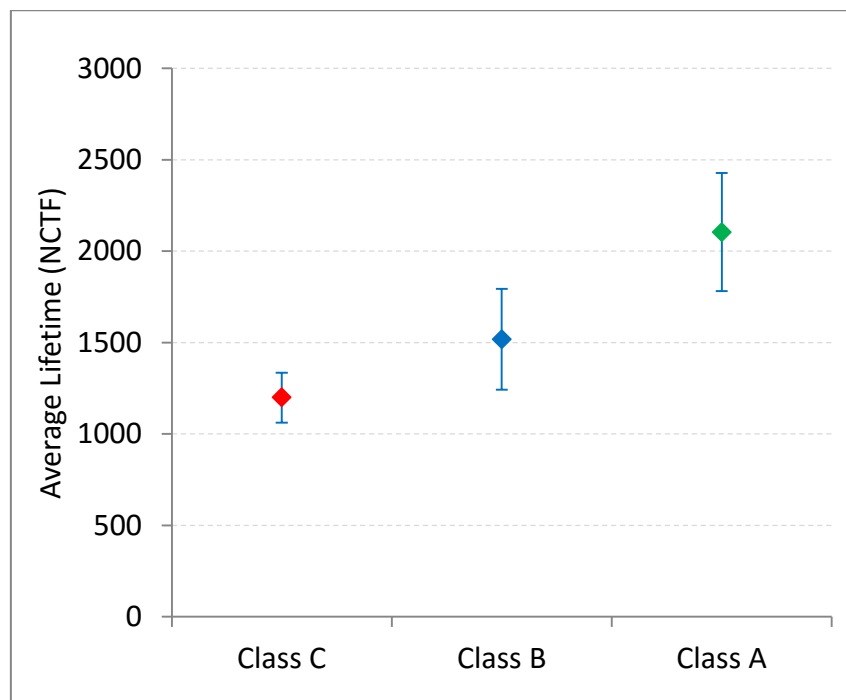


Figure 5.7: Average lifetime of predicted classes

Cumulative frequency curves for the lifetime of the three classes are shown in Fig. 5.8. Clear separation of the lifetimes of the three classes can be observed, the onset of lift-off for class "A" bonds being almost a factor of two higher than for those in class "C".



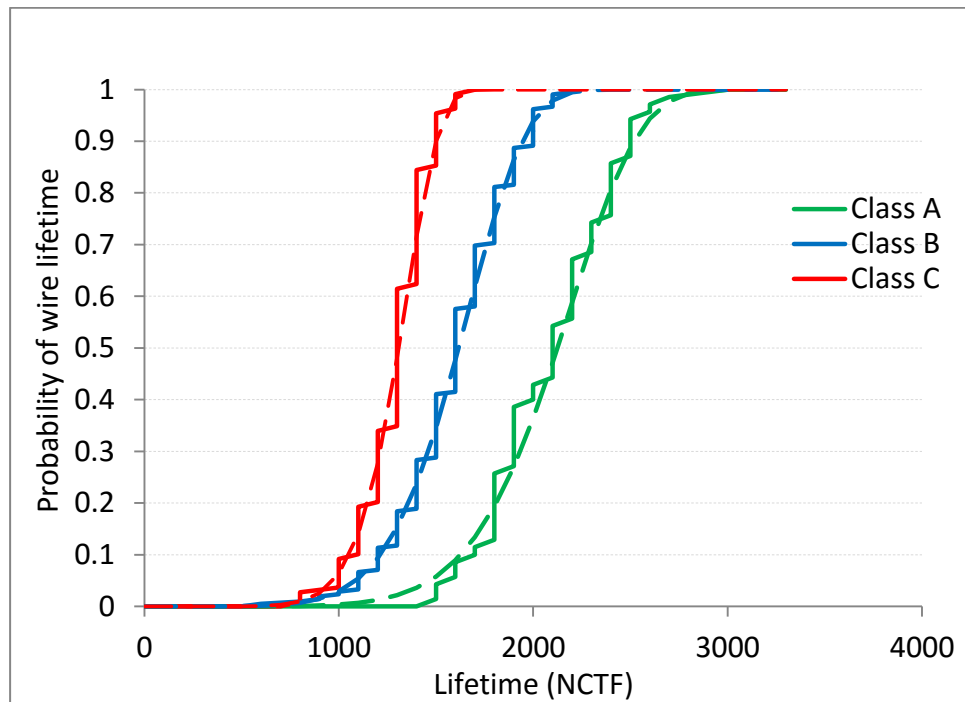


Figure 5.8: Cumulative frequency curve of three classes

The data were analysed using a one-way Analysis of Variance (ANOVA) by MINITAB software to perform hypothesis tests to determine whether the means of the three classes differ. In ANOVA, the most important statistic is P-value. The results one-way ANOVA shown in Table 5.4 confirm a significant difference in lifetime of wire bonds among the three classes since, p-value is less than the  $\alpha$ -level which is 0.05. This affirms the suitability of the method for monitoring the quality of the bonding process. The Individual 95% confidence interval for mean of three classes also is given in Table 5.5. The details of contents in ANOVA table (Table 5.4) are given in Appendix III.

Table 5.4: One-way ANOVA for wire bonds lifetime data

Source	SS	DF	MS	F	P-value
Class	27862909	2	13931454	198.24	0.000
Error	27566861	388	702775		
Total	55129770	390			
S = 265.1    R-Sq=50.54%    R-Sq(adj)=50.29%					

Table 5.5: Individual 95% confidence interval for mean of wire bonds lifetime data

Individual 95% CIs For Mean Based on Pooled StDev			
Level	Mean	StDev	
1	2100.0	320.3	(-*)
2	1594.8	283.5	(-*)
3	1291.7	172.7	(-*)

### 5.3.2. Setting Target for On-Line Monitoring Assessment

High product quality requires continuous monitoring and well-controlled manufacturing. In our case, the proposed method can automatically predict the class of individual bonded wires and hence the expected life. However, arbitrary target limits need to be set in order to predict process performance. One of the advantages of setting target is that the detection technique would be very easy to understand and use. Below, an example of setting a target limits for each different class is given (see Fig. 5.9).

- *Class A > 1800 cycles*
- *1400 cycles ≤ Class B ≤ 1800 cycles*
- *Class C < 1400 cycles*

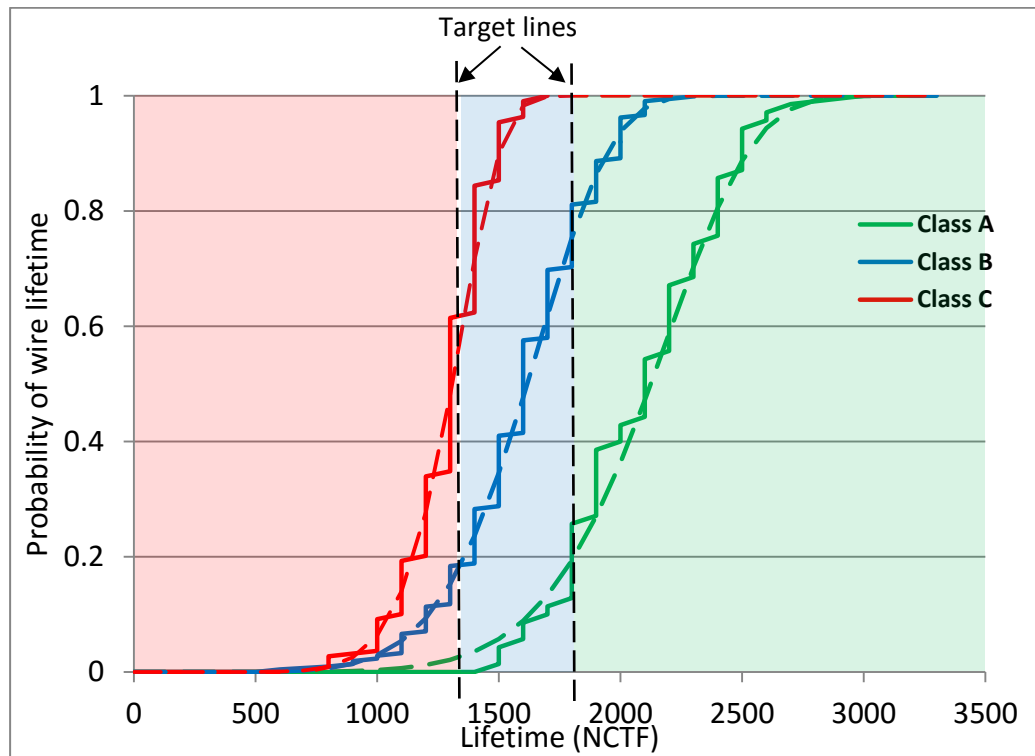


Figure 5.9: Using arbitrary limits for the on-line process monitoring technique

The target limits represent the variation in the process performance which allows us to understand the process capability, to detect process improvement/malfunctions and to take appropriate action when the process makes weak bonds continuously. In next section, the classifier performance is evaluated using the above target limits.

### 5.3.3. Model Performance Evaluation

The performance of a classification algorithm is a complex and open problem to debate although it is most commonly defined in terms of accuracy[145]. The assessment of accuracy is an important part of any classification process and it is usually assessed by comparing the predicted classes computed using the classification algorithm with the real/reference data. Commonly, accuracy is evaluated using an error matrix. The error matrix is a table which is often used to describe the performance of a classifier[146].

### 5.3.3.1. Accuracy

In our case, we have the predicted class of the 391 bonds of the test set and their actual lifetimes (i.e. number of cycles to failure). The error matrix of the model classifier considering actual lifetimes can be determined based on the target limits set in section 5.3.2 (see Fig. 5.9).

- *Class A > 1800 cycles*
- $1400 \text{ cycles} \leq \text{Class B} \leq 1800 \text{ cycles}$
- *Class C < 1400 cycles*

Table 5.6: The error matrix of the bond quality classifier

		Actual lifetime data			
		A	B	C	Sum
Predicted classes	A	82	31	0	113
	B	8	137	17	162
	C	0	30	86	116
	Sum	90	198	103	<b>391</b>

From the above matrix, the overall accuracy of the model can be derived by the sum of all correct classified bonds over the total number of bonds.

$$Accuracy = \frac{82 + 137 + 86}{391} = 78.00\%$$

The value of the overall accuracy can, however be misleading and does not represent the effectiveness of a classifier in an individual class. In order to estimate the performance of the classification method concentrating on the individual class, precision and recall are the best performance measures [147].

### 5.3.3.2. Precision and Recall

Originally, Kent et al. defined precision and recall in the area of information retrieval. Both terms can show the effectiveness of the predictions in a model classifier [148].

The precision of individual classes can be derived as the number of correctly predicted bonds over the total number of predicted bonds in that class. The individual precision of the bonds classes are given in Table 5.7.

$$Precision_{class "A"} = \frac{82}{90} = 91\%$$

Table 5.7: Precision value for each class

Precision [%]		
Class "A"	Class "B"	Class "C"
0.91	0.69	0.83

The recall value can be derived as the total number of correctly predicted bonds over the total number of actual bonds in each class. The individual recall values of the bonds classes are given in Table 5.8.

$$Recall_{class "A"} = \frac{82}{113} = 84\%$$

Table 5.8: Recall value for each class

Recall values [%]		
Class "A"	Class "B"	Class "C"
0.72	0.84	0.74

Ideally, a good model can be described with high precision and high recall values. Overall, the model shows precision and recall values above 69% for individual classes.

### 5.3.4. Estimating Die/Substrate/Module Life from Wire Bond Process Classifier Data

In robust process design and control, not only setting a target life but also the maximum allowable probability of not reaching the target life is necessary. In this part, estimating die/substrate/module life from wire bond process classifier data is presented.

#### 5.3.4.1. Assumptions and Models for Life Expectancy

As mentioned earlier, wire bonds are classified into one of three classes: “A”, “B” and “C”. The lifetime statistics of each of these classes is described by a cumulative probability distribution that approximates a Weibull distribution (see Fig. 5.8). Each wire is assumed to behave independently of the others i.e. the failure of a one wire does not affect the life of any of the others.

For a die with a number of wires bonded onto it is desired to determine the life expectancy or probability of failure after a prescribed number of thermal cycles, since the class of each bond is known. For the purposes of this analysis, it is considered the case where each bond wire has a single bond on the die surface (i.e. no stitch bonds). Then it is assumed that the die interconnect has failed when more than a certain number of the wires have failed. Let’s define this number to be  $N_f$ .

For any die, it is assumed a total of  $N$  bonds of which  $n_A$  are in class “A”,  $n_B$  are in class “B” and  $n_C$  are in class “C”. The respective cumulative probabilities of failure, as a function of thermal cycles, for each of the wires in each of these classes, are given respectively by  $P_A$ ,  $P_B$ , and  $P_C$ .

It is determined the probability of failure of a given sample of the wires on the die by considering the probability of failure of each of those wires in the sample and the probability that all other wires have not failed. Within the sample, the number of wires in class “A” is  $a$ , the number of wires in class “B”

is  $b$  and the number of wires in class “C” is  $c$ , based on binomial probability formula:

$$p_B^b (1 - P_B)^{(n_B - b)} p_{abc} = \frac{n_A!}{a! (n_A - a)!} \frac{n_B!}{b! (n_B - b)!} \frac{n_C!}{c! (n_C - c)!} p_A^a (1 - P_A)^{(n_A - a)} p_C^c (1 - P_C)^{(n_C - c)} \quad (5.2)$$

### 5.3.4.2. Wire Bond Failure on a Single Die

To determine the probability of die interconnect failure, it is needed to determine the probability that more than a given number of wires has failed. First, it is considered the possible combinations of wire failures from each of the classes that can result in a given total number of wire failures,  $m$ , (i.e. all the possible wire samples that contain a total of  $m$  wires are selected) and sum the probabilities to find the probability of an  $m$ -wire failure:

$$p_m = \sum_{a=0}^{n_A} \sum_{\substack{b=0 \\ a+b+c=m}}^{n_B} \sum_{c=0}^{n_C} \frac{n_A!}{a! (n_A - a)!} \frac{n_B!}{b! (n_B - b)!} \frac{n_C!}{c! (n_C - c)!} p_A^a (1 - P_A)^{(n_A - a)} p_B^b (1 - P_B)^{(n_B - b)} p_C^c (1 - P_C)^{(n_C - c)} \quad (5.3)$$

Next we determine the cumulative probability of there being up to  $N_f$  wire failures on the die.

$$p_{N_f} = \sum_{m=0}^{N_f} p_m \quad (5.4)$$

Finally, the probability of there being more than  $N_f$  wire failures on a die is

$$1 - p_{N_f}.$$

### 5.3.4.3. Substrate Tile Failure

Different dies will have different populations of the wire bond classes and so the probability of failure will in general be different for each die. If it is desired to calculate the probability of failure of a substrate containing say  $M$  dies we can determine this through the probability that no dies have failed:

$$p_{sf} = 1 - p_{\text{no die failures}} \quad (5.5)$$

$$p_{sf} = 1 - \prod_{i=1}^M p_{N_{fi}} \quad (5.6)$$

### 5.3.4.4. Module Level Failure

The method for determining the probability of substrate tile failure can be extended to module level assuming that the failure of a single substrate tile will result in failure of the module.

### 5.3.4.5. Example

Consider a die with 8 wire bonds with a mixture of class “A” & “C” bonds. Table 5.9 shows the probabilities of failure determined for the die as a function of the number of class “C” bonds for several failure criteria when the target life is 1500 cycles (using data from Fig. 5.8/Fig. 5.10b). The final column shows the probability of failure of a substrate with 6 dies using a failure criterion of > 2 wire failures for each die. The impact of the number of class “C” bonds on the probability of failure after 1500 cycles is dramatic.



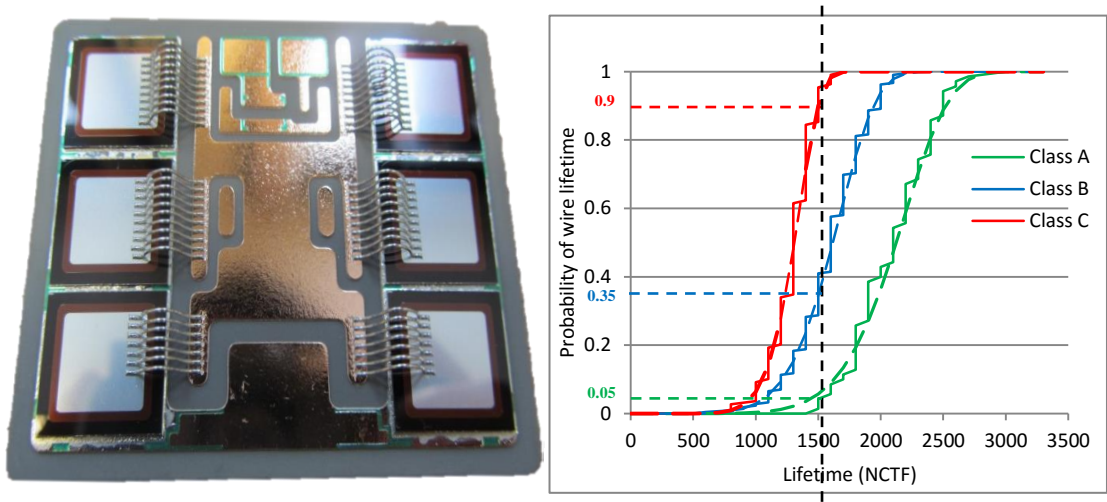


Figure 5.10: a) A typical substrate tile, b) cumulative frequency curve

Table 5.9 : Example of probabilities of failure for eight wires mix of class “A” and class “C”

8 wires mix of class “A” and class “C”						Substrate
number “C”- class	p >0 wire failures	p > 1	p > 2	p > 3	p > 4 lifts @ 1500 cycles	6 dies p>2
0	0.33658	0.057245	0.005788	0.000372	1.54E-05	0.034231
1	0.930166	0.275934	0.040318	0.003401	0.000175	0.218798
2	0.992649	0.858011	0.220497	0.026949	0.001822	0.77566
3	0.999226	0.978131	0.784582	0.170435	0.016752	0.9999
4	0.999919	0.996969	0.956766	0.710873	0.125814	1
5	0.999991	0.999604	0.992599	0.928996	0.637808	1
6	0.999999	0.99995	0.998849	0.985575	0.895367	1
7	1	0.999994	0.999832	0.9974	0.975457	1
8	1	0.999999	0.999977	0.999568	0.994976	1

Table 5.10 gives values for the same set of conditions but this time with a mixture of class “A” & “B” bonds. Although less dramatic than that observed for the class “C” bonds, the impact of the class “B” bonds on die and substrate lifetime is still highly significant.

Table 5.10: Example of probabilities of failure for eight wires mix of class “A” and class “B”

8 wires mix of class “A” and class “B”						Substrate
Number “B”- class	p > 0	p > 1	p > 2	p > 3	p > 4 lifts @ 1500 cycles	6 dies p>2
0	0.33658	0.057245	0.005788	0.000372	1.54E-05	0.034231
1	0.546081	0.134429	0.017975	0.001441	7.17E-05	0.10312
2	0.689424	0.25688	0.048305	0.005066	0.000313	0.257006
3	0.7875	0.388311	0.107254	0.015618	0.001259	0.493746
4	0.854606	0.510839	0.18956	0.040224	0.004498	0.716648
5	0.90052	0.61698	0.28543	0.082337	0.013563	0.866872
6	0.931934	0.704866	0.385505	0.141204	0.032183	0.946159
7	0.953429	0.77544	0.482641	0.213239	0.062819	0.980824
8	0.968136	0.830873	0.572186	0.293601	0.106091	0.993869

#### 5.3.4.6. Determining expected life at die, substrate or module level

The expressions for the probabilities of failure are functions of the cumulative probability density functions for each of the wire classes which are, themselves defined as functions of the number of thermal cycles. Each of the expressions can therefore be inverted (numerically) to determine the life in cycles for a given probability of failure.

#### 5.3.5. Determination of Degradation Rate

The bonds randomly selected for X-ray tomography were imaged at zero cycles (in the as-bonded condition), 700 cycles and 1400 cycles. The reduction of bonded area was measured to obtain the rate of degradation for the different classes. Fig. 5.11 & Fig. 5.12 show the results for both two classes of bonds. In the as-bonded condition, the bonds attached from the middle and significant pre-cracks appear around the edge and in particular at the toe and heel of the bonds. After 700 cycles, cracks have started to grow inwards from the edge

and micro-voids have begun to coalesce. After 1400 cycles, the bond has almost lifted off as illustrated in the X-Z plane image inset in Fig. 5.11.

Fig. 5.12 shows that in the as-bonded state the bonds in class “A” have a more uniform shape compared to those in class “C”. Again, pre-cracks are evident around the edge of the bond and in particular at the heel and toe. After 1400 cycles micro-voids have started to join together. The rate of degradation, for all bonds were measured in terms of the remaining bonded area, for both classes is shown Fig. 5.13. The results indicate that both classes degrade at almost the same rate, although the initial bonded area of the class “A” bonds is significantly higher, leading to longer life.

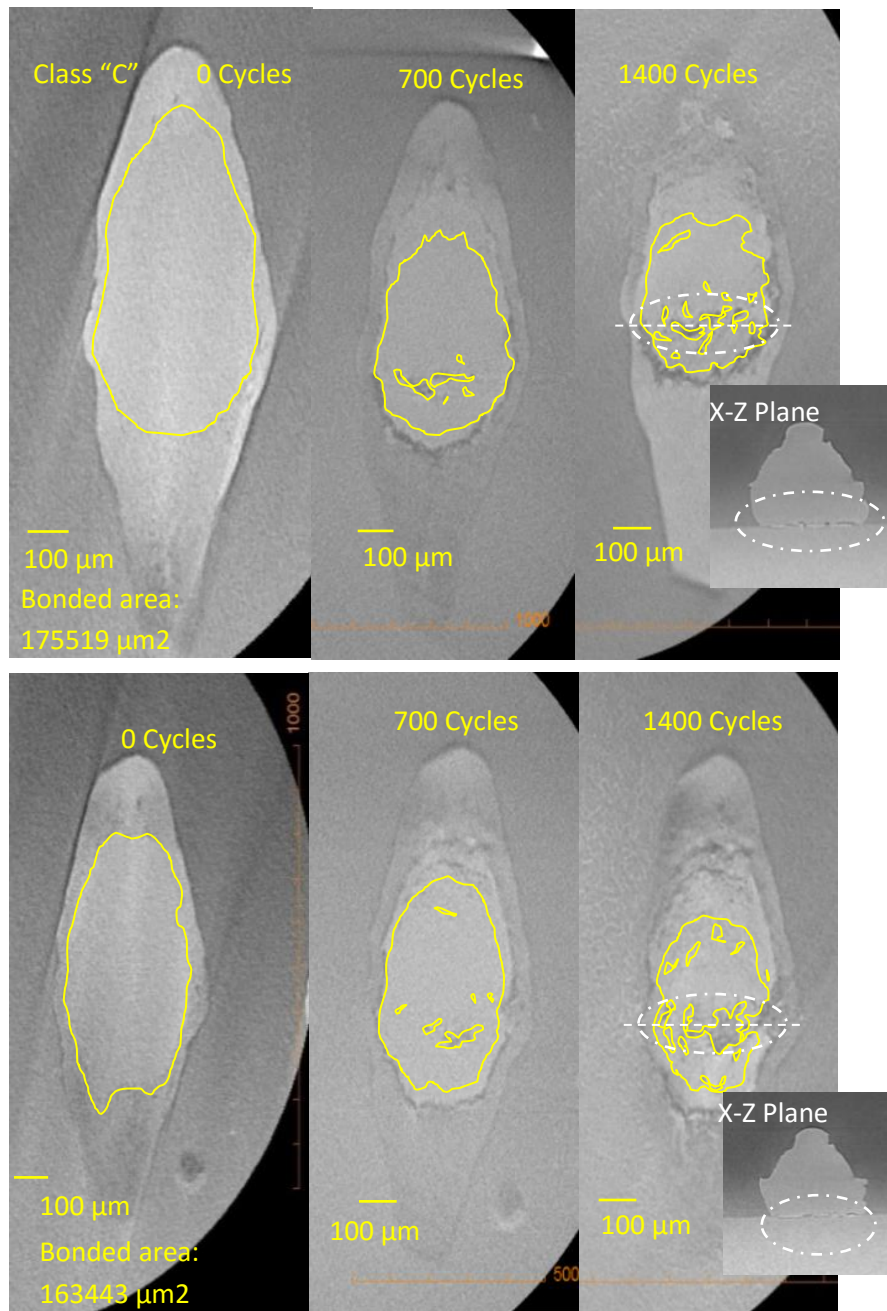


Figure 5.11: Virtual cross-section images of two bonds in class "C" in X-Y plane in as-bonded condition, 700 cycles and 1400 cycles

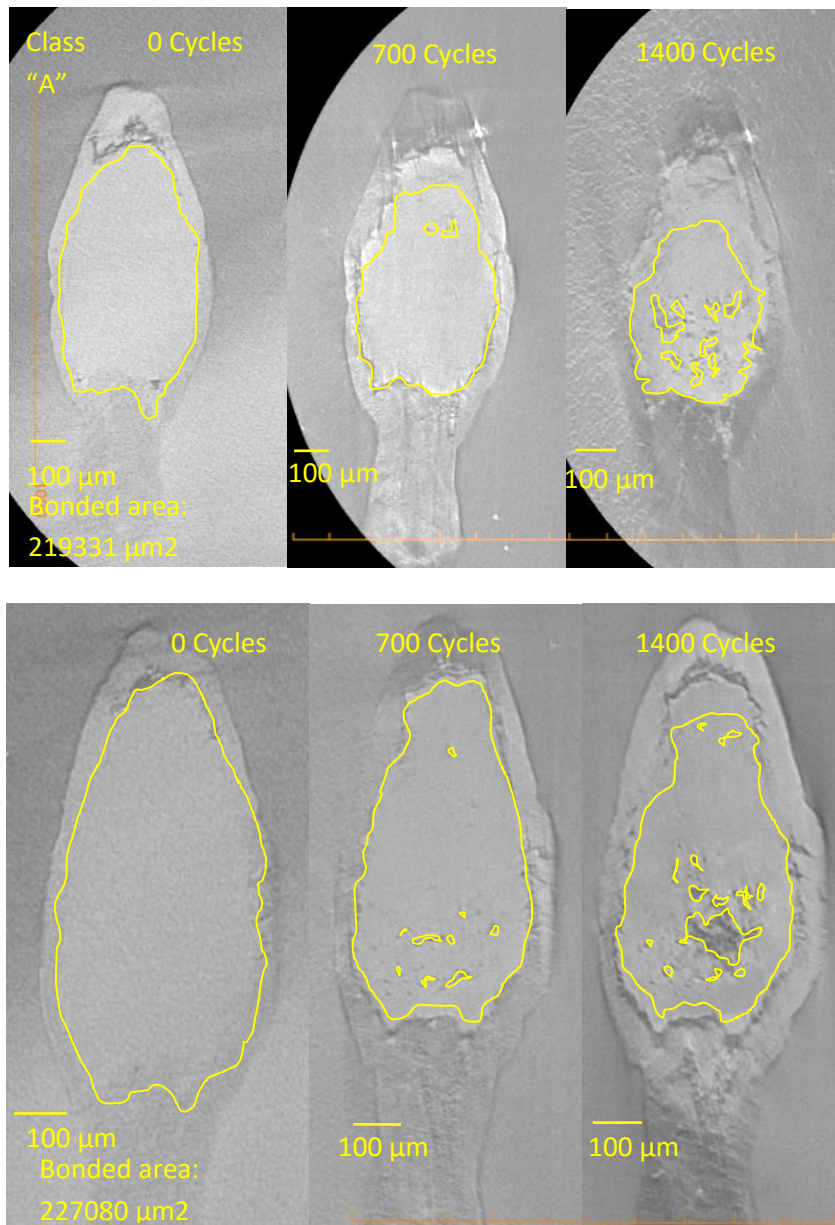


Figure 5.12: Virtual cross-section images of two bonds in class "A" in X-Y plane in as-bonded condition, 700 cycles and 1400 cycles

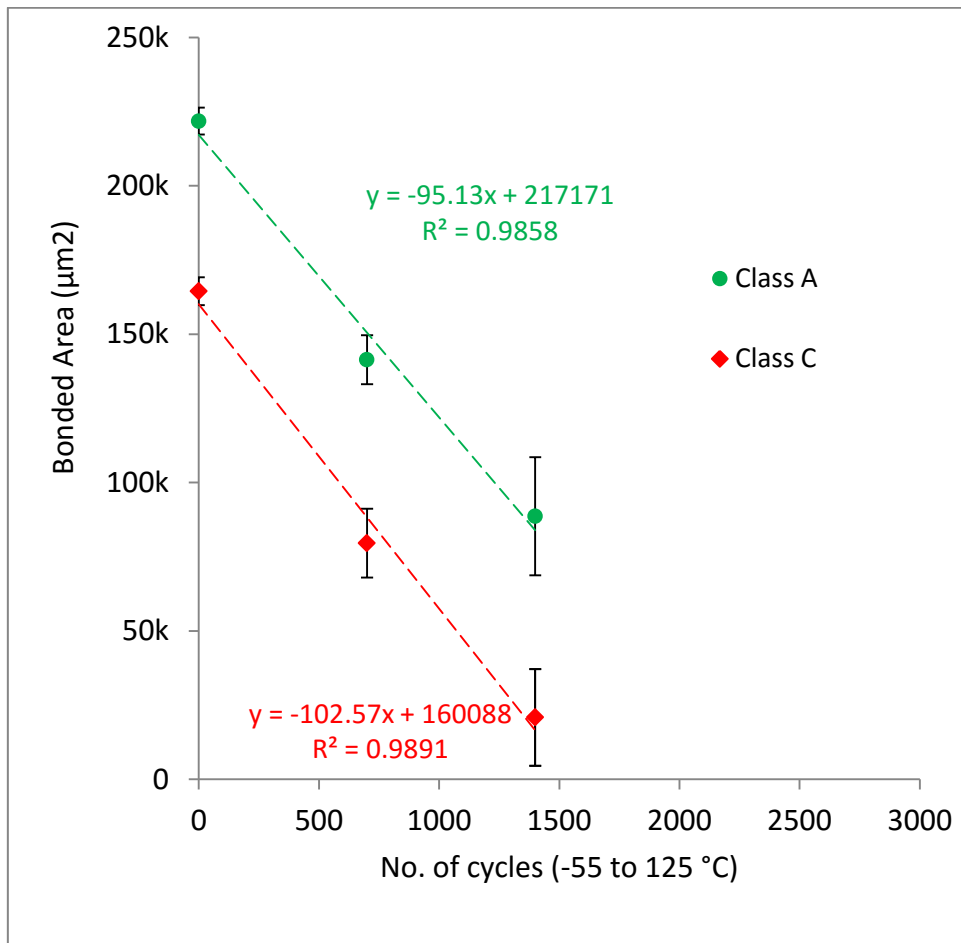


Figure 5.13: Bonds degradation rate in class “A” and “C”

The estimated lifetime from the linear regression lines in Fig. 5.13 agree very well with the actual average lifetime of the predicted class “A” in Fig. 5.7 (see Table 5.11). In Class “C”, there is a bit difference between the estimated lifetime and the actual average lifetime. This might be because bonds with very small bonded area are prone to lift-off as a result of gentle prodding with the tweezer. Therefore, it might be a reason that the actual (tweezer test) lifetime is less than the lifetime estimated from the residual bonded area.

Table 5.11: Details of actual and lifetime values for class “A” and “C”

	Class “A” (NCTF)	Class “C” (NCTF)
<b>Actual Lifetime</b> (see Fig. 5.7)	2104	1198
<b>Estimated Lifetime</b> (see Fig. 5.13)	2278	1560

### 5.3.6. Surface Treatment

Evidence from previous work obtained from the literature confirms that appropriate surface treatment prior to wire bonding improves wire bonding strength by removing contamination [42-45]. In this work, we also checked the performance of the presented method for three different bond pad conditions, namely: freshly manufactured dies with plasma cleaning (condition “i”), freshly manufactured dies without plasma cleaning (condition “ii”) and manufactured dies which had been stored in a argon purged cabinet for 4 days at room temperature (condition “iii”).

The freshly manufactured dies were taken and plasma cleaned for 15 minutes with argon. Immediately after etching, 59 bonds were made on the clean devices. Fig. 5.14 shows the envelope of current signals for the bonded wires.

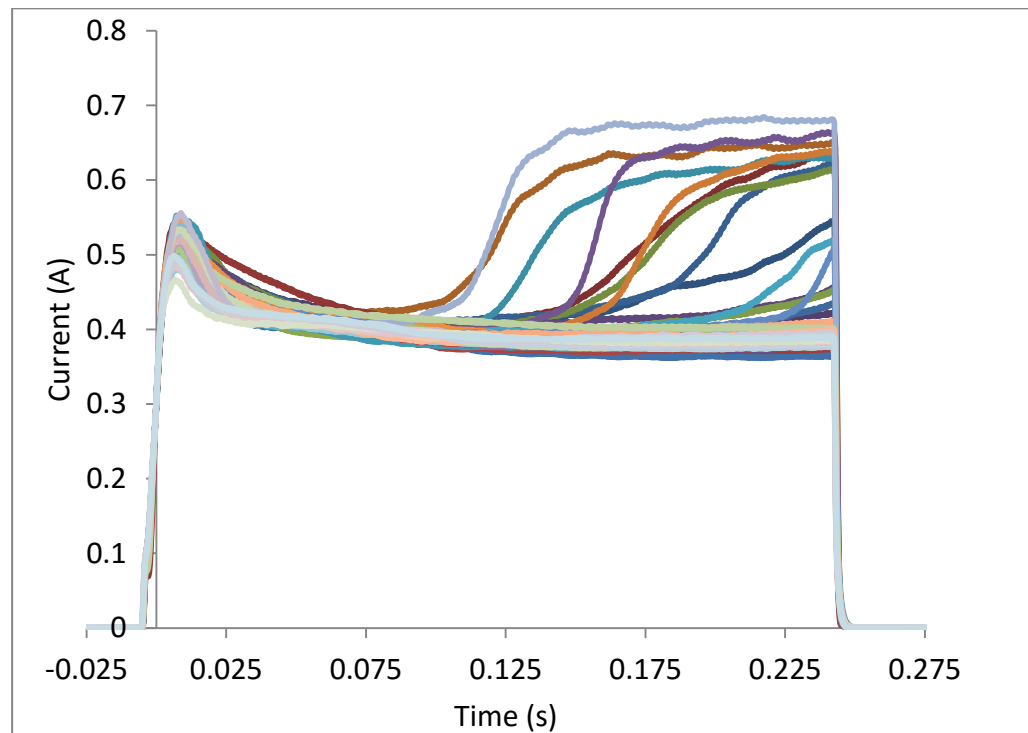


Figure 5.14: Envelope of current signals of plasma cleaned sample (condition “i”)

As can be seen in Fig. 5.14, most of the bonds received a constant level of power which indicates consistent mechanical conditions at the bond foot.

Then, freshly manufactured dies were bonded. The envelope of the signals of 65 bonds indicates greater inconsistency in transferring energy compared to the plasma cleaned sample (see Fig. 5.15). This could be because of the presence of contamination and or oxide on the top of the die's surface.

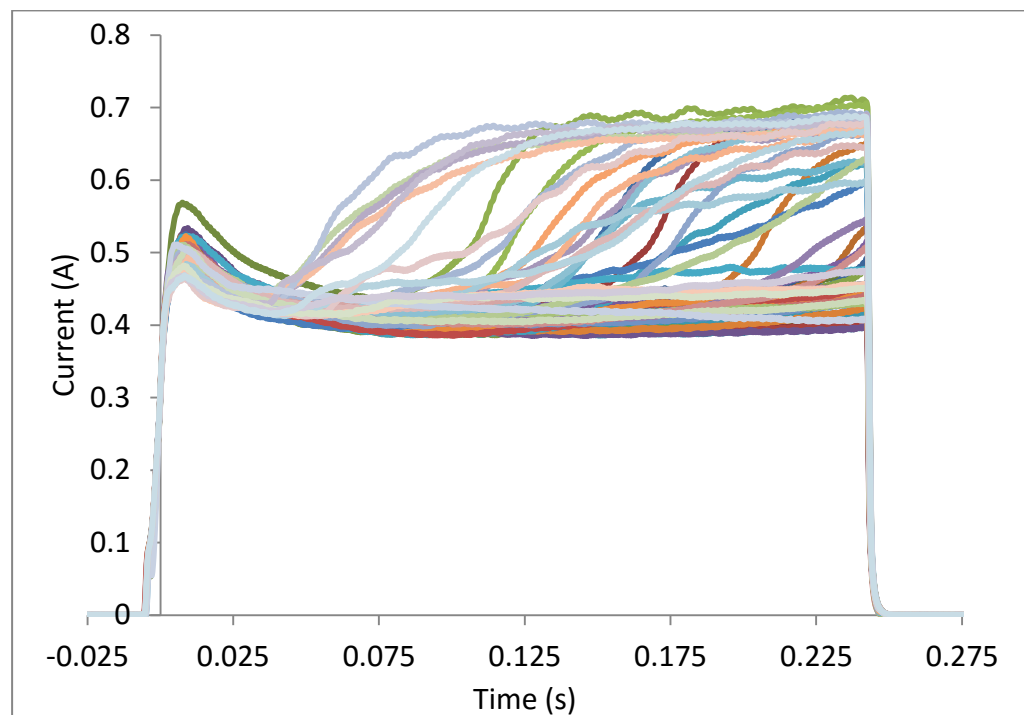


Figure 5.15: Envelope of current signals of freshly manufactured sample without plasma cleaning (condition “ii”)

Next, 63 bonds were made on dies which were kept in the argon cabinet for 4 days. The envelopes of signals show significant differences compared to the plasma-cleaned and freshly manufactured (see Fig. 5.16). Signal characteristics indicate inconsistent transfer of energy at the bond interface, which might indicate changing mechanical conditions at the interface during bonding.



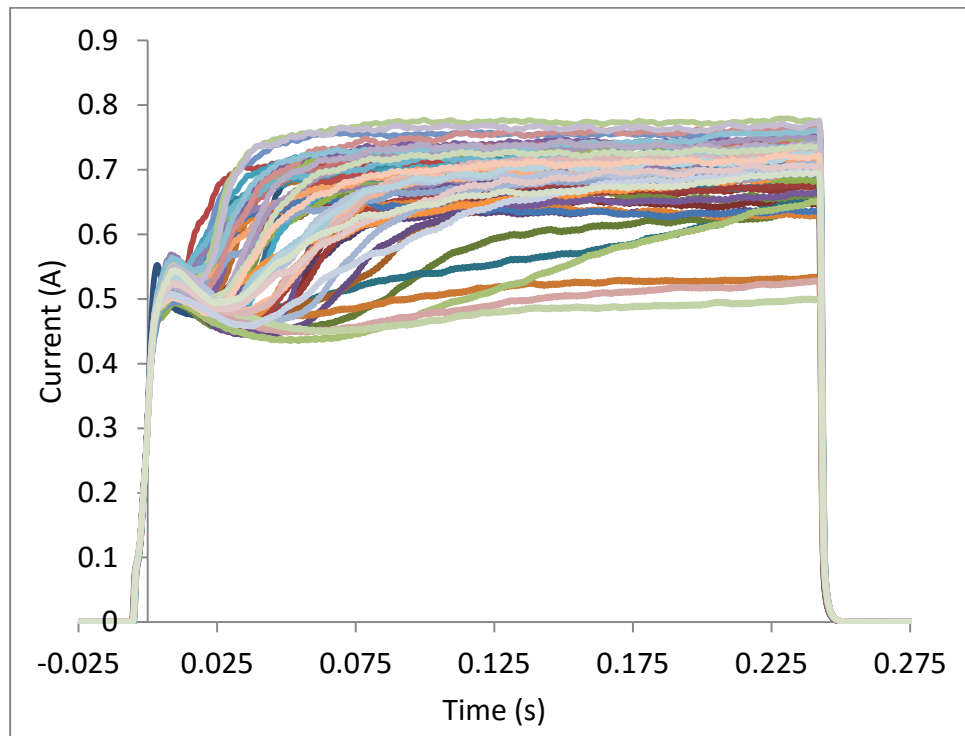
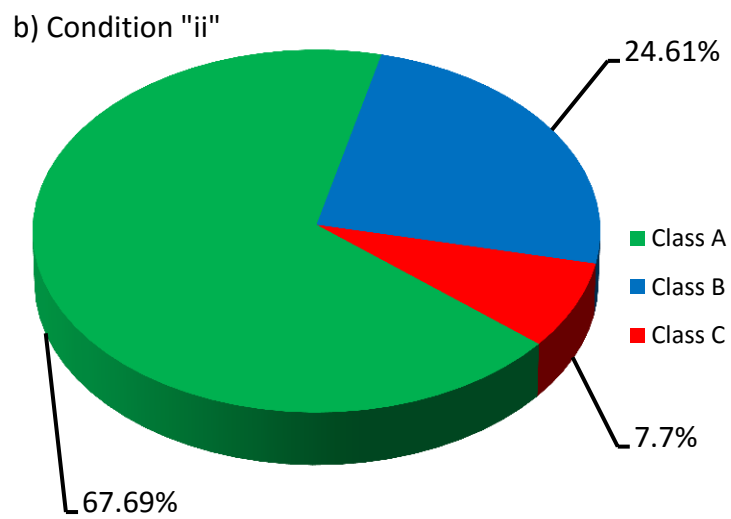
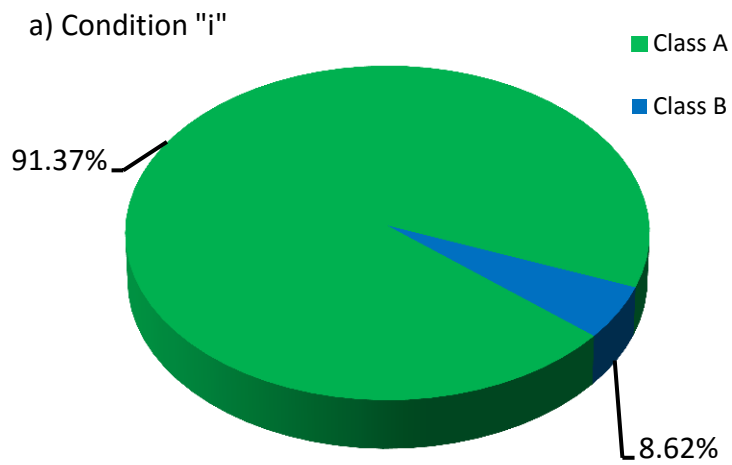


Figure 5.16: Envelope of current signals of manufactured dies which were kept in argon purged cabinet for 4 days (condition “iii”)

The signals of three different bond conditions were fed into the SDA classifier algorithm in order to predict the class of bonds. This is illustrated in Fig. 5.17, which shows the effect of bond surface condition on bond quality. The results show that the plasma cleaned samples contain no class “C” bonds, in other words no weak bonds. This also confirms the work of Nowfult et al. that plasma cleaning can provide the best wire bonding quality [42]. The results from the stored samples condition clearly illustrate how bond quality is reduced due to using ‘old’ dies.



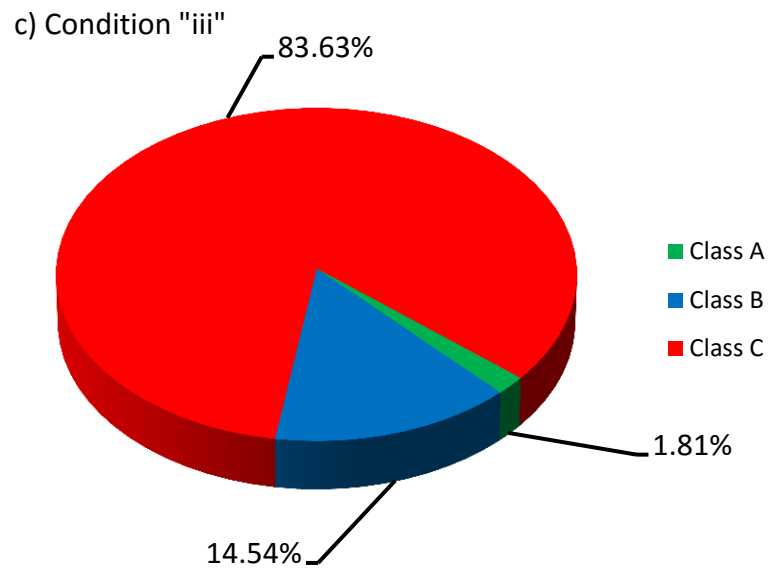


Figure 5.17: Classification results in a) using fresh and plasma cleaned dies, b) fresh and without plasma cleaning c) old dies (stored for 4 days in purged cabinet) and without plasma cleaning

Following bonding, all samples were subjected to passive thermal cycling, and the lifetime of each bond was determined with tweezer test. Fig. 5.18 shows the average lifetime of the bonded wire vs. bond pad condition. The result shows plasma-cleaned samples have longer life in average compare to the other bond pad conditions.

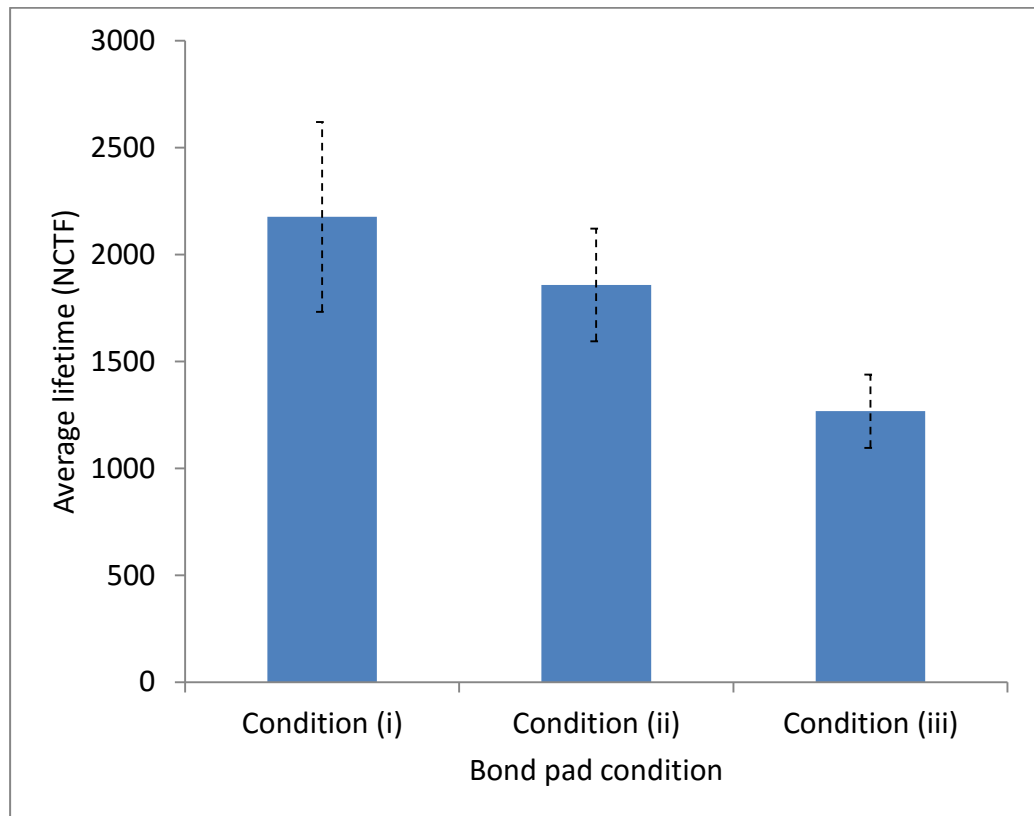


Figure 5.18: Average lifetime of wire bonds in different bond pad conditions

#### 5.4. Summary

Overall, the method for bond quality assessment proposed in this work has been shown to be capable of distinguishing between the differing levels of bond quality expected within a batch of bonds exhibiting typical variation which are not solely due to the wire bonding machine and its parameters, but also due to other factors, including the condition of bond surface such as cleanliness of die surface, freshness of die and bonding environment condition.

Although the lifetime of the predicted classes of bond quality show some variation, especially in bonds classified as class “A”. However, the classification is strong enough to demonstrate that the bonds may be separated into different quality groups for the purposes of on-line quality monitoring and evaluation of the wire bonding process. In addition, it is important to note that

the accuracy of prediction of the model classifier can be improved by adding more labelled signals and increasing the size of the training set.

In this chapter, a non-destructive on-line technique for detecting the quality of ultrasonically bonded wires by application of a semi-supervised algorithm to process signals obtained from the ultrasonic generator was presented. The role of the semi-supervised algorithm was to find the best model classifier using labelled data and a training set.

Experimental tests verified that the classification method is capable of accurately predicting bond quality, indicated by bonded area measured by X-ray tomography. Samples classified during bonding were subjected to temperature cycling between  $-55^{\circ}\text{C}$  and  $+125^{\circ}\text{C}$  and the distribution of bond life amongst the different classes analysed. It is demonstrated that the as-bonded quality classification is closely correlated with thermal cycling life and can therefore be used as a non-destructive tool for monitoring bond quality and predicting useful service life.

The remaining useful life of die/substrate/module from as-bonded condition can be determined using the presented probabilistic assessment method.

In the next chapter, same classification technique was applied on a few samples which are subjected to active power cycling test.

# **Chapter 6      Classifier Performance for Samples Subjected to Active Power Cycling**

The aim of this chapter is to examine the performance of the model classifier achieved in Chapter 5 with samples which were subjected to power cycling test from +40 to +120°C. The bonds were made under different bond pad conditions in order to create different bond strengths. The electrical signals obtained from ultrasonic generator were recorded during bonding and logged as unlabelled data and then classified with the model classifier. The bonds were imaged in the as-bonded condition and over their lifetime using 3D x-ray tomography. In this chapter, firstly, sample preparation method is explained, then a brief overview of the active power cycling rig is presented, and finally the results of classification and lifetime estimation are presented and discussed.

## 6.1. Experimental procedure

Similar to the experiments done in previous chapters, the substrate and silicon dies which have been previously soldered onto substrates were provided by Dynex Semiconductor Ltd.

### 6.1.1. Active Power Cycling Set-up

The power cycling rig used in this research applies a constant current to heat up samples while a cold-plate connected to a temperature-controlled circuit cools down the samples. Each sample consists of a single silicon die soldered onto substrate and eight wire bonds (see Fig. 6.3). Each sample was fixed to the cold plate with two thick copper plates (See Fig. 6.1).

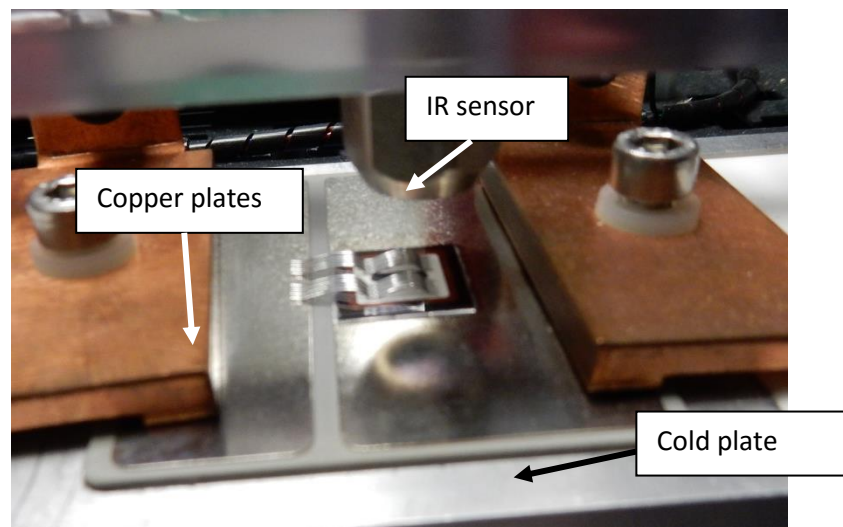


Figure 6.1: Fixing the sample on cold plate with copper plates

For achieving the best measure of junction temperature, the infrared (IR) sensor lenses were closely focused on the black strip on the silicon dies (see Fig. 6.2). The current is controlled by a set of metal-oxide semiconductor field-effect transistors (MOSFETs). When the temperature of silicon dies reaches to the upper temperature limit, the MOSFETs are activated and the load current is

diverted to a bypass circuit. When the temperature drops lower than lower temperature limit, the bypass device is switched off and the load current goes through the devices again [35]. In this experiment, the power cycling rig was set to apply a constant current of about 70 A. Each cycle was about eight seconds long (one second heating and seven seconds cooling) and the temperature amplitude was approximately 80K (from 40°C to 120°C). The power cycling rig and a snapshot of the temperature profile are given in Chapter 3, Figs. 3.8 and 3.9, respectively. Similar to the passive thermal cycling samples, the degradation behaviour of the wire bonds was evaluated by measuring the reduction in bonded area using x-ray tomography images of the same bonds in the as-bonded condition and over its lifetime.

### 6.1.2. Sample Preparation

In order to prepare samples for active power cycling test before wire bonding, firstly the centre of the silicon dies were painted with matt black spray as an emissivity reference in order to create temperature measurement spot for IR sensor lenses (see Fig. 6.2).

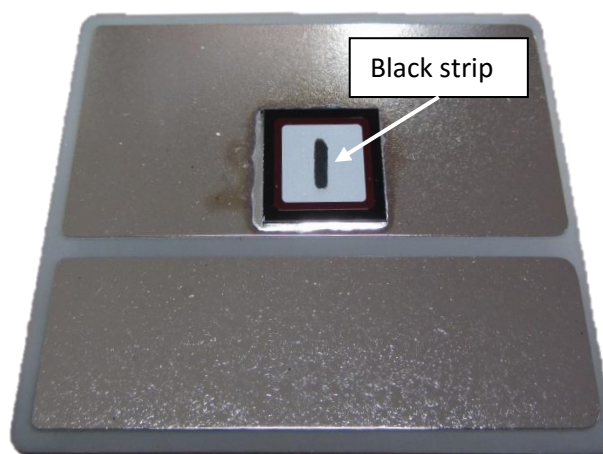


Figure 6.2: Substrate preparation for wire bonding



### 6.1.3. Bond Parameter Setting

In total 16, 99.999% pure aluminium wires, 375  $\mu\text{m}$  in diameter, were ultrasonically bonded at room temperature onto silicon dies with a 5- $\mu\text{m}$ -thick aluminium top metallization with the optimized bonding parameters described in Chapter 4 and shown in Table 5.1& 5.2 (Chapter 5). Similar to the experiment done in Chapter 5 (section 5.3.6.), bonds were made onto different bond surfaces. First, eight bonds were made on a die which had been kept in an argon-purged cabinet for one day (condition “1”) and then eight bonds were made on a die which had been kept in the argon-purged cabinet for seven days (condition “2”). In addition, it should be noted that the wire bonding layout in this experiment contains stitch bonds. A stitch bond has wire loops at both ends of the bond (see Fig. 6.3).

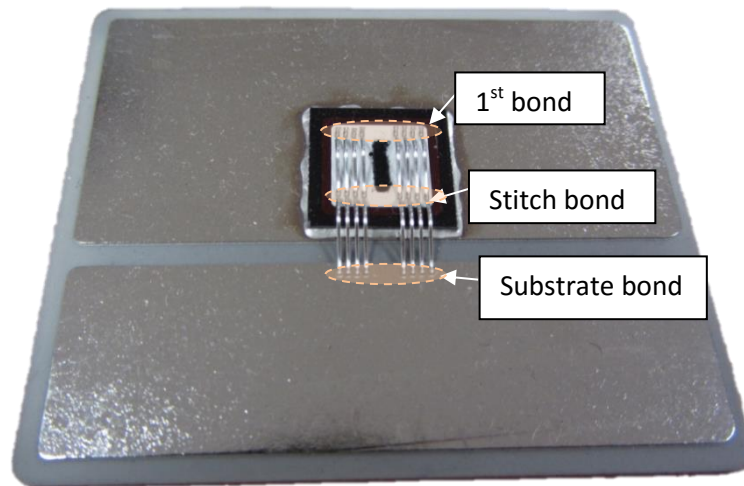


Figure 6.3: Aluminium wires bonded onto silicon dies for active power cycling test

### 6.1.4. Signal Detection

Similar to the previous experiment in Chapters 4 & 5, electrical signatures were recorded for each first bond at a sampling rate of 12.5 MHz. and the

envelopes of the ultrasonic generator currents were computed using MATLAB codes available in Appendix I.

### **6.1.5. Description of Samples for the SDA Algorithm**

In order to predict the class of the bonds, all 16 bonds were logged as unlabelled data and introduced to the model classifier which was developed in Chapter 5. In more detail, the labelled data are the 24 bonds used in Chapter 5 and the training data set remains the same. These 16 bonds were added to the test data for classification.

### **6.1.6. 3D X-ray Tomography**

In order to evaluate the quality and lifetime of all the bonded wires 3D x-ray tomography were used. All bonds are imaged in their as-bonded condition, and then after approximately 50k and 110k cycles.

## **6.2. Results and Discussions**

As the first bonds are the focus for quality assessment and lifetime prediction, their electrical signals were recorded. The envelopes of signals for the two types of bond surface are given in Fig. 6.4 & Fig. 6.5. Again, the envelope of signals indicates significant differences for the different bond pad conditions. Almost all bonds on condition “2” sample generated unstable signal during bonding. The non-uniformity of the waveforms indicates poor energy transfer at the bond interface, probably because deterioration in the quality of the surfaces of the substrates after storage in the argon-purged cabinet for seven days. The majority of bonds made on condition “1” sample generated more stable and uniform signal shape and received more constant level of power compared to the condition “2” sample.

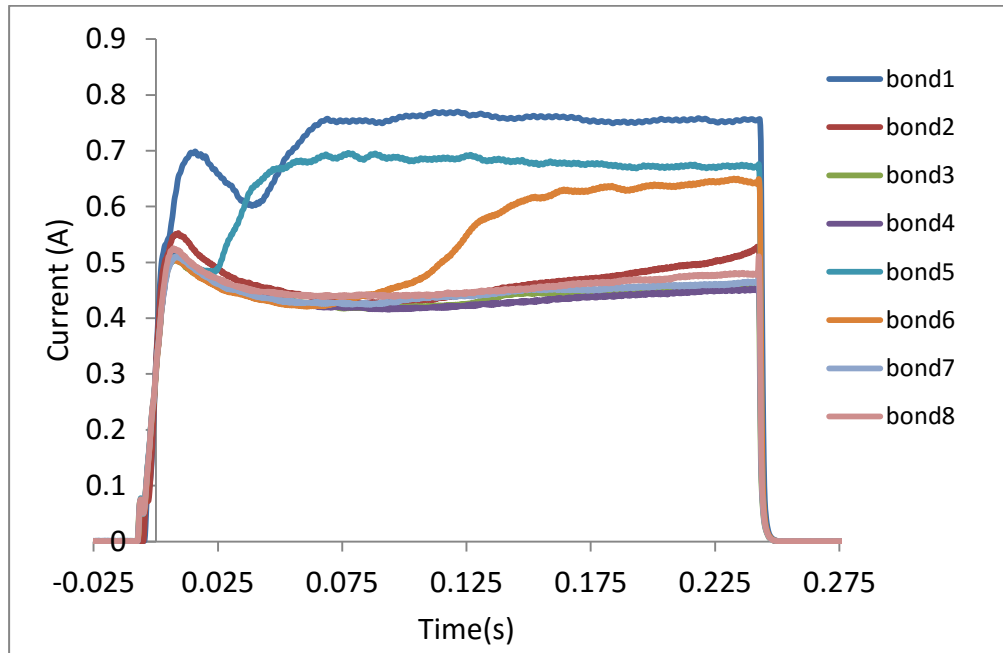


Figure 6.4: Current envelopes of the eight bonds on a freshly manufactured die

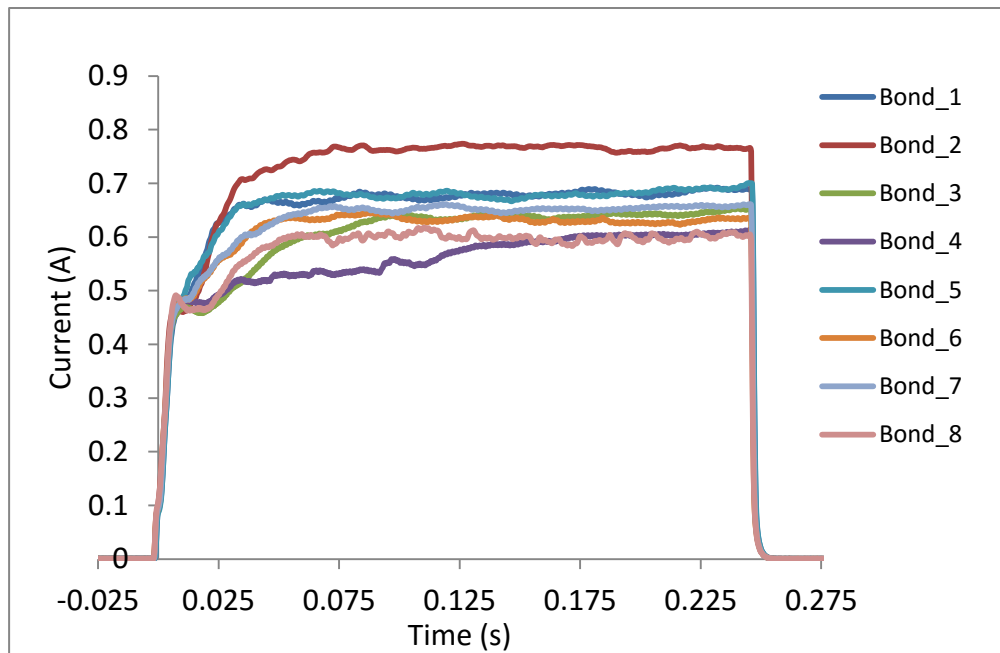


Figure 6.5: Current envelope of the 8 bonds on a die which were kept in an argon-purged cabinet for seven days

The model classifier built in Chapter 5 was used to predict the class of these 16 bonds. The results of the predicted class of bonds are given in below table (see table 6.1).

Table 6.1: The predicted class of bonds for active power cycling

	Bond_1	Bond_2	Bond_3	Bond_4	Bond_5	Bond_6	Bond_7	Bond_8
<b>Condition</b>	Class	Class	Class	Class	Class	Class	Class	Class
<b>“1”</b>	“C”	“A”	“A”	“A”	“B”	“B”	“A”	“A”
<b>Condition</b>	Class	Class	Class	Class	Class	Class	Class	Class
<b>“2”</b>	“C”	“C”	“C”	“C”	“C”	“C”	“C”	“C”

As table 6.1 shows, and as expected from the bond signal envelopes, condition “2” produced only weak bonds, classified as class “C” and bond pad condition “1” mostly contains strong bonds classified as “A”. In the next section, the degradation behaviour of bonds in different classes was observed in the as-bonded condition, after about 50k cycles and about 110k cycles.

### 6.2.1. Determination of Degradation Rate

The bonded wires were imaged by 3D x-ray tomography in the as-bonded condition, and then after 50k and approximately 100k cycles. The reduction of bonded area as visualised in the X-Y plane was measured using the polygon tool in ImageJ software to obtain the rate of degradation for the first bonds shown in Fig. 6.6.

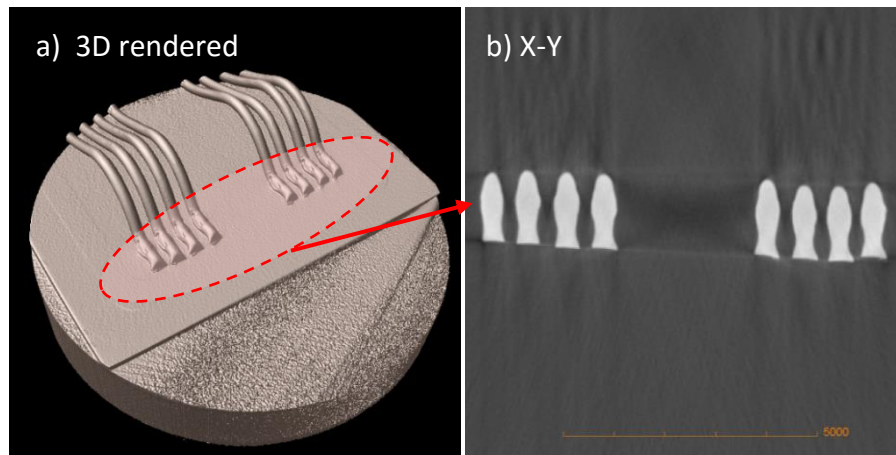


Figure 6.6: An overview of sample for active power cycling test, a) 3D rendered view, b) Selected wires in X-Y plane

Bonded area in the as-bonded condition was measured by looking at the virtual cross-section of the bonds parallel to the interface in the X-Y plane, similar to Chapter 5. However, for bonded wires which had been power cycled, measuring bonded area was more challenging, as the crack-propagation is not restricted to one plane, and therefore damage can be seen not only at the bond interface but also above the interface. Therefore, in order to quantify bonded area, several layers parallel to interface in X-Y plane and other planes were examined. In order to explain the procedure that was followed for measuring bonded area for cycled bonds, virtual cross-sections of different plane view of two bonds in different classes are given in Figs. 6.7- 6.10.

Fig. 6.7 shows the virtual cross-sectional view of a class “A” bond (bond no. 8) after 45k cycles from different Z heights –about 3 $\mu$ m- (indicated with red dash lines). Some lifted area can be seen in the bond tail area and rising heel region (see Fig. 6.7a). At the interface, some cracks can be seen at the rising heel region and small are voids observed in the middle of the bond (see Fig. 6.7b). A few microns above interface more cracks at rising heel can be observed (see Fig.6.7c & 6.7d). Figs. 6.7b, 6.7c and 6.7d, shows the depth of the voids is different inside the bonds near the interface, as some can be seen in all the X-Y sections but some appears on one or two sections.

Fig. 6.8 illustrates the damage such as lifted area and voids within the selected bond after 45k cycles in the X-Y and X-Z planes. Cross-sections made along X-Z plane are indicated by the yellow dashed lines. By looking at the plane views as explained above, the region indicated by long dashed red line is considered for measuring bonded area (see Fig. 6.8).

Figs. 6.9 & 6.10 show a class “C” bond in different plane views after 50k cycles. Virtual cross-sections from different Z heights are presented in Fig. 6.9. Lifted area and cracks can be seen in these X-Y views. For further illustration, X-Z plane views are also presented that mainly show lifted area, crack and voids within the bonds. Again, the region that is indicated by long dash red line is considered for measuring bonded area (see Fig. 6.10).

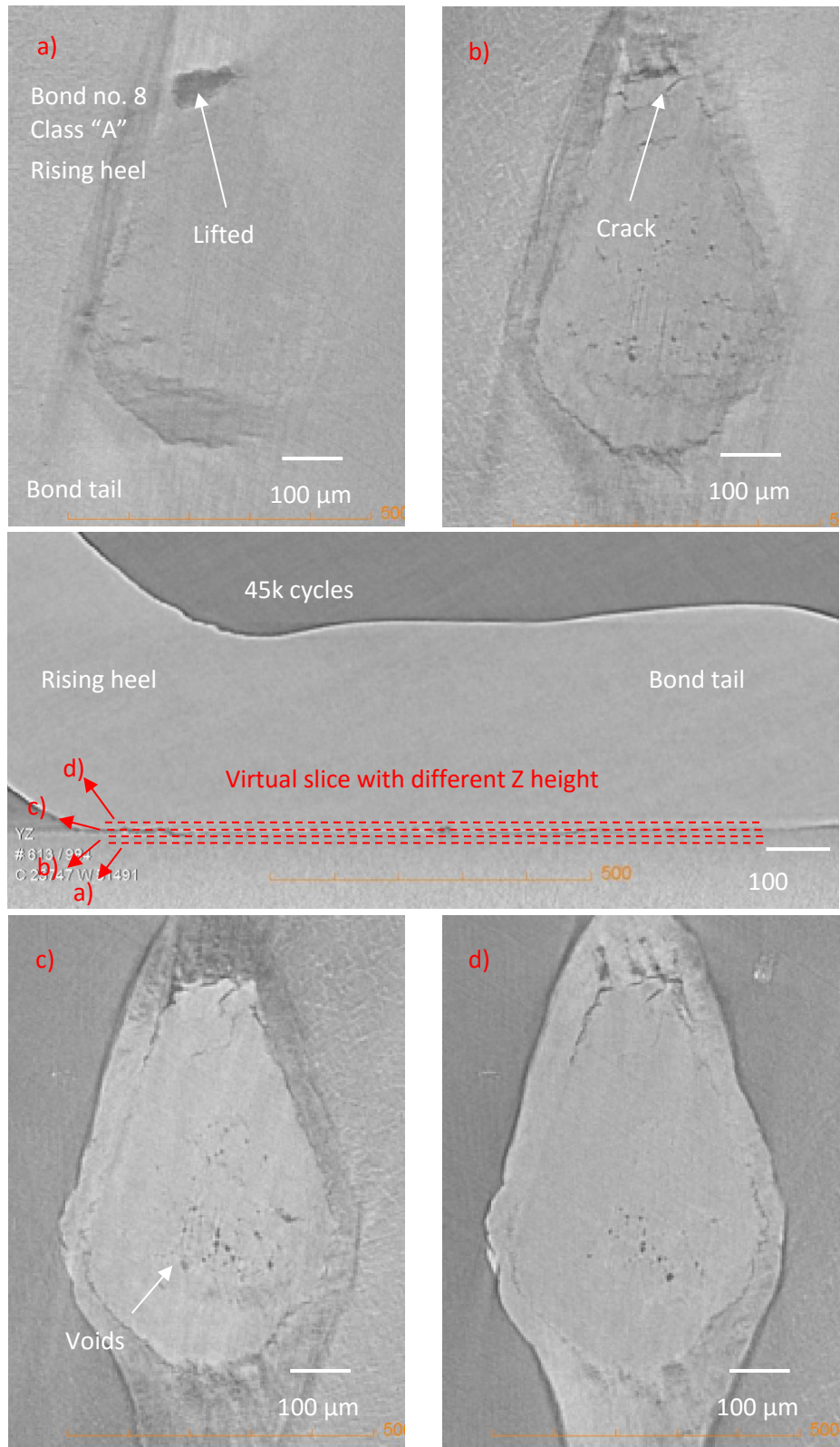


Figure 6.7: Virtual cross-sections with different Z height in the X-Y planes and Y-Z plane, bond no. 8, condition "1", Class "A"

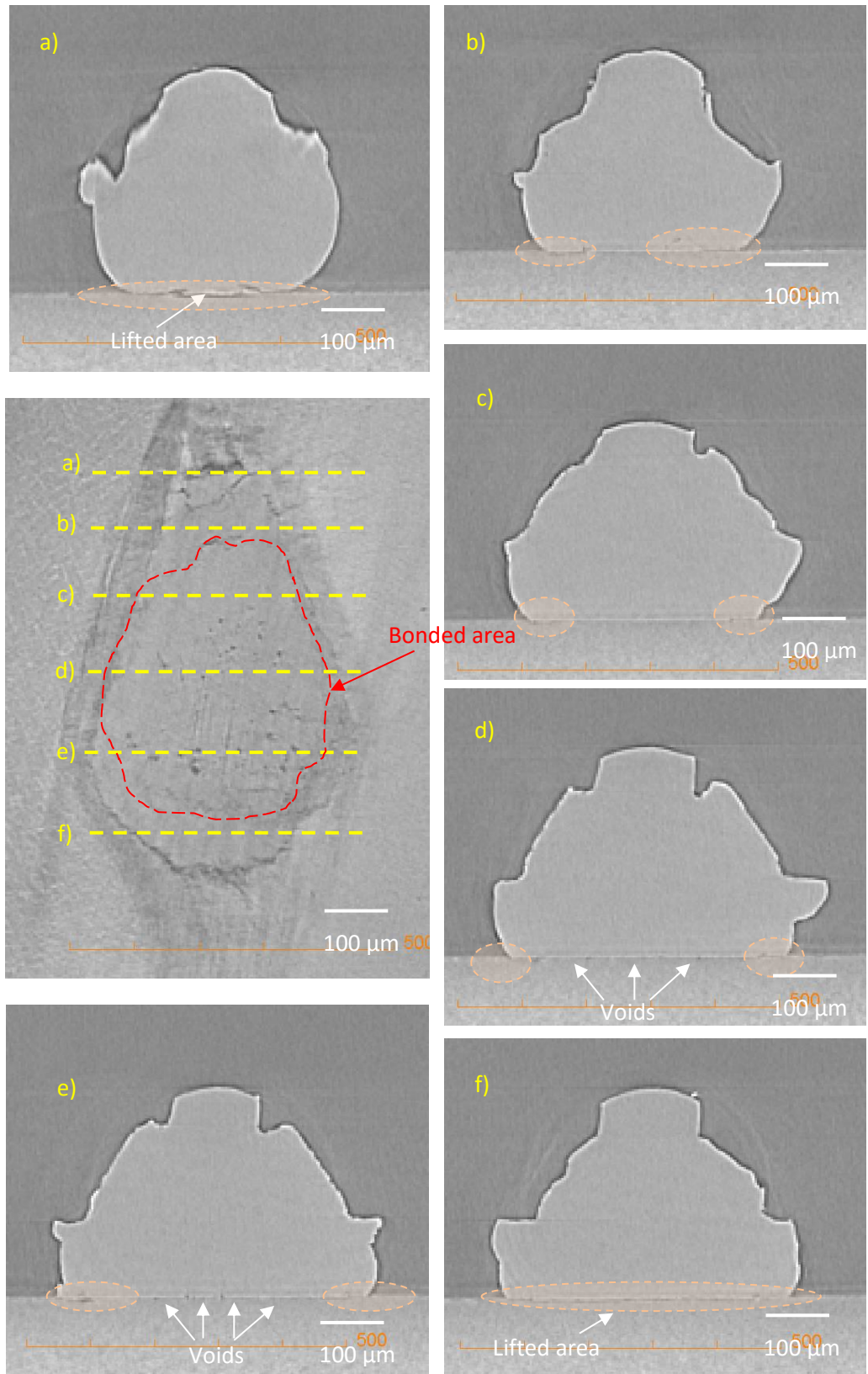


Figure 6.8: Virtual cross-sections with different X position in the, X-Y plane and X-Z planes, bond no. 8, condition “1”, Class “A”



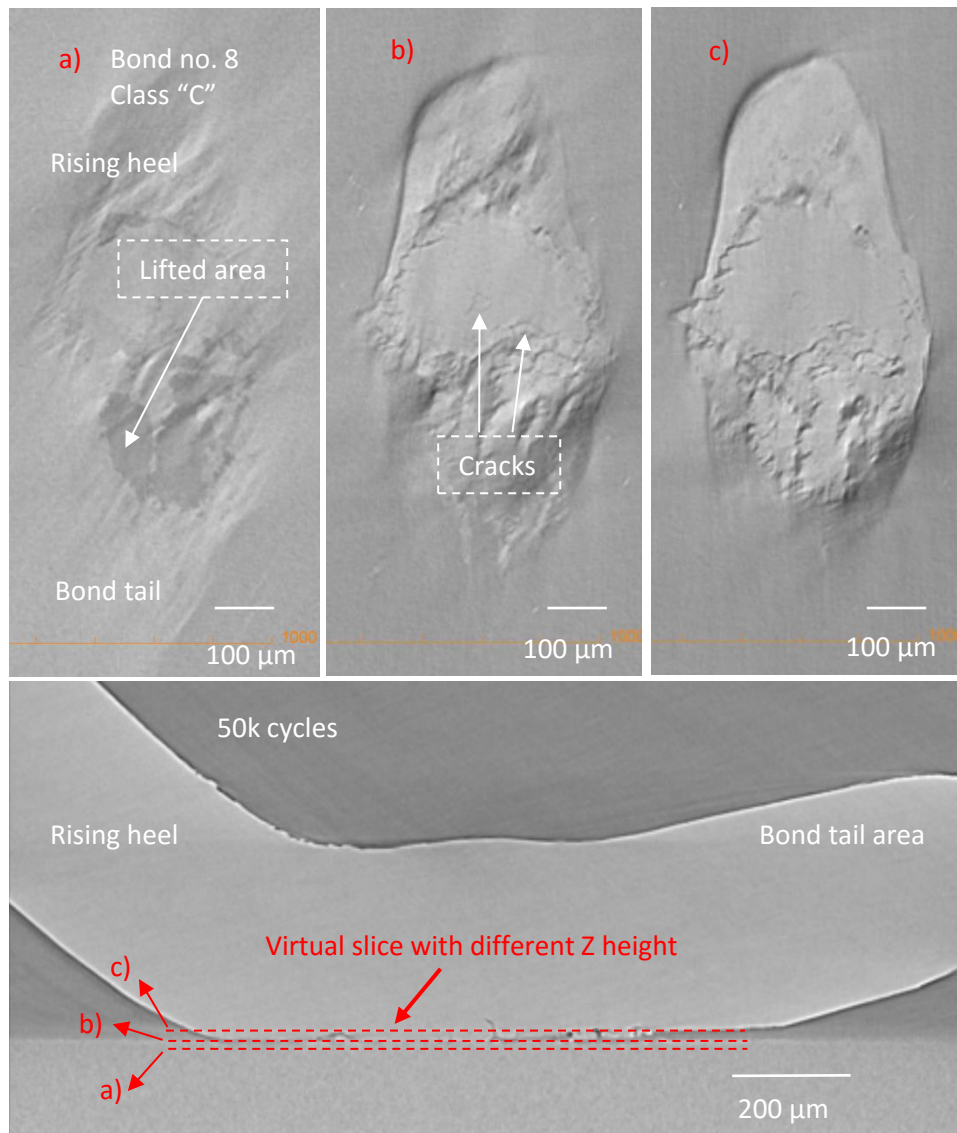


Figure 6.9: Virtual cross-sections with different Z height in the X-Y planes and Y-Z plane, bond no. 8, condition “2”, Class “C”

The bonds within class “A” had the largest bonded area and those within class “C” had the least bonded area. The bonded area reduced with increasing number of cycles.



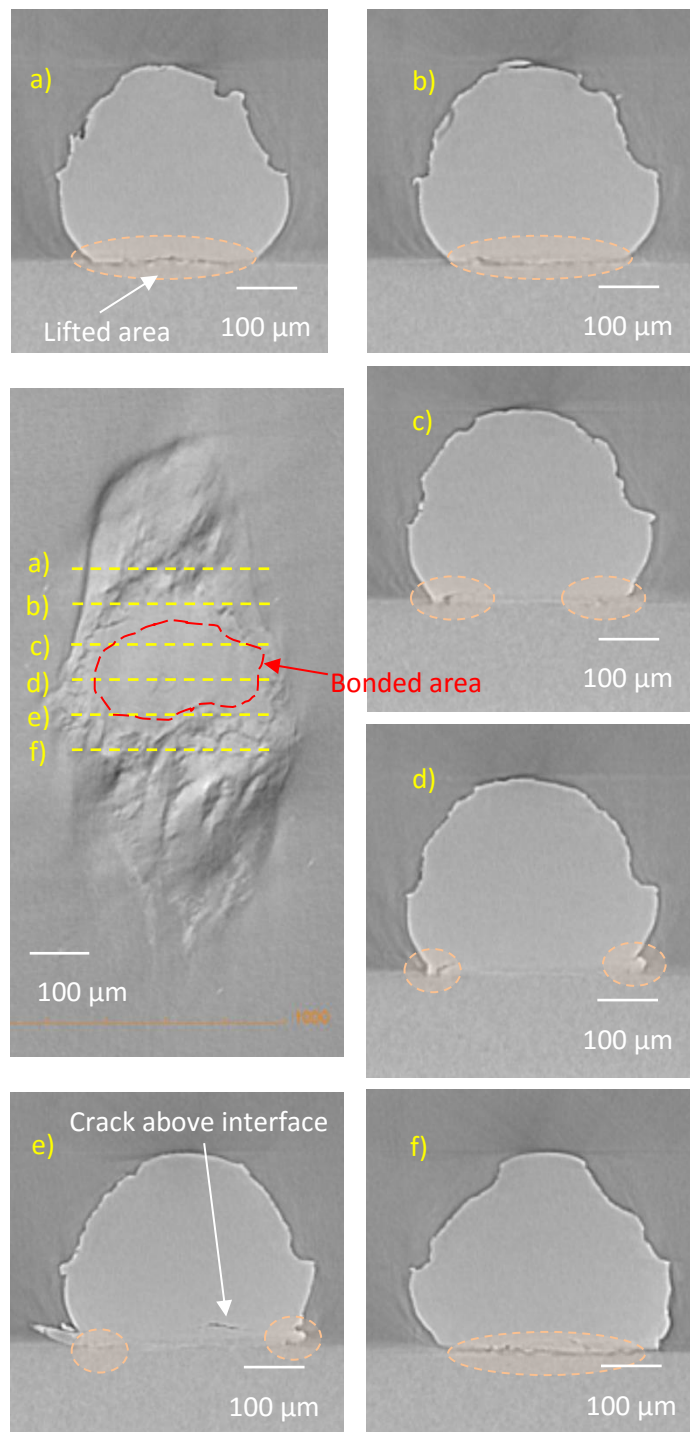


Figure 6.10: Virtual cross-sections with different X position in the, X-Y plane and X-Z planes, bond no. 8, condition “2”, Class “C”

The observed results from virtual cross-sections in different plane views show that damage occurs initially at the bond peripheries, particularly in the rising heel. Initial damage could occur during the bonding process, which flexes the wire at the heels during loop formation [149]. Further damage will accumulate during power cycling, for example as explained in Onuki et al.'s study and illustrated schematically Fig. 6.11. During power cycling, heating causes compressive stress at the bond periphery while cooling causes tensile stress in around the periphery of the bonded wire and cracks propagate during the cooling process at both bond ends and more generally around the periphery [33, 150].

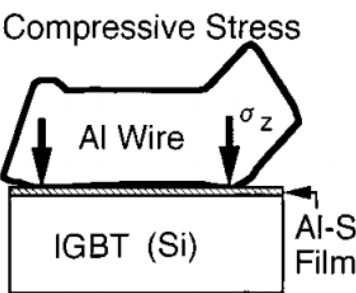
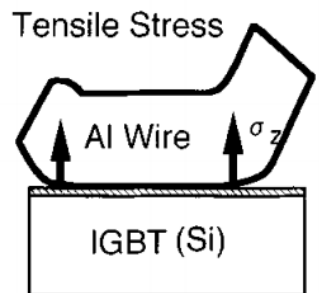
Process	Heating Process (Current On)	Cooling Process (Current Off)
Stress at both ends of bonds	<p>Compressive Stress</p> 	<p>Tensile Stress</p> 
Crack	No Propagation	Propagation

Figure 6.11: Region of stress in Al wire during active power cycling [150]

### 6.2.2. Estimation of Lifetime

The rate of degradation for both classes (“A” and “C”), measured following the above observations in terms of the remaining bonded area. Fig. 6.12 shows the average bonded area across all bonds of the same class versus lifetime. The results indicate that the rate of degradation in both classes at about the same, although the bonded area in the as-bonded condition of class “A” is significantly higher. End of life values determined by extrapolating the linear

regression lines of the selected bonds for class “A” and “C” bonds are about 116k cycles and 78k cycles, respectively.

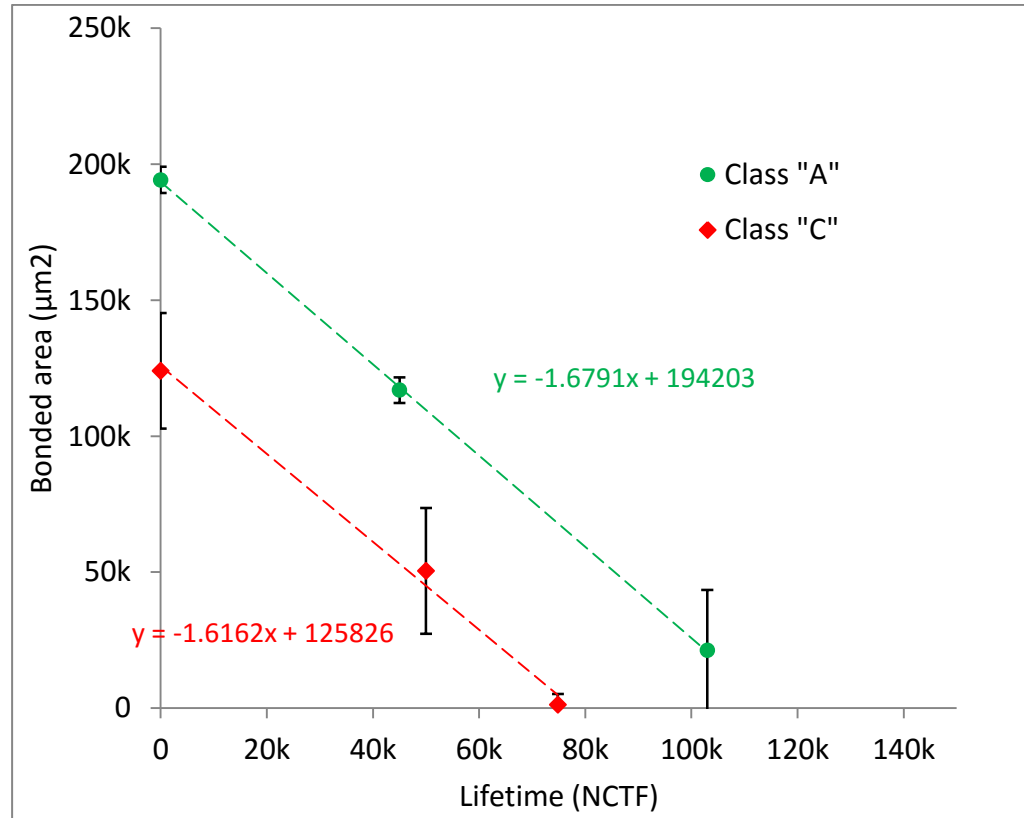


Figure 6.12: Bonds degradation rate in class “A” and “C” (active power cycling)

Based on the Coffin-Manson model, these results have been compared with the lifetime estimation curve of Held et al.[57] and Ramminger et al [41] shown in Fig. 6.13. Held et al. lifetime estimation graph is based on lifetime  $N_f$  vs  $\Delta T_j$  with  $T_m$  (mean cycling temperature) as parameters. In present experiment,  $\Delta T_j$  is 80K and  $T_m$  is 80 °C. Lifetime of predicted class “C” agrees with the both models but class “A” shows longer lifetime. Again, the results of lifetime indicate that the model classifier bond class is closely correlated to both the as-bonded area, estimated by X-ray tomography, and the cyclic lifetime. Furthermore, as the model classifier used in this experiment is the same as that built in Chapter 5, then it is safe to assume that the predicted class for the

bonds made in the previous chapter would have similar lifetimes as above if they were subjected to the same active power cycling test.

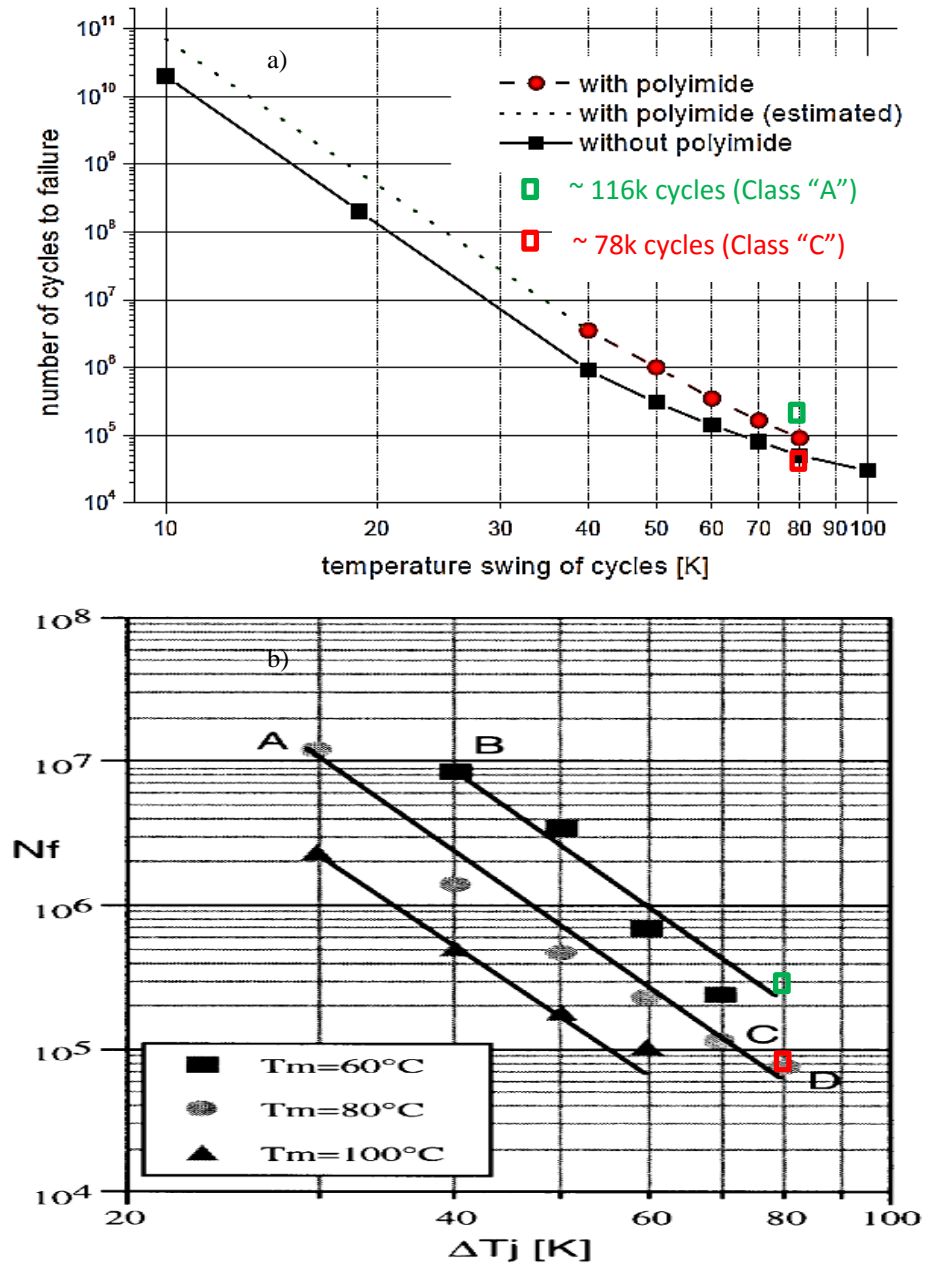


Figure 6.13: Comparing the results of lifetime with a) Ramminger et al. [41] and b) Held et al. [57] lifetime curve

### **6.3. Summary**

In this chapter, the performance of the model classifier described in Chapter 5 was examined on bonded wires subjected to active power cycling from +40 to +120 °C. Firstly, the classes of the bonded wires were predicted. Then, the degradation rate and end of life were estimated using non-destructive 3D X-ray tomography. The results again confirmed the capability of the presented model classifier for predicting bond quality. End of life estimation for the samples were compared with existing works and the results for class “C” bonds agree with the previous study.

# **Chapter 7      Conclusions and Recommendations for Future work**

## **7.1. Conclusions**

This thesis presents a new non-destructive technique for the real-time assessment of bond quality and prediction of lifetime, based on signals acquired during the ultrasonic bonding process

The presented work covered a number of key steps in the quest to identify an appropriate non-destructive bond quality monitoring tool.

Chapter 3 established the use of x-ray tomography as a non-destructive technique for evaluating the bonded area and therefore the initial quality and subsequent extent of degradation of thermally cycled bonds.

In Chapter 4, the effects of bonding parameters such as ultrasonic power, pre-compression steps and initial bond force on the reliability of wire bonds in power electronic modules is studied. Analysis of virtual cross-sections obtained from X-ray tomography images before and after passive thermal

cycling indicated good correlation between the bonds signal (i.e. an indicator of the initial bond quality) and wire bond lifetime.

The experimental results presented in Chapter 5 verified that the non-destructive method is able to separate a normal batch of bonded wires into quality classes. The bonded area measurements agreed with the results of the classification algorithm. More interestingly, the lifetime data for these bonds linked perfectly with the initial quality classifications made from the ultrasonic signals. In addition, the results indicated that poor initial bond quality led to shorter lifetimes but the observed damage mechanisms and degradation rates were more or less the same.

The results from the study of different bond pad conditions clearly show how that bond quality is influenced by the bond pad conditions.

With the aid of the probabilistic assessment method presented in Chapter 5, it is possible to determine important properties of remaining useful life of die/substrate/module from as-bonded condition, without simulating system until failure.

The results of the lifetime estimation were compared with previous works in the literature and shown a good agreement. Again, it indicates the capability of the method in real time lifetime prediction. However, a larger sample size and more labelled data would boost statistical confidence levels in the accuracy of the lifetime predictions made.

In conclusion, the main findings from the studies can be summarised as follows.

- The developed method provides a non-destructive way of evaluating wire bond quality in real time and all the steps followed in this method such as the signal acquisition, data analysis, classification and lifetime production can be carried out instantaneously on the production line with minimal additional infrastructural requirements. Therefore, it can be used to detect any fault or abnormality continuously and in real-

time, instead of having relying on quality measurements at the end of a batch or at given sampling intervals.

- The findings from the estimation of probability of failure of die/substrate/module suggest that the method can be applied to streamline production processes by, for example, grading predicted product life based on the proportion of high-quality bonds and in the development of improved bonding processes, or as illustrated, in the identification of optimised handling and cleaning methods.
- The present study can predict wire bond lifetime from initial bond quality without any destructive test such as shear test, therefore, the information obtained from this method can also be used for wire bonds lifetime models in order to provide uncertainty quantification for life prediction.
- Finally, the proposed method possesses significant improvement and effectiveness compared with other existing methods of real-time bond-quality monitoring.

## **7.2. Future Work**

In future work, it would be interesting to use additional cross-validation datasets to evaluate and improve the model classifier performance. In addition, more research is required to evaluate the accuracy of the model performance on new and more extensive datasets which represent typical production batches. Ideally such studies would be carried out in collaboration with a power module manufacturer.

The presented work considers degradation under a limited range of temperature and power cycling conditions. It would be very interesting to evaluate the same technique for the prediction of the useful in-service life of bonded wires over a wider range of thermal and power cycling conditions and with wires of different diameter.



Lastly, it has been proposed that Aluminium wire bonds might be replaced by Copper wire bonds. As Copper wire offers greater current carrying capacity (higher electrical and thermal conductivity) and longer lifetime as the lower coefficient of thermal expansion reduces fatigue stress at the wire-die interface. However, replacing existing technologies with new ones presents new challenges. Therefore, another possible area of future research would be applying the same approach for on-line quality monitoring of copper wire bonding.

## Appendix I

MATLAB codes for calculating envelope of current signal

```
clc
clear all
close all
count=0;
a = dir('*.dat');
load time.dat
all_rms=ones(1000,170);
for j = 37 %length(a)
fileName=['bond' num2str(j)];% ID_1 to n
d= load ([fileName '.dat']);
count=count;

dd=-d(1:end,1); %-
counter = 0;

for i=1:4999:4995000 %4900000
counter = counter+1;
y= dd(i:i+4999,1);

N = 4999;          % number of points
fs = 12500000;     % sample rate
t = (0 : N-1) / fs;

h = fft(y);

% Scale frequency and amplitude.
freq = fs * (0 : N/2) / N;

data= 2/N * abs(h(1 : N/2+1));

selectregion=data(21:27,:);
selectregion2(:,counter)=data(21:27,:);
% RMS
rms_data(counter,:)=sqrt(sum(selectregion.^2));
tt(counter,1)=time(i,1);

end

count=count+1;
all_rms(:,count)=rms_data(1:counter,1);
end

hold on
plot (time, d); hold on
plot (tt, rms_data); hold on
```

## Appendix II

SDA algorithm MATLAB codes[136] :

```
function [eigvector, eigvalue] = SDA(gnd,fea,semiSplit,options)
% SDA: Semi-supervised Discriminant Analysis
%
%      [eigvector, eigvalue] =
SDA(gnd,feaLabel,feaUnlabel,options)
%
%      Input:
%      gnd      - Label vector.
%      fea      - data matrix. Each row vector of fea
is a data point.
%
%      semiSplit - fea(semiSplit,:) is the labeled data
matrix.
%                  - fea(~semiSplit,:) is the unlabeled
data matrix.
%
%      options - Struct value in Matlab. The fields in
options
%                  that can be set:
%
%      WOptions   Please see ConstructW.m for
detailed options.
%      or
%      W          You can construct the W
outside.
%
%      ReguBeta   Paramter to tune the weight
between
%                  supervised info and local
info
%                  Default 0.1.
%                  beta*L+\tilde{I}
%      ReguAlpha  Paramter of Tinkhonov
regularizer
%                  Default 0.1.
%
%                  Please see LGE.m for other options.
%
%      Output:
%      eigvector - Each column is an embedding
function, for a new
%                  data point (row vector) x, y =
x*eigvector
%                  will be the embedding result of x.
%      eigvalue  - The eigvalue of SDA eigen-problem.
sorted from
%                  smallest to largest.
%
%
%
% See also LPP, LGE
%
```

```

%Reference:
%
%   Deng Cai, Xiaofei He and Jiawei Han, "Semi-Supervised
Discriminant
%   Analysis ", IEEE International Conference on Computer
Vision (ICCV),
%   Rio de Janeiro, Brazil, Oct. 2007.
%
%   version 2.0 --July/2007
%   version 1.0 --May/2006
%
%   Written by Deng Cai (dengcai2 AT cs.uiuc.edu)

%   Examples:
%

if ~isfield(options, 'ReguType')
    options.ReguType = 'Ridge';
end
if ~isfield(options, 'ReguAlpha')
    options.ReguAlpha = 0.1;
end

[nSmp, nFea] = size(fea);
nSmpLabel = sum(semiSplit);
nSmpUnlabel = sum(~semiSplit);

if nSmpLabel+nSmpUnlabel ~= nSmp
    error('input error!');
end

if ~isfield(options, 'W')
    options.WOptions.gnd = gnd;
    options.WOptions.semiSplit = semiSplit;
    W = constructW(fea, options.WOptions);
else
    W = options.W;
end

gnd = gnd(semiSplit);

```

```

classLabel = unique(gnd);
nClass = length(classLabel);
Dim = nClass;

D = full(sum(W,2));
W = -W;
for i=1:size(W,1)
    W(i,i) = W(i,i) + D(i);
end

ReguBeta = 0.1;
if isfield(options, 'ReguBeta') && (options.ReguBeta > 0)
    ReguBeta = options.ReguBeta;
end

LabelIdx = find(semiSplit);
D = W*ReguBeta;
for i=1:nSmpLabel
    D(LabelIdx(i),LabelIdx(i)) = D(LabelIdx(i),LabelIdx(i)) +
1;
end

%=====
% If data is too large, the following centering codes can be
commented
%=====
if isfield(options, 'keepMean') && options.keepMean
else
    if issparse(fea)
        fea = full(fea);
    end
    sampleMean = mean(fea,1);
    fea = (fea - repmat(sampleMean,nSmp,1));
end
%=====

```

```

DPrime = fea'*D*fea;

switch lower(options.ReguType)
    case {lower('Ridge')}
        for i=1:size(DPrime,1)
            DPrime(i,i) = DPrime(i,i) + options.ReguAlpha;
        end
    case {lower('RidgeLPP')}
        for i=1:size(DPrime,1)
            DPrime(i,i) = DPrime(i,i) + options.ReguAlpha;
        end
    case {lower('Tensor')}
        DPrime = DPrime +
options.ReguAlpha*options.regularizerR;
    case {lower('Custom')}
        DPrime = DPrime +
options.ReguAlpha*options.regularizerR;
    otherwise
        error('ReguType does not exist!');
end

DPrime = max(DPrime,DPrime');

feaLabel = fea(LabelIdx,:);

Hb = zeros(nClass,nFea);
for i = 1:nClass,
    index = find(gnd==classLabel(i));
    classMean = mean(feaLabel(index,:),1);
    Hb (i,:) = sqrt(length(index))*classMean;
end
WPrime = Hb'*Hb;
WPrime = max(WPrime,WPrime');

dimMatrix = size(WPrime,2);

if Dim > dimMatrix

```

```

        Dim = dimMatrix;
end

if isfield(options, 'bEigs')
    if options.bEigs
        bEigs = 1;
    else
        bEigs = 0;
    end
else
    if (dimMatrix > 1000 && Dim < dimMatrix/20)
        bEigs = 1;
    else
        bEigs = 0;
    end
end

if bEigs
    %disp('use eigs to speed up!');
    option = struct('disp',0);
    [eigvector, eigvalue] =
eigs(WPrime,DPrime,Dim,'la',option);
    eigvalue = diag(eigvalue);
else
    [eigvector, eigvalue] = eig(WPrime,DPrime);
    eigvalue = diag(eigvalue);

    [junk, index] = sort(-eigvalue);
    eigvalue = eigvalue(index);
    eigvector = eigvector(:,index);

    if Dim < size(eigvector,2)
        eigvector = eigvector(:, 1:Dim);
        eigvalue = eigvalue(1:Dim);
    end
end
end

```

```
for i = 1:size(eigvector,2)
    eigvector(:,i) = eigvector(:,i)./norm(eigvector(:,i));
end
```



### Appendix III

The details of contents of ANOVA table presents in Table 5.5 are summarised in below Tables:

Table Appendix III.1: List of abbreviations

<b>Source of variations</b>	
<i>df</i>	Degree of freedom
<i>SS</i>	Sum of squares
<i>MS</i>	Mean squares
F-ratio	A ratio of mean squares
P-value	Probability more than F-value

Table Appendix III.1: List of equations [151]

<b>Source of variations</b>	<b>SS</b>	<b>df</b>	<b>MS</b>	<b>F</b>	<b>P &gt; F</b>
<b>Factors</b>	$SS_t = n \sum_{i=1}^a (\bar{y}_{i.} - \bar{y}_{..})^2$	$a - 1$	$MS_t$	$F = \frac{MS_t}{MS_E}$	
<b>Error</b>	$SS_E = SS_T - SS_t$	$N - a$	$MS_E$		
<b>Total</b>	$SS_T = \sum_{i=1}^a \sum_{j=1}^n (\bar{y}_{ij} - \bar{y}_{..})^2$	$N - 1$			

## References

- [1] X. Luo, J. Wang, M. Dooner, and J. Clarke, "Overview of current development in electrical energy storage technologies and the application potential in power system operation," *Applied Energy*, vol. 137, pp. 511-536, 1/1/ 2015.
- [2] IEA, *Key World Energy Statistics 2014*: OECD Publishing.
- [3] F. Blaabjerg, Y. Yongheng, and M. Ke, "Power electronics - Key technology for renewable energy systems - Status and future," in *Electric Power and Energy Conversion Systems (EPECS), 2013 3rd International Conference on*, 2013, pp. 1-6.
- [4] M. Elbuluk and N. R. N. Idris, "The role power electronics in future energy systems and green industrialization," in *Power and Energy Conference, 2008. PECon 2008. IEEE 2nd International*, 2008, pp. 1-6.
- [5] A. Azarpour, S. Suhaimi, G. Zahedi, and A. Bahadori, "A Review on the Drawbacks of Renewable Energy as a Promising Energy Source of the Future," *Arabian Journal for Science and Engineering*, vol. 38, pp. 317-328, 2013/02/01 2013.
- [6] C. Blake and C. Bull, "International Rectifier," *IGBT or MOSFET: Choose Wisely*, 2000.
- [7] L. Hua and C. Bailey, "Lifetime prediction of an IGBT power electronics module under cyclic temperature loading conditions," in *Electronic Packaging Technology & High Density Packaging, 2009. ICEPT-HDP '09. International Conference on*, 2009, pp. 274-279.
- [8] C. Bailey, H. Lu, C. Yin, and S. Ridout, "Predictive Reliability, Prognostics and Risk Assessment for Power Modules," *Integrated Power Systems (CIPS), 2008 5th International Conference on*, pp. 1-7, 2008.
- [9] L. Y. Pearl A Agyakwa, Martin R Corfield & C Mark Johnson, "A nondestructive study of crack development during thermal cycling of Al wire bonds using x-ray computed tomography," presented at the CIPS 2014 Germany, 2014.
- [10] S. W. Or, H. L. W. Chan, V. C. Lo, and C. W. Yuen, "Sensors for automatic process control of wire bonding," in *Applications of Ferroelectrics, 1996. ISAF '96., Proceedings of the Tenth IEEE International Symposium on*, 1996, pp. 991-994 vol.2.
- [11] S. W. Or, H. L. W. Chan, V. C. Lo, and C. W. Yuen, "Ultrasonic wire-bond quality monitoring using piezoelectric sensor," *Sensors and Actuators A: Physical*, vol. 65, pp. 69-75, 1998.
- [12] W. Feng, Q. Meng, Y. Xie, and H. Fan, "Wire bonding quality monitoring via refining process of electrical signal from ultrasonic generator," *Mechanical Systems and Signal Processing*, vol. 25, pp. 884-900, 2011.
- [13] F. Wuwei, Z. Yulian, and M. Qingfeng, "Monitoring of the Ultrasonic Wire Bonding Quality Based on System Impedance," in *Computer Science & Service System (CSSS), 2012 International Conference on*, 2012, pp. 2013-2016.
- [14] F. Wuwei, M. Qingfeng, X. Youbo, and M. Qinghu, "Online Quality Evaluation of Ultrasonic Wire Bonding Using Input Electrical Signal of Piezoelectric Transducer," in *Computer Science and Information Engineering, 2009 WRI World Congress on*, 2009, pp. 462-466.
- [15] E. Arjmand, P. Agyakwa, and C. M. Johnson, "Methodology for identifying wire bond process quality variation using ultrasonic current frequency

- spectrum," in *Power Electronics and Applications (EPE), 2013 15th European Conference on*, 2013, pp. 1-8.
- [16] J. Pan and P. Fraud, "Wire Bonding Challenges in Optoelectronics Packaging," 2004.
- [17] C. Hager, "Lifetime estimation of aluminum wire bonds based on computational plasticity," Ph.D., Engineering, Technische Wissenschaften ETH Zürich, ETH. Zürich, 2000.
- [18] S. C. H. W.-S. Loh, R. J. Ikujeniya, M. R. Corfield, P. Agyakwa and C. M. Johnson, "Effect of bonding temperature, post-bond heat treatment and extended range thermal cycling on the reliability of al wire bonds," presented at the IMAPS, USA, 2008.
- [19] M.-N. B. R. J. R. Le, "Advanced thermosonic wire bonding using high frequency ultrasonic power optimization, bondability, and reliability : a thesis," California Polytechnic State University], San Luis Obispo, Calif., 2009.
- [20] C. D. Breach and F. W. Wulff, "A brief review of selected aspects of the materials science of ball bonding," *Microelectronics Reliability*, vol. 50, pp. 1-20, 1// 2010.
- [21] B. Langenecker, "Effects of Ultrasound on Deformation Characteristics of Metals," *Sonics and Ultrasonics, IEEE Transactions on*, vol. 13, pp. 1-8, 1966.
- [22] W. S. Loh, "Studies of Avalanche Breakdown Characteristics in 4H-SiC and reliability of pure aluminium wire bonds for high power and high temperature applications," PhD, University of Sheffield, University of Sheffield, 2008.
- [23] P. F. J. Pan, "Wire Bonding Challenges in Optoelectronics Packaging," presented at the Manufacturing Technology Symposium, California Polytechnic State University, 2004.
- [24] W. S. a. M. Tirakanogsathit, "Design of Experiments Approach for Improving Wire Bonding Quality," *International Journal of Innovation, Management and Technology*, vol. 3, 2012.
- [25] H. Berg and E. Wolfgang, "Advanced IGBT modules for railway traction applications: Reliability testing," *Microelectronics Reliability*, vol. 38, pp. 1319-1323, 6// 1998.
- [26] S. Lijie, B. Shengxiang, H. Yongda, J. Wei, and L. Qiang, "The optimization of process parameters based on the orthogonal experiments in wire bonding," in *Electronic Packaging Technology (ICEPT), 2015 16th International Conference on*, 2015, pp. 1180-1183.
- [27] R. S. Caiyuan Wang, "The Quality Test of Wire Bonding," *Modern Applied Science*, vol. 3, 2009.
- [28] M. L. Sheaffer, L. Grove, W., "How to Optimize and Control the Wire Bonding Process: Part I & Part II," *Solid State Technology*, vol. 34, pp. 67-70, 1991.
- [29] R. Pufall, "Automatic process control of wire bonding," in *Electronic Components and Technology Conference, 1993. Proceedings., 43rd*, 1993, pp. 159-162.
- [30] E. L. R. L. H. Chiang, R. D. Braatz, *Fault detection and diagnosis in industrial systems*. New York: Springer-Verlag, 2001.
- [31] X. Saint-Martin and C. Yuan, "Wire-bonding machine optimization using Taguchi method," in *Electronic Manufacturing Technology Symposium, 1992. IEMT 1992. 12th International*, 1992, pp. 74-83.
- [32] L. Yumin, L. Yong, S. Irving, A. Zhu, and F. Xingquan, "Optimization of 2 Mil Al Wire Wedge Bond of D-PAK," in *Electronic Packaging Technology, 2006. ICEPT '06. 7th International Conference on*, 2006, pp. 1-5.

- [33] J. Onuki and M. Koizumi, "Reliability of thick Al wire bonds in IGBT modules for traction motor drives," in *Power Semiconductor Devices and ICs, 1995. ISPSD '95., Proceedings of the 7th International Symposium on*, 1995, pp. 428-433.
- [34] J.-M. Göhre, "Entwicklung und Implementierung einer verbesserten Lastwechselfestmethode zur experimentellen Bestimmung der Zuverlässigkeit von Dickdrahtbonds in Leistungsmodulen, Development and Implementation of an Improved Active Power Cycling Test Method for Experimentally Determining the Reliability of Heavy Wire Bonds in Power Semiconductor Modules," 2013.
- [35] L. Yang, "A damage-based time-domain wear-out model for wire bond interconnects in power electronic modules," Ph.D., Department of Electrical and Electronic Engineering, University of Nottingham, Nottingham, UK, 2013.
- [36] G. Khatibi, B. Weiss, J. Bernardi, and S. Schwarz, "Microstructural Investigation of Interfacial Features in Al Wire Bonds," *Journal of electronic materials*, vol. 41, pp. 3436-3446, 2012.
- [37] C. Dresbach, M. Mittag, M. Petzold, E. Milke, and T. Müller, "Mechanical properties and microstructure of heavy aluminum bonding wires for power applications," in *Microelectronics and Packaging Conference, 2009. EMPC 2009. European*, 2009, pp. 1-8.
- [38] L. Wei-Sun, M. Corfield, L. Hua, S. Hogg, T. Tilford, and C. M. Johnson, "Wire Bond Reliability for Power Electronic Modules - Effect of Bonding Temperature," in *Thermal, Mechanical and Multi-Physics Simulation Experiments in Microelectronics and Micro-Systems, 2007. EuroSime 2007. International Conference on*, 2007, pp. 1-6.
- [39] Y. Yamada, Y. Takaku, Y. Yagi, I. Nakagawa, T. Atsumi, M. Shirai, *et al.*, "Reliability of wire-bonding and solder joint for high temperature operation of power semiconductor device," *Microelectronics Reliability*, vol. 47, pp. 2147-2151, 12// 2007.
- [40] K. Pedersen, D. Benning, P. Kristensen, V. Popok, and K. Pedersen, "Interface structure and strength of ultrasonically wedge bonded heavy aluminium wires in Si-based power modules," *Journal of Materials Science: Materials in Electronics*, vol. 25, pp. 2863-2871, 2014/07/01 2014.
- [41] S. Ramminger, N. Seliger, and G. Wachutka, "Reliability model for Al wire bonds subjected to heel crack failures," *Microelectronics Reliability*, vol. 40, pp. 1521-1525, 8// 2000.
- [42] J. M. Nowful, S. C. Lok, and S. W. R. Lee, "Effects of plasma cleaning on the reliability of wire bonding," in *Electronic Materials and Packaging, 2001. EMAP 2001. Advances in*, 2001, pp. 39-43.
- [43] R. Guan, X. Wang, F. Zhu, Z. Gan, S. Liu, and D. Huang, "Study on plasma cleaning and strength of wire bonding," in *Business of Electronic Product Reliability and Liability, 2004 International Conference on*, 2004, pp. 65-71.
- [44] R. D. Rust, D. A. Doane, and I. Sawchyn, "Improvements in wire bonding and solderability of surface mount components using plasma cleaning techniques," *Components, Hybrids, and Manufacturing Technology, IEEE Transactions on*, vol. 14, pp. 573-579, 1991.
- [45] L. Wood, C. Fairfield, and K. Wang, "Plasma cleaning of chip scale packages for improvement of wire bond strength," in *Electronic Materials and Packaging, 2000. (EMAP 2000). International Symposium on*, 2000, pp. 406-408.
- [46] A. Hamidi, S. Kaufmann, and E. Herr, "Increased lifetime of wire bonding connections for IGBT power modules," in *Applied Power Electronics*

- Conference and Exposition, 2001. APEC 2001. Sixteenth Annual IEEE, 2001, pp. 1040-1044 vol.2.*
- [47] L. Hua, L. Wei-Sun, C. Bailey, and C. M. Johnson, "Computer Simulation of Aluminium Wirebonds with Globtop in Power Electronics Modules," in *Microsystems, Packaging, Assembly & Circuits Technology Conference, 2008. IMPACT 2008. 3rd International, 2008*, pp. 348-351.
  - [48] L. Hua, L. Wei-Sun, C. Bailey, and C. M. Johnson, "Computer modelling analysis of the globtop's effects on aluminium wirebond reliability," in *Electronics System-Integration Technology Conference, 2008. ESTC 2008. 2nd, 2008*, pp. 1369-1374.
  - [49] C. T. Leonard, "ON UNITED-STATES MIL-HDBK-217 AND RELIABILITY PREDICTION," ed: IEEE-INST ELECTRICAL ELECTRONICS ENGINEERS INC 345 E 47TH ST, NEW YORK, NY 10017-2394, 1988.
  - [50] I. Knowles, "Reliability prediction or reliability assessment," in *Systems Reliability and Maintainability (Ref. No. 1999/189), IEE Seminar, 1999*, pp. 1/1-1/5.
  - [51] A. Siemens, "Siemens Company Standard SN29500," ed: Version.
  - [52] C. T. Leonard and M. Pecht, "How failure prediction methodology affects electronic equipment design," *Quality and Reliability Engineering International*, vol. 6, pp. 243-249, 1990.
  - [53] M. Pecht and A. Dasgupta, "Physics-of-Failure: An Approach to Reliable Product Development," *Journal of the IES*, vol. 38, pp. 30-34, 1995.
  - [54] S. Jiang, L. Fengming, Z. Chenhui, and X. Ming, "The Principle and application of physics-of-failure based reliability technology," in *Prognostics and System Health Management Conference (PHM-2014 Hunan), 2014, 2014*, pp. 75-78.
  - [55] J. G. McLeish, "Enhancing MIL-HDBK-217 reliability predictions with physics of failure methods," in *Reliability and Maintainability Symposium (RAMS), 2010 Proceedings - Annual, 2010*, pp. 1-6.
  - [56] M. Ciappa, "Selected failure mechanisms of modern power modules," *Microelectronics reliability*, vol. 42, pp. 653-667, 2002.
  - [57] M. Held, P. Jacob, G. Nicoletti, P. Scacco, and M.-H. Poech, "Fast power cycling test of IGBT modules in traction application," in *Power Electronics and Drive Systems, 1997. Proceedings., 1997 International Conference on, 1997*, pp. 425-430.
  - [58] M. Ciappa, P. Malberti, W. Fichtner, P. Cova, L. Cattani, and F. Fantini, "Lifetime extrapolation for IGBT modules under realistic operation conditions," *Microelectronics Reliability*, vol. 39, pp. 1131-1136, 6// 1999.
  - [59] K. Norris and A. Landzberg, "Reliability of controlled collapse interconnections," *IBM Journal of Research and Development*, vol. 13, pp. 266-271, 1969.
  - [60] K. J. Chung, L. Yang, B.-Y. Wang, and C.-C. Wu, "The investigation of modified Norris-Landzberg acceleration models for reliability assessment of Ball Grid Array packages," in *Microsystems Packaging Assembly and Circuits Technology Conference (IMPACT), 2010 5th International, 2010*, pp. 1-4.
  - [61] R. Bayerer, T. Herrmann, T. Licht, J. Lutz, and M. Feller, "Model for Power Cycling lifetime of IGBT Modules - various factors influencing lifetime," in *Integrated Power Systems (CIPS), 2008 5th International Conference on, 2008*, pp. 1-6.
  - [62] B. Czerny, M. Lederer, B. Nagl, A. Trnka, G. Khatibi, and M. Thoben, "Thermo-mechanical analysis of bonding wires in IGBT modules under

- operating conditions," *Microelectronics Reliability*, vol. 52, pp. 2353-2357, 9// 2012.
- [63] P. A. Agyakwa, M. R. Corfield, L. Jian Feng, L. Wei-Sun, E. Liotti, S. C. Hogg, *et al.*, "Unusual Observations in the Wear-Out of High-Purity Aluminum Wire Bonds Under Extended Range Passive Thermal Cycling," *Device and Materials Reliability, IEEE Transactions on*, vol. 10, pp. 254-262, 2010.
- [64] P. A. Agyakwa, V. M. F. Marques, M. R. Corfield, J. F. Li, L. Yang, and C. M. Johnson, "Room-Temperature Nanoindentation Creep of Thermally Cycled Ultrasonically Bonded Heavy Aluminum Wires," *Journal of Electronic Materials*, vol. 42, pp. 537-544, 2013/03/01 2013.
- [65] J. Albers, *The Destructive bond pull test*. Washington,U.S. Dept. of Commerce, National Bureau of Standards, 1976.
- [66] G. Harman and C. Cannon, "The Microelectronic Wire Bond Pull Test-How to use It, How to Abuse It," *Components, Hybrids, and Manufacturing Technology, IEEE Transactions on*, vol. 1, pp. 203-210, 1978.
- [67] S. M. Polcari, and Bowe, J.J., "Evaluation of Non-Destructive Tensile Testing," Report No. DOT-TSC- NASA-71-101971.
- [68] G. G. Harman, *Wire Bonding in Microelectronics*. New York: McGraw-Hill, 1997.
- [69] V. Sundararaman, D. R. Edwards, W. E. Subido, and H. R. Test, "Wire pull on fine pitch pads: an obsolete test for first bond integrity," in *Electronic Components & Technology Conference, 2000. 2000 Proceedings. 50th*, 2000, pp. 416-420.
- [70] M. Pecht, D. Barker, and P. Lall, "Development of an alternative wire bond test technique," *Components, Packaging, and Manufacturing Technology, Part A, IEEE Transactions on*, vol. 17, pp. 610-615, 1994.
- [71] A. Jalar, M. N. Zulkifli, N. K. Othman, and S. Abdullah, "The re-evaluation of mechanical properties of wire bonding," in *Advanced Packaging Materials (APM), 2011 International Symposium on*, 2011, pp. 226-233.
- [72] J. A. a. D. Arleth, R. D., "A New Test for Thermocompression Microbonds," *Electronic Products*, vol. 9, pp. pp. 92-94, 1967.
- [73] W. Gill and W. Workman, "Reliability Screening Procedures for Integrated Circuits," in *Physics of Failure in Electronics, 1966. Fifth Annual Symposium on the*, 1966, pp. 101-142.
- [74] J. Jellison, "Effect of Surface Contamination on the Thermocompression Bondability of Gold," *Parts, Hybrids, and Packaging, IEEE Transactions on*, vol. 11, pp. 206-211, 1975.
- [75] MIL-STD-883B, "Test methods and procedures for microelectronics," in *U. S. D. Defense*, ed. Washington, D.C., 1977.
- [76] W. Fuliang, L. Junhui, L. Shaohua, and H. Lei, "Heavy Aluminum Wire Wedge Bonding Strength Prediction Using a Transducer Driven Current Signal and an Artificial Neural Network," *Semiconductor Manufacturing, IEEE Transactions on*, vol. 27, pp. 232-237, 2014.
- [77] P. J. Withers and M. Preuss, "Fatigue and damage in structural materials studied by X-ray tomography," *Annual Review of Materials Research*, vol. 42, pp. 81-103, 2012.
- [78] P. J. Withers, "Mechanical failure: Imaging cracks in hostile regimes," *Nat Mater*, vol. 12, pp. 7-9, 01//print 2013.
- [79] H. Tsuritani, T. Sayama, Y. Okamoto, T. Takayanagi, K. Uesugi, and T. Mori, "Application of Synchrotron Radiation X-Ray Microtomography to Nondestructive Evaluation of Thermal Fatigue Process in Flip Chip

- Interconnects," *Journal of Electronic Packaging*, vol. 133, pp. 021007-021007, 2011.
- [80] P. W.-P. Chu, H.-L. Li, H. L.-W. Chan, K. M.-W. Ng, and P. C.-K. Liu, "Smart ultrasonic transducer for wire-bonding applications," *Materials Chemistry and Physics*, vol. 75, pp. 95-100, 4/28/ 2002.
- [81] K. S. G. Z.W. Zhonga, "Investigation of ultrasonic vibrations of wire bonding capillaries," *Microelectronics Journal*, vol. 37, pp. 107-113, 2006.
- [82] H. Gaul, M. Schneider-Ramelow, K. D. Lang, and H. Reichl, "Predicting the Shear Strength of a Wire Bond Using Laser Vibration Measurements," in *Electronics Systemintegration Technology Conference, 2006. 1st*, 2006, pp. 719-725.
- [83] J. L. Landes, "Ultrasonic bond energy monitor," U.S. Classification Patent, 1982.
- [84] L. K. Chan, "Apparatus and method for automatic evaluation of a bond created by an ultrasonic transducer," US Patent, 1982.
- [85] M. Brökelmann, R. Krol, J. Wallaschek, and H. J. Hesse, "A self-sensing transducer for ultrasonic wire bonding," in *Proceedings of the 18th International Congress on Acoustics (ICA 2004)*, 2004, pp. 4-9.
- [86] A. Hamidi, N. Beck, K. Thomas, and E. Herr, "Reliability and lifetime evaluation of different wire bonding technologies for high power IGBT modules," *Microelectronics reliability*, vol. 39, pp. 1153-1158, 1999.
- [87] M. Tounsi, A. Oukaour, B. Tala-Ighil, H. Gualous, B. Boudart, and D. Aissani, "Characterization of high-voltage IGBT module degradations under PWM power cycling test at high ambient temperature," *Microelectronics Reliability*, vol. 50, pp. 1810-1814, 9// 2010.
- [88] V. Sankaran, C. Chen, C. Avant, and X. Xu, "Power cycling reliability of IGBT power modules," in *Industry Applications Conference, 1997. Thirty-Second IAS Annual Meeting, IAS'97., Conference Record of the 1997 IEEE*, 1997, pp. 1222-1227.
- [89] W. W. Tian-Hong Yan 1, Xue-Dong Chen 2, Qing Li 1,\* and Chang Xu, "Design of a Smart Ultrasonic Transducer for Interconnecting Machine Applications," *Sensors*, vol. 9, pp. 4986-5000, 2009.
- [90] J. Lutz, H. Schlangenotto, U. Scheuermann, and R. Doncker, "Packaging and reliability of power devices," *Semiconductor Power Devices*, pp. 343-418, 2011.
- [91] L. Josef, S. Heinrich, S. Uwe, and D. Rik De, *Semiconductor Power Devices Physics, Characteristics, Reliability*, 2011.
- [92] W. Kanert, "Active cycling reliability of power devices: Expectations and limitations," *Microelectronics Reliability*, vol. 52, pp. 2336-2341, 2012.
- [93] S. M. Sze and K. K. Ng, *Physics of semiconductor devices*: John Wiley & Sons, 2006.
- [94] U. Scheuermann and R. Schmidt, "Impact of load pulse duration on power cycling lifetime of Al wire bonds," *Microelectronics Reliability*, vol. 53, pp. 1687-1691, 2013.
- [95] M. S. Broll, U. Geissler, J. Höfer, S. Schmitz, O. Wittler, and K. D. Lang, "Microstructural evolution of ultrasonic-bonded aluminum wires," *Microelectronics Reliability*, vol. 55, pp. 961-968, 5// 2015.
- [96] O. S. Marc Schäfer, Chen Yue, Tatyana Kashko, "Comparison between active and passive thermal cycling stress with respect to substrate solder reliability in IGBT modules with Cu baseplates," presented at the PCIM, 2014.
- [97] R. Schmidt and U. Scheuermann, "Using the chip as a temperature sensor- The influence of steep lateral temperature gradients on the Vce(T)-

- measurement," in *Power Electronics and Applications, 2009. EPE '09. 13th European Conference on*, 2009, pp. 1-9.
- [98] S. Beczkowski, P. Ghimre, A. R. de Vega, S. Munk-Nielsen, B. Rannestad, and P. Thogersen, "Online Vce measurement method for wear-out monitoring of high power IGBT modules," in *Power Electronics and Applications (EPE), 2013 15th European Conference on*, 2013, pp. 1-7.
- [99] D. C. Katsis, "Thermal characterization of die-attach degradation in the power MOSFET," Virginia Polytechnic Institute and State University, 2003.
- [100] U. Scheuermann and F. Ebersberger, "Packaging of Large Area Power Chips - Extending the Limits of Standard Module Technology," in *Integrated Power Systems (CIPS), 2006 4th International Conference on*, 2006, pp. 1-6.
- [101] T.-Y. Hung, L.-L. Liao, C. C. Wang, W. Chi, and K.-N. Chiang, "Life Prediction of High-Cycle Fatigue in Aluminum Bonding Wires Under Power Cycling Test," *Device and Materials Reliability, IEEE Transactions on*, vol. 14, pp. 484-492, 2014.
- [102] J. Kastner, D. Heim, D. Salaberger, C. Sauerwein, and M. Simon, "Advanced applications of computed tomography by combination of different methods," in *Proceedings of the European conference on nondestructive testing, Berlin, Germany*, 2006.
- [103] T. Wuest, C. Irgens, and K.-D. Thoben, "An approach to monitoring quality in manufacturing using supervised machine learning on product state data," *Journal of Intelligent Manufacturing*, vol. 25, pp. 1167-1180, 2013.
- [104] A. Bartkowiak and R. Zimroz, *Data dimension reduction and visualization with application to multi-dimensional gearbox diagnostics data: comparison of several methods* vol. 180: Trans Tech Publications, Switzerland, 2012.
- [105] A. Navot, "On the role of feature selection in machine learning," Hebrew University, 2006.
- [106] R. O. Duda, P. E. Hart, and D. G. Stork, *Pattern Classification: Wiley*, 2012.
- [107] R. L. Eshleman and J. Nagle- Eshleman, *Basic machinery vibrations : an introduction to machine testing, analysis, and monitoring*. Clarendon Hills, Ill.: VIPress, 1999.
- [108] X. Fan and M. J. Zuo, "Gearbox fault detection using Hilbert and wavelet packet transform," *Mechanical Systems and Signal Processing*, vol. 20, pp. 966-982, 5// 2006.
- [109] H. Cuayáhuitl, M. van Otterlo, N. Dethlefs, and L. Frommberger, "Machine learning for interactive systems and robots: a brief introduction," in *Proceedings of the 2nd Workshop on Machine Learning for Interactive Systems: Bridging the Gap Between Perception, Action and Communication*, 2013, pp. 19-28.
- [110] B. Chizi and O. Maimon, "Dimension Reduction and Feature Selection," in *Data Mining and Knowledge Discovery Handbook*, O. Maimon and L. Rokach, Eds., ed: Springer US, 2005, pp. 93-111.
- [111] Z. Ge, Z. Song, and F. Gao, "Review of recent research on data-based process monitoring," *Industrial & engineering chemistry research*, vol. 52, pp. 3543-3562, 2013.
- [112] C. Zhao, F. Wang, N. Lu, and M. Jia, "Stage-based soft-transition multiple PCA modeling and on-line monitoring strategy for batch processes," *Journal of Process Control*, vol. 17, pp. 728-741, 10// 2007.
- [113] G. Li, S.-Z. Qin, Y.-D. Ji, and D.-H. Zhou, "Total PLS Based Contribution Plots for Fault Diagnosis," *Acta Automatica Sinica*, vol. 35, pp. 759-765, 6// 2009.
- [114] L. Gao, B. Zhang, X. Sun, S. Li, Q. Du, and C. Wu, "Optimized maximum noise fraction for dimensionality reduction of Chinese HJ-1A hyperspectral



- data," *EURASIP Journal on Advances in Signal Processing*, vol. 2013, pp. 1-12, 2013.
- [115] J. H. Krijthe and M. Loog, "Implicitly Constrained Semi-supervised Linear Discriminant Analysis," in *Pattern Recognition (ICPR), 2014 22nd International Conference on*, 2014, pp. 3762-3767.
- [116] Z.-H. Zhou and M. Li, "Semi-supervised learning by disagreement," *Knowledge and Information Systems*, vol. 24, pp. 415-439, 2010.
- [117] X. Zhu, A. B. Goldberg, R. Brachman, and T. Dietterich, *Introduction to Semi-Supervised Learning*: Morgan and Claypool Publishers, 2009.
- [118] X. Zhu, "Semi-supervised learning literature survey," 2005.
- [119] C. Deng, H. Xiaoferi, and H. Jiawei, "Semi-supervised Discriminant Analysis," in *Computer Vision, 2007. ICCV 2007. IEEE 11th International Conference on*, 2007, pp. 1-7.
- [120] M. Belkin, P. Niyogi, and V. Sindhwani, "Manifold Regularization: A Geometric Framework for Learning from Labeled and Unlabeled Examples," *J. Mach. Learn. Res.*, vol. 7, pp. 2399-2434, 2006.
- [121] D. Zhou, O. Bousquet, T. N. Lal, J. Weston, and B. Schölkopf, "Learning with local and global consistency," *Advances in neural information processing systems*, vol. 16, pp. 321-328, 2004.
- [122] X. Zhu, Z. Ghahramani, and J. Lafferty, "Semi-supervised learning using gaussian fields and harmonic functions," in *ICML, 2003*, pp. 912-919.
- [123] J. He, J. G. Carbonell, and Y. Liu, "Graph-Based Semi-Supervised Learning as a Generative Model," in *IJCAI, 2007*, pp. 2492-2497.
- [124] Z. Xuran, N. Evans, and J. L. Dugelay, "Open-set semi-supervised audio-visual speaker recognition using co-training LDA and Sparse Representation Classifiers," in *Acoustics, Speech and Signal Processing (ICASSP), 2013 IEEE International Conference on*, 2013, pp. 2999-3003.
- [125] (2015). *Semi-supervised Classification*. Available: <http://www.nltk.org/book/ch06.html>
- [126] V. N. Vapnik and V. Vapnik, *Statistical learning theory* vol. 1: Wiley New York, 1998.
- [127] S. M. Chu, T. Hao, and T. S. Huang, "Fishervoice and semi-supervised speaker clustering," in *Acoustics, Speech and Signal Processing, 2009. ICASSP 2009. IEEE International Conference on*, 2009, pp. 4089-4092.
- [128] A. M. Martinez and A. C. Kak, "PCA versus LDA," *Pattern Analysis and Machine Intelligence, IEEE Transactions on*, vol. 23, pp. 228-233, 2001.
- [129] C. McCool, S. Marcel, A. Hadid, M. Pietikainen, P. Matejka, J. Cernocky, *et al.*, "Bi-Modal Person Recognition on a Mobile Phone: Using Mobile Phone Data," in *Multimedia and Expo Workshops (ICMEW), 2012 IEEE International Conference on*, 2012, pp. 635-640.
- [130] G. Jie, S. Zhenan, C. Jun, J. Shuiwang, and W. Xindong, "How to Estimate the Regularization Parameter for Spectral Regression Discriminant Analysis and its Kernel Version?," *Circuits and Systems for Video Technology, IEEE Transactions on*, vol. 24, pp. 211-223, 2014.
- [131] T. Sim, S. Baker, and M. Bsat, "The CMU pose, illumination, and expression database," *Pattern Analysis and Machine Intelligence, IEEE Transactions on*, vol. 25, pp. 1615-1618, 2003.
- [132] M. Turk and A. Pentland, "Eigenfaces for Recognition," *Journal of Cognitive Neuroscience*, vol. 3, pp. 71-86, 1991/01/01 1991.
- [133] H. Xiaoferi, Y. Shuicheng, H. Yuxiao, P. Niyogi, and Z. Hong-Jiang, "Face recognition using Laplacianfaces," *Pattern Analysis and Machine Intelligence, IEEE Transactions on*, vol. 27, pp. 328-340, 2005.

- [134] D. Cai, "Spectral Regression: A Regression for Efficient Regularized Subspace Learning," Ph.D., Computer Science, University of Illinois at Urbana-Champaign, Urbana, Illinois, 2009.
- [135] C. Deng, H. Xiaofei, and H. Jiawei, "SRDA: An Efficient Algorithm for Large-Scale Discriminant Analysis," *Knowledge and Data Engineering, IEEE Transactions on*, vol. 20, pp. 1-12, 2008.
- [136] C. Deng. *Matlab Codes and Datasets for Feature Learning*. Available: <http://www.cad.zju.edu.cn/home/dengcai/Data/data.html>
- [137] K. Tang, C. Yu, R. Liu, and Z. Su, "A Semi-supervised Dimensionality Reduction Framework for Face Recognition Based on Sparse Lorentzian Metric Tensors\*," *Journal of Information & Computational Science*, vol. 8, pp. 601-608, 2011.
- [138] M. Zhao, Z. Zhang, T. W. S. Chow, and B. Li, "A general soft label based Linear Discriminant Analysis for semi-supervised dimensionality reduction," *Neural Networks*, vol. 55, pp. 83-97, 7// 2014.
- [139] K. Fukunaga, *Introduction to statistical pattern recognition (2nd ed.)*: Academic Press Professional, Inc., 1990.
- [140] F. Chung, *Spectral Graph Theory (CBMS Regional Conference Series in Mathematics, No. 92)*: American Mathematical Society, 1996.
- [141] J. Goehre, U. Geissler, M. Schneider-Ramelow, and K. Lang, "Influence of Bonding Parameters on the Reliability of Heavy Wire Bonds on Power Semiconductors," in *Integrated Power Electronics Systems (CIPS), 2012 7th International Conference on*, 2012, pp. 1-6.
- [142] D. M. Byrne, "The Taguchi approach to parameter design," *Quality Progress*, vol. 20, pp. 19-26, 1987.
- [143] W. G. Cochran, *Sampling Techniques, 3rd Edition*: John Wiley, 1977.
- [144] W. W. Daniel, "Biostatistics: a foundation for analysis in the health sciences," *New York*, 1987.
- [145] V. Labatut and H. Cherifi, "Accuracy measures for the comparison of classifiers," *arXiv preprint arXiv:1207.3790*, 2012.
- [146] M. Makhtar, D. Neagu, and M. Ridley, "Comparing Multi-class Classifiers: On the Similarity of Confusion Matrices for Predictive Toxicology Applications," in *Intelligent Data Engineering and Automated Learning - IDEAL 2011*. vol. 6936, H. Yin, W. Wang, and V. Rayward-Smith, Eds., ed: Springer Berlin Heidelberg, 2011, pp. 252-261.
- [147] L. Torgo and R. Ribeiro, "Utility-based regression," in *Knowledge Discovery in Databases: PKDD 2007*, ed: Springer, 2007, pp. 597-604.
- [148] A. Kent, M. M. Berry, F. U. Luehrs, and J. W. Perry, "Machine literature searching VIII. Operational criteria for designing information retrieval systems," *American documentation*, vol. 6, pp. 93-101, 1955.
- [149] K. N. Meyyappan, "Failure Prediction of Wire Bonds Due to Flexure " PhD Thesis, University of Maryland, 2004.
- [150] J. Onuki, M. Koizumi, and M. Suwa, "Reliability of thick Al wire bonds in IGBT modules for traction motor drives," *Advanced Packaging, IEEE Transactions on*, vol. 23, pp. 108-112, 2000.
- [151] D. C. Montgomery, *Design and analysis of experiments*: John Wiley & Sons, 2008.